TUNING THE OPTOELECTRONIC PROPERTIES OF CONJUGATED POLYMERS VIA DONOR-ACCEPTOR-DONOR ARCHITECTURES

A THESIS SUBMITTED TO
THE GRADUATE SCHOOL OF NATURAL AND APPLIED SCIENCES
OF
MIDDLE EAST TECHNICAL UNIVERSITY

BY

SİMGE TARKUÇ

IN PARTIAL FULFILLMENT OF THE REQUIREMENTS
FOR
THE DEGREE OF DOCTOR OF PHILOSOPHY
IN
CHEMISTRY

JUNE 2010

Approval of the thesis:

TUNING THE OPTOELECTRONIC PROPERTIES OF CONJUGATED POLYMERS VIA DONOR-ACCEPTOR-DONOR ARCHITECTURES

submitted by **SİMGE TARKUÇ** in partial fulfillment of the requirements for the degree of **Doctor of Philosophy in Chemistry Department, Middle East Technical University** by,

Prof. Dr. Canan Özgen _____
Dean, Graduate School of **Natural and Applied Sciences**

Prof. Dr. İlker Özkan _____
Head of Department, **Chemistry**

Prof. Dr. Levent Toppare
Supervisor, **ChemistryDept., METU** _____

Asst. Prof. Dr. Erdal Onurhan
Co-Supervisor,**ChemistryDept.,METU** _____

Examining Committee Members:

Prof. Dr. Leyla Aras _____
Chemistry Dept., METU

Prof. Dr. Levent Toppare _____
Chemistry Dept., METU

Prof. Dr. Erdal Bayramlı _____
Chemistry Dept., METU

Prof. Dr. Cihangir Tanyeli _____
Chemistry Dept., METU

Assoc. Prof. Dr. Yasemin Arslan Udum _____
Institute of Science and Technology,
Department of Advanced Technologies,
Gazi University

Date: 25/06/2010

I hereby declare that all information in this document has been obtained and presented in accordance with academic rules and ethical conduct. I also declare that, as required by these rules and conduct, I have fully cited and referenced all material and results that are not original to this work.

Name, Last name:

Signature :

ABSTRACT

TUNING THE OPTOELECTRONIC PROPERTIES OF CONJUGATED POLYMERS VIA DONOR-ACCEPTOR-DONOR ARCHITECTURES

Tarkuç, Simge
Ph.D., Department of Chemistry
Supervisor: Prof. Dr. Levent Toppare
Co-Supervisor: Asst. Prof. Dr. Erdal Onurhan

June 2010, 148 pages

A new class of π-conjugated monomers was synthesized with combination of electron donating and electron-withdrawing heterocyclics to understand the effects of structural differences on electrochemical and optoelectronic properties of the resulting polymers. The use of this alternating donor-acceptor-donor strategy allows the synthesis of low band gap polymers in which the redox, electronic, and optical properties are controlled through easily approachable synthetic modification of the polymer backbone. This control allows fine-tuning of the band gap to values between 1.0 and 1.8 eV by making structural changes. These structural manipulations yield varied electronic absorption energies for a range of colors in the neutral polymer films, multi-colored electrochromism, and accessible states for reduction leading to n-type doping. The polymers prepared were characterized using cyclic voltammetry, colorimetry, and UV-Vis-NIR spectroscopy demonstrating that the polymers can undergo both p- and n-type doping and color changes in both redox states.

Keywords: Electrochemical polymerization; Conducting polymer; Low band gap polymer; Electrochromism.

ÖZ

DONÖR-AKSEPTÖR-DONÖR YAPILARI İLE KONJUGE POLİMERLERİN OPTOELEKTRONİK ÖZELLİKLERİNİN AYARLANMASI

Tarkuç, Simge
Doktora, Kimya Bölümü
Tez Yöneticisi: Prof. Dr. Levent Toppare
Ortak Tez Yöneticisi: Y. Doç. Dr. Erdal Onurhan

Haziran 2010, 148 sayfa

Yapısal farklılıkların sentezlenen polimerlerin elektrokimyasal ve optoelektronik özellikleri üzerindeki etkisinin anlaşılabilmesi için elektron donör ve elektron akseptör heterosiklik yapıların birleştirilmesi ile yeni bir π-konjuge monomer sınıfı sentezlendi. Alternatif donör-akseptör-donör stratejisinin kullanılması ile π-konjuge moleküllerin yapılarında kolaylıkla değişikler yapıldı. Bunun sonucunda polimerlerin redoks, elektronik ve optik özellikleri kontrol edildi. Bu kontrol ile polimerlerin bant aralık değerleri 1.0 eV ile 1.8 eV arasında değiştiği gözlendi. Yapısal değişiklikler ile değişen elektronik soğurma enerjisi polimerlerin nötral durumda farklı renklere sahip olmasını sağlarken, multi-elektrokromik özellik gösteren polimerlerinde sentezlenmesini sağladı. Sentezlenen iletken polimerlerin elektronik ve elektrokromik özellikleri dönüşümlü voltametre, UV-Vis-NIR spektroelektrokimyasal ve kolorimetrik çalışmalarla araştırılmıştır. Polimerlerin p- ve n- tipi katkılama ile renklerindeki değişim spektroelektrokimyasal çalışmalar ile analiz edildi.

Anahtar sözcükler: Elektrokimyasal polimerleşme; iletken polimerler; düşük bant aralıklı polimerler; elektrokromizm.

To My Family

ACKNOWLEDGMENTS

I would like to express my sincere gratitude to the excellent and diligent guidance of Prof. Dr. Levent Toppare for his valuable suggestion, stimulating advice, creative and energetic instructions.

I would like to acknowledge Asst. Prof. Dr. Erdal Onurhan who provides me opportunities to complete a part of my thesis studies at Middle East Technical University Northern Cyprus Campus.

I would like to thank Assoc. Prof. Dr. Yasemin Arslan Udum for her valuable discussions, endless helps, stimulating conversations besides her kind friendship.

I would like to give a special thanks to Dr. Elif Köse Ünver for the collaborative spirit of the synthetic chemists. I always appreciated her help.

Special thanks go to Görkem Günbaş for his invaluable guidance at the initial stages of organic synthesis. To Aslı Tuba Taşkın, Funda Uçal, Ayşe Gül Varış, Başak Yiğitsoy and Asuman Durmuş, thanks go for their endless patience and friendship.

I also would like to thank Özlem Türkarslan and Yusuf Nur for their friendship, useful conversations and cooperation.

Over the past five years, there have been a large number of people come and go from the group and each individual has leant their personality to the dynamics of the Toppare Research Group. I would like to thank those who have been there for their friendship, helping, making lab-life more fun.

Also, thanks to my friends Ahmet Melih Selçuk, Cem Yıldırım, İlknur Demirtaş and Özcan Kasal for the early morning and midnight coffee breaks.

I would especially like to thank Aysun, with whom I struggle the challenges that we met over 3 years as resident at “3101”. To Aysun, thanks also go for a continuing friendship, her endless patience and encouragement through Ph.D. proficiency exam.

I would like to extend my deepest gratitude to “Kuzen” for always believing in me and making me feel strong enough to achieve everything.

I would like to extend my deepest gratitude to Nurten Serger for 14 years that we have survived many things that life threw our way.

Words fail to express my eternal gratitude to my parents for their continuous support and attempts to understand and encourage me during what has been simultaneously the most enjoyable and most stressful part of my life. I would like to thank my sister Sinem Tarkuç for always being there for me and her unwavering support of my decision.

Finally, I would like thank the Scientific and Technological Research Council of Turkey (TUBITAK) for financial support which enabled me to carry out this work.

TABLE OF CONTENTS

ABSTRACT iv
ÖZ v
ACKNOWLEDGMENTS vii
TABLE OF CONTENTS ix
LIST OF FIGURES xiii
LIST OF TABLES xviii
ABBREVIATIONS xix
CHAPTERS
1.INTRODUCTION 1
1.1. Brief History of Conducting Polymers 1
1.2. Band Theory 3
1.3. Conductivity in π-Conjugated Organic Materials 5
1.4. Doping Types in Conducting Polymers 8
1.5. Polymerization Methods 10
1.5.1. Chemical Polymerization 10
1.5.2. Electrochemical Polymerization 12
1.6. Band Gap 14
1.6.1. Factors effecting band gap 14
1.6.2. Band gap control in π-conjugated polymers 17
1.6.2.1. Low band gap conducting polymers with increased quinoid character 17
1.6.2.2. Low band gap conducting polymers with alternating donor-acceptor moieties along the chain 19
1.6.3. Structural Design and Synthetic Methodology for Low Band Gap Materials 20
1.7. Chromism 24
1.7.1. Electrochromism 25
1.8. Electrochromism in Conducting Polymers 27
1.9. Application Areas of Conducting Polymers 30
1.9.1. Absorption/Transmission ECDs 31

1.9.2. Light Emitting Diodes....32
1.9.3. Solar Cell....34
2.EXPERIMENTAL....35
2.1. Materials and Methods....35
2.2. Syntheses of π-Conjugated D-A-D Type Monomers....36
2.2.1. Preparation of Donor Moieties....36
2.2.1.1. Tributyl(thiophen-2-yl)stannane (1)....36
2.2.1.2. Tributyl(4-hexylthiophen-2-yl)stannane (2)....37
2.2.1.3. Tributyl(2,3-dihydrothieno[3,4-*b*][1,4]dioxin-7-yl)stannane (3)....38
2.2.2. Syntheses of Quinoxaline Derivatives....39
2.2.2.1. 4,7-Dibromobenzo[*c*][1,2,5]thiadiazole (5)....39
2.2.2.2. 3,6-Dibromobenzene-1,2-diamine (6)....40
2.2.2.3. 1-(2,3-Dihydrobenzo[b][1,4]dioxin-6-yl)-2-(2,3-dihydrobenzo[b][1,4] dioxin 7-yl) ethane-1,2-dione (8)....40
2.2.2.4. 5,8-Dibromo-2-(2,3-dihydrobenzo[b][1,4]dioxin-6-yl)-3-(2,3-dihydro benzo[b] [1,4]dioxin-7-yl)quinoxaline (9)....41
2.2.2.5. General Procedure for the Synthesis of 14, 15, 16 via Stille coupling....42
2.2.2.5.1. 2-(2,3-Dihydrobenzo[*b*][1,4]dioxin-6-yl)-3-(2,3-dihydrobenzo[*b*][1,4] dioxin-7-yl)-5,8-di(thiophen-2-yl)quinoxaline (14)....42
2.2.2.5.2. 5,8-Bis(4-hexylthiophen-2-yl)-2-(2,3-dihydrobenzo[*b*][1,4]dioxin-6-yl)-3-(2,3-dihydrobenzo[*b*][1,4]dioxin-7-yl)quinoxaline (15)....43
2.2.2.5.3. 2-(2,3-dihydrobenzo[*b*][1,4]dioxin-6-yl)-3-(2,3-dihydrobenzo[*b*][1,4] dioxin-7-yl)-8-(2,3-dihydrothieno[3,4-*b*][1,4]dioxin-5-yl)-5-(2,3-dihydrothieno [3,4-*b*][1,4]dioxin-7-yl)quinoxaline (16)....44
2.2.2.6. 10,13-Dibromodibenzo[*a,c*]phenazine (10)....44
2.2.2.7. General Procedure for the Synthesis of 17, 18 via Stille coupling....45
2.2.2.7.1. Synthesis of DAD monomer based on dibenzo [a,c] phenazine and....45
3-hexylthiophene....45
2.2.2.7.2. Synthesis of DAD monomer based on dibenzo [a,c] phenazine and....46
EDOT....46
2.2.2.8. 1,10-Phenanthroline-5,6-dione (12)....46
2.2.2.9. 3-(2,3-Dihydrothieno[3,4-b][1,4]dioxin-5-yl)-6-(2,3-dihydrothieno[3,4-b][1,4] dioxin-7-yl)benzene-1,2-diamine (20)....47
2.2.2.10. Synthesis of DAD monomer based on 1,10-phenanthroline..48
2.2.3. Thienopyrazine Derivative....49
2.2.3.1. 2,5-Dibromo-3,4-dinitrothiophene (23)....49

2.2.3.2. 2,5-Bis(4-hexylthiophen-2-yl)-3,4-dinitrothiophene (24).....49
2.2.3.3. 2,5-Bis(4-hexylthiophen-2-yl)thiophene-3,4-diamine (25) 50
2.2.3.4. 5,7-Bis(4-hexylthiophen-2-yl)-2-(2,3-dihydrobenzo[b][1,4]dioxin-6-yl)-3-(2,3-dihydrobenzo[b][1,4]dioxin-7-yl)thieno[3,4-b]pyrazine (26).....51
2.3. Electrochemical Method 51
2.3.1. Electrochemical cells 52
2.3.2. Cyclic Voltammetry 53
2.4. Optical Methods 56
2.4.1. Spectroelectrochemistry 56
2.4.2. Electrochromic Switching 58
2.4.3. Colorimetry 59
2.5. Electrochromic Devices 60
2.5.1. Device Construction 61
2.5.2. Preparation of Gel Electrolyte 62
2.5.3. Characterization of ECDs 63
2.5.3.1. Spectroelectrochemistry 63
2.5.3.2. Switching Studies 63
2.5.3.3. Open Circuit Memory 63
3.RESULTS AND DISCUSSION 64
3.1. Donor-Acceptor-Donor Type π-Conjugated Monomers 64
3.1.1. Quinoxaline Derivatives 64
3.1.2. Thienopyrazine Derivative 66
3.1. 3. Donor Moieties 66
3.1.4. Acceptor Moieties 67
3.1.4.1. Synthesis of 5,8-dibromo-2-(2,3-dihydrobenzo[*b*][1,4]dioxin-6-yl)-3-(2,3-di hydrobenzo[*b*][1,4]dioxin-7-yl)quinoxaline (9).....67
3.1.4.2. Synthesis of 10,13-dibromodibenzo [a,c] phenazine (10) 69
3.1.4.3. Synthesis of 10,13- dibromodipyrido[3,2-a:2,3-c]phenazine ..70
3.1.4.4. Characterization of Acceptor Moieties 72
3.2. Syntheses of Donor-Acceptor-Donor Type Quinoxaline Derivatives ...73
3.3. Synthesis of DAD monomer based on 1,10-phenanthroline.....78
3.4. Synthesis of Thienopyrazine Derivative 80
3.4.1. 5,7-bis(4-hexylthiophen-2-yl)-2-(2,3-dihydrobenzo[b][1,4]dioxin-6-yl)-3-(2,3-dihydrobenzo[b][1,4]dioxin-7-yl)thieno[3,4-b]pyrazine 80
3.5. Characterization of Conducting Polymers 81
3.5.1. Ethylenedioxy Benzene Substituted Quinoxaline Derivatives 81
3.5.1.1. Electrochemistry 81

3.5.1.2. Spectroelectrochemistry 86
3.5.1.3. Electrochromic Switching Studies 90
3.5.1.4. Colorimetry Studies 93
3.5.2. Dibenzo[*a,c*]phenazine Inserted Quinoxaline Derivatives 95
3.5.2.1. Electrochemistry 95
3.5.2.2. Spectroelectrochemistry 98
3.5.2.3. Electrochromic Switching 102
3.5.2.4. Colorimetry 104
3.6. Dipyrido[3,2-*a*:2,3-*c*]phenazine Inserted Quinoxaline Derivative 105
3.6.1. Electrochemistry 105
3.6.2. Spectroelectrochemistry 107
3.6.3. Electrochromic Switching Studies 109
3.6.4. Colorimetry 110
3.7. Thienopyrazine Derivative 111
3.7.1. Cyclic Voltammetry 111
3.7.2. Spectroelectrochemistry 112
3.7.3. Electrochromic Switching Studies 113
3.7.4. Colorimetry 114
3.8. Electrochromic Device 115
3.8.1. Spectroelectrochemistry of ECD 115
3.8.2. Electrochromic switching studies of ECDs 116
3.8.3. Open circuit memory 117
4.CONCLUSION 119
REFERENCES 121
APPENDIX A: SELECTED NMR DATA 129
CURRICULUM VITAE 146

LIST OF FIGURES

FIGURES

Figure 1.1. Structures of some common π-conjugated monomers 2
Figure 1.2. Simple band picture explaining the difference between an insulator, a semiconductor and a metal [24] 4
Figure 1.3. The formation of a band structure as conjugation increases from thiophene to polythiophene 5
Figure 1.4. (a) Degenerate polyacetylene; and (b) non-degenerate polypyrrole [25] 6
Figure 1.5. Charge carries in PEDOT and its corresponding energy bands in the mid- gap. 7
Figure 1.6. Doping mechanisms and related applications 8
Figure 1.7. Synthesis of polythiophene via a) metal catalyzed coupling and b) chemical oxidation 11
Figure 1.8. McCullough method for the synthesis of regioregular poly(alkylthiophenes) [34] 12
Figure 1.9. Mechanism of oxidative polymerization of thiophene 13
Figure 1.10. Overview of methods for the modification of band gap [37] 15
Figure 1.11. The nondegenerate ground state resonance of polythiophene 15
Figure 1.12. Interannular rotation in conjugated polymer 16
Figure 1.13. Mesomeric forms of polyisothianaphthene 17
Figure 1.14. Overview of some synthesized PITN derivatives 18
Figure 1.15. The donor-acceptor approach, alternating donor and acceptor moieties results in a polymer that has the combined optical properties of the parent donor or acceptor monomers [37]. 20
Figure 1.16. The three common redox states of viologens 27
Figure 1.17. Polaron and bipolaron in non-degenerate ground state polymers: band diagrams for (a) neutral, (b) polaron, (c) bipolaron [24] 29

Figure 1.18. Schematic illustration of dual type absorptive/transmissive type ECD configuration [74].....32
Figure 1.19. Schematic representation of polymer light emitting diode [76] ...33
Figure 2.1. A three electrode electrochemical cell set up 52
Figure 2.2. Typical (a) Potential−time excitation signal in CV (b) cyclic voltammogram of a reversible O + ne$^-$ ↔R redox process [79].....53
Figure 2.3. Cyclic voltammogram of a representative electroactive monomer 54
Figure 2.4. Cyclic voltammogram of a representative type of electroactive monomer at scan rates of 100, 150,200, 250 and 300 mV/s. 55
Figure 2.5. p-Doping spectroelectrochemistry of a representative electrochromic conducting polymer.....57
Figure 2.6. Switching studies of a representative electrochromic conducting polymer 58
Figure 2.7. CIE 1931 Yxy color space [82] 59
Figure 2.8. ECDs.....61
Figure 2.9. Schematic representation of a typical absorptive/transmissive electrochromic device [83].....62
Figure 3.1. Donor-Acceptor-Donor Type Thienopyrazine Derivative 66
Figure 3.2. Aromatic chemical shifts of π-conjugated monomers.....72
Figure 3.3. Aromatic chemical shifts of π-conjugated monomers.....75
Figure 3.4. Aromatic chemical shifts of π-conjugated monomers.....77
Figure 3.5. Repeated potential scan electropolymerization of a) 14 c) 16 in 0.1 M $TBABF_4$/ACN/DCM, b) 15 in 0.1 M $NaClO_4$/ACN at 100 mV/s on the ITO electrode. 82
Figure 3.6 Cyclic voltammograms of a) P14 b) P15 c) P16 in 0.1 M $TBABF_4$/ACN/DCM at scan rates of 100, 150, 200, 250 and 300 mV/s. 85
Figure 3.7. p-Doping spectroelectrochemistry of P14 film on an ITO coated glass slide in monomer free, 0.1 M $TBAPF_6$/DCM electrolyte-solvent couple at applied potentials.....87

Figure 3.8. p-Doping spectroelectrochemistry of P15 film on an ITO coated glass slide in monomer free, 0.1 M $NaClO_4$/ACN electrolyte-solvent couple at applied potentials 88
Figure 3.9. p-Doping spectroelectrochemistry of P16 film on an ITO coated glass slide in monomer free, 0.1 M $TBAPF_6$/DCM electrolyte-solvent couple at applied potentials.....88
Figure 3.10. n-Doping spectroelectrochemistry of P16 at -0.2 V, -1.7 V and + 1.1. V.....90
Figure 3.11. Electrochromic switching and optical absorbance change monitored at a) 395, 630 and 1560 nm for P14 in 0.1 M $TBABF_4$/ACN, b) 530 and 1640 nm for P15 in 0.1 M $NaClO_4$/ACN, c) 423, 738 and 1780 nm for P16 in 0.1 M $TBABF_4$/ACN. 92
Figure 3.13. Cyclic voltammograms of P17 in 0.1 M $TBAPF_6$/DCM at scan rates of 100, 150, 200, 250 and 300 mV/s. 98
Figure 3.14. a) p-doping spectroelectrochemistry of P17 film on an ITO coated glass slide in monomer free, in 0.1 M $NaClO_4$/ACN electrolyte-solvent couple at applied potentials, b) p-doping Spectroelectrochemistry of P18 film on an ITO coated glass slide in monomer free, 0.1 M $TBAPF_6$/DCM electrolyte-solvent couple at applied potentials. 100
Figure 3.15. Electrochromic switching, optical absorbance change monitored at a) 570 and 1850 nm for P17 b) 470, 790 and 1600 nm for P18 in 0.1 M $TBAPF_6$/DCM.....103
Figure 3.16. Repeated potential scan electropolymerization of 21 at 100 mVs^{-1} in 0.1 M $TBAPF_6/CH_2Cl_2$ on an ITO electrode 105
Figure 3.17. Cyclic voltammograms of P21 in 0.1 M $TBAPF_6$/DCM at scan rates of 100, 150, 200, 250 and 300 mV/s. 106
Figure 3.18. p-Doping spectroelectrochemistry of P21 film on an ITO-coated glass slide in monomer-free, 0.1 M $TBAPF_6$/DCM electrolyte–solvent couple at applied potentials.....107
Figure 3.19. Electrochromic switching and optical absorbance change monitored at 460 nm and 1460 nm for P21 in 0.1 M $TBAPF_6$/DCM.....109

Figure 3.20. Repeated potential scan electropolymerization of P26 at 100 mV/s in 0.1 M $TBAPF_6$/DCM on ITO electrode. 111
Figure 3.21. p-Doping spectroelectrochemistry of P26 film on an ITO coated glass slide in monomer free, 0.1M $TBAPF_6$/DCM electrolyte-solvent couple at applied potentials. 113
Figure 3.22. Electrochromic switching and optical absorbance change monitored at 410 nm, 751 nm and 1550 nm for P26 in 0.1M $TBAPF_6$/DCM. 114
Figure 3.23. Optoelectrochemical spectrum of P18/PEDOT device 116
Figure 3.24. Electrochromic switching, optical absorbance monitored for P18/PEDOT device. 117
Figure 3.25. Open circuit memory of P18/PEDOT device monitored at −1.8 V and +1.8 V potentials were applied for one second for each 200 s time interval. 118
Figure A.1. ^{1}H-NMR spectrum of 4,7-dibromobenzo[c][1,2,5]thiadiazole (5) 129
Figure A.2. ^{13}C-NMR spectrum of 4,7-dibromobenzo[c][1,2,5]thiadiazole (5) 130
Figure A. 3. ^{1}H-NMR spectrum of 3,6-dibromobenzene-1,2-diamine (6) 131
Figure A.4. ^{13}C-NMR spectrum of 3,6-dibromobenzene-1,2-diamine (6) 132
Figure A.6. ^{1}H-NMR spectrum of 5,8-dibromo-2-(2,3-dihydrobenzo[b][1,4]dioxin-6-yl)-3-(2,3-dihydrobenzo[b][1,4]dioxin-7-yl)quinoxaline (9) 134
Figure A.7. ^{13}C-NMR spectrum of 5,8-dibromo-2-(2,3-dihydrobenzo[b][1,4]dioxin-6-yl)-3-(2,3-dihydrobenzo[b][1,4]dioxin-7-yl)quinoxaline (9) 135
Figure A.8. ^{1}H-NMR spectrum of 2-(2,3-dihydrobenzo[b][1,4]dioxin-6-yl)-3-(2,3-dihydrobenzo [b][1,4]dioxin-7-yl)-5,8-di(thiophen-2-yl)quinoxaline (14) 136
Figure A. 9. ^{1}H-NMR spectrum of 5,8-bis(4-hexylthiophen-2-yl)-2-(2,3-dihydro benzo[b] [1,4] dioxin-6-yl)-3-(2,3-dihydrobenzo[b][1,4]dioxin-7-yl)quinoxaline(15) 137

Figure A. 10. ^{13}C-NMR spectrum of 5,8-bis(4-hexylthiophen-2-yl)-2-(2,3-dihydro benzo[b] [1,4] dioxin-6-yl)-3-(2,3-dihydrobenzo[b][1,4]dioxin-7-yl)quinoxaline (15).....138
Figure A. 11. ^{1}H-NMR spectrum of 2-(2,3-dihydrobenzo[b][1,4]dioxin-6-yl)-3-(2,3-dihydrobenzo [b][1,4]dioxin-7-yl)-8-(2,3-dihydrothieno[3,4-b][1,4]dioxin-5-yl)-5-(2,3-dihydrothieno[3,4-b] [1,4]dioxin-7-yl)quinoxaline (16).....139
Figure A. 12. ^{1}H-NMR spectrum of 10,13-dibromobenzo[*a,c*]phenazine (10) 140
Figure A. 13. ^{1}H-NMR spectrum of 17.....141
Figure A. 14. ^{1}H-NMR spectrum of 18.....142
Figure A. 15. ^{1}H-NMR spectrum of 21.....143
Figure A. 16. ^{1}H-NMR spectrum of 5,7-bis(4-hexylthiophen-2-yl)-2-(2,3-dihydro- benzo[b][1,4] dioxin-6-yl)-3-(2,3-dihydrobenzo[b][1,4]dioxin-7-yl)thieno[3,4-b] pyrazine (26).....144
Figure A. 17. ^{13}C-NMR spectrum of 5,7-bis(4-hexylthiophen-2-yl)-2-(2,3-dihydro- benzo[b][1,4] dioxin-6-yl)-3-(2,3-dihydrobenzo[b][1,4]dioxin-7-yl)thieno[3,4-b] pyrazine (26).....145

LIST OF TABLES

TABLES

Table 3.1. Donor-Acceptor-Donor Type Quinoxaline Derivatives 65
Table 3.2. Electrochromic properties of a) P14, b) P15,c) P16 94
Table 3.3. Effects of changes in π-system of the central aromatic group on the absorption onset and electronic band gap of the resulting polymers 101
Table 3.4. Electrochromic properties of a) P17, b) P18.....104
Table 3.5. Effects of changes in π-system of the central aromatic group on the absorption onset and electronic band gap of the resulting polymers 108
Table 3.6. Electrochromic properties of P21 110
Table 3.7. Electrochromic properties of P26. 115

ABBREVIATIONS

EDOT	3,4-Ethylenedioxythiophene
Th	Thiophene
Py	Pyrrole
PEDOT	Poly(3,4-ethylenedioxythiophene)
ACN	Acetonitrile
DCM	Dichloromethane
TBAFB	Tetrabutylammonium tetrafluoroborate
TBAPF	Tetrabutylammonium hexafluorophosphate
PMMA	Poly(methylmethacrylate)
PC	Propylene carbonate
NMR	Nuclear Magnetic Resonance
CV	Cyclic Voltammetry
ECD	Electrochromic Device
PVD	Photovoltaic Device
TFT	Thin Film Transistor
LED	Light-Emitting Diode
HOMO	Highest Occupied Molecular Orbital
LUMO	Lowest Unoccupied Molecular Orbital
E_g	Band Gap Energy
CIE	La Commission Internationale de l'Eclairage
L a b	Luminance, hue, saturation

CHAPTER 1

INTRODUCTION

1.1. Brief History of Conducting Polymers

The field of conducting polymers dates to as far back as 1862 when Letheby produced a dark green film on an electrode by the electrolytic oxidation of aniline under acidic conditions [1]. The most studied conducting polymer, polyacetylene (PAc) can even be dated to 1955 when Natta described the production of the polymer using the coordination catalyst system commonly used to polymerize ethylene and propylene [2]. PAc was even found to behave as a semiconductor by various researchers in the 1960s on treatment with different catalyst systems, producing dramatic changes in electrical conductivity [3-5]. However, the idea of using polymers for their electrical conducting properties actually emerged in 1977 with the findings of H. Shirakawa, A. McDiarmid, A. J. Heeger et al., that the oxidatively doped trans-polyacetylene, (CH)x, exhibits the metallic electrical conductivity [6,7].
Since then, the conducting polymers were proclaimed as futuristic new materials which exhibit the electrical properties of metals or semiconductors and which retain the known advantageous properties of polymer. The high conductivity of PAc found by Shirakawa, McDiarmid, Heeger opened up the field of “plastic electronics”. Alan Heeger, Alan MacDiarmid, and Hideki Shirakawa were awarded the Nobel Prize in Chemistry in 2000 "for the discovery and development of electrically conducting polymers" [8].

Although polyacetylene exhibits a very high conductivity in the doped form, the material is unstable to oxygen and humidity. Also characterization and processing of the polymer cannot be performed since the material is insoluble. The synthesis of new conducting polymer with improved/desired properties has been the subject of research in the field of conducting polymers over the years.

Polyacetylene is the archetype of conducting polymer that has the characteristic structure of a π-conjugated system with alternating double and single bonds over a large number of chain. The idea that any conjugated system might be capable of conduction directs the studies on aromatic and heteroaromatic compounds such as thiophene, furan, pyrrole, benzene, aniline, indole and carbazole (Figure 1.1).

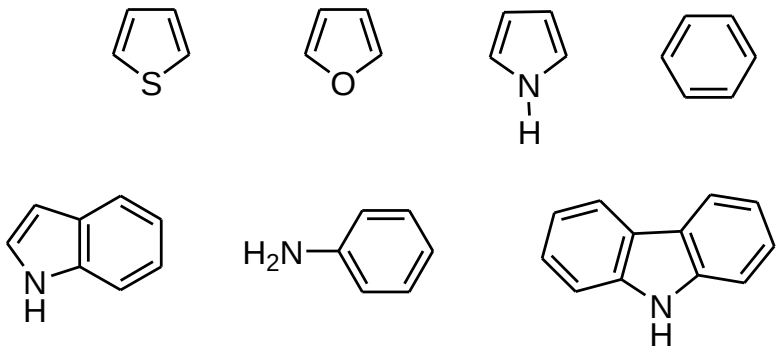

Figure 1.1. Structures of some common π-conjugated monomers

Diaz et al. showed that electrochemically polymerized pyrrole produced free-standing, air-stable polymer films with conductivities of 100 $S.cm^{-1}$ [9]. The method they used was a modification of that originally reported by Dall'Olio in 1968 with the main difference being that Diaz et al, obtained a strongly adhered, durable film that could be peeled off the platinum electrodes as opposed to a powdery, insoluble precipitate [10]. Not only did this demonstrate the ability to electrochemically polymerize directly onto an electrode surface and reversibly switch the polymer between a neutral and oxidized state, but it introduced the field to polyheterocyclic systems, which would become the most important class of conducting polymer

to date. The impact of electron rich heterocyclic systems such as pyrrole and thiophene stems from several factors that include stability of the polymers, the ease of preparation of polymer films, and the ability to synthesize derivatives that allow for modification of the electrical and physical properties of the final polymer. The higher stability of polyheterocyclics resulted from the stabilizing effect of sulfur and nitrogen on the positive charge.

Combining the electrical properties of semiconductors with the properties of polymers makes these compounds excellent materials for a large extent of applications such as thin film transistors [11-13], sensors [14,15], polymer light emitting diodes [16,17], photovoltaics [18,19] and electrochromic devices [20,21].

Various strategies have been used to design and synthesis of new precursor structures to combine good electrical, optical and mechanical properties with processability and environmental stability. In order to enhance a specific property desired for end use application, a basic understanding of how structural modification is related to the material properties is needed. Recent studies indicate that the magnitude of the band gap and position of the edges of the conduction band and valence band are most important factors to the control of conducting polymer properties [22, 23]. Developing methodologies to attain such precise control over the electronic band structure of the polymer is a key aspect for the advancement of the conducting polymer field.

1.2. Band Theory

Conducting polymers are classified as semiconductors according to their conductivity. Therefore, the band model that explains the electrical behavior of semiconductors, have been used to describe the electronic properties of conducting polymers. The band gap of semiconductors lies between those of metals and insulators (Figure 1.2). According to band theory, a metal has a zero band gap since the conduction band and valence band is overlapped to form a single band.

Movement of the charge carriers (electrons) freely within partially filled bands leads to metallic conductivity. On the other hand, the transition of electrons from the valence band to the conduction band is not possible for an insulator due to the large band gap.

In a semiconductor, there is a filled valence band and an empty conduction band separated by a band gap where no energy levels are present. The conduction band of semiconductors is lightly populated by exciting electrons across the band gap either thermally or photochemically at ambient temperature. This gives rise to charge carriers are available for electrical charge flow in semiconductors [24].

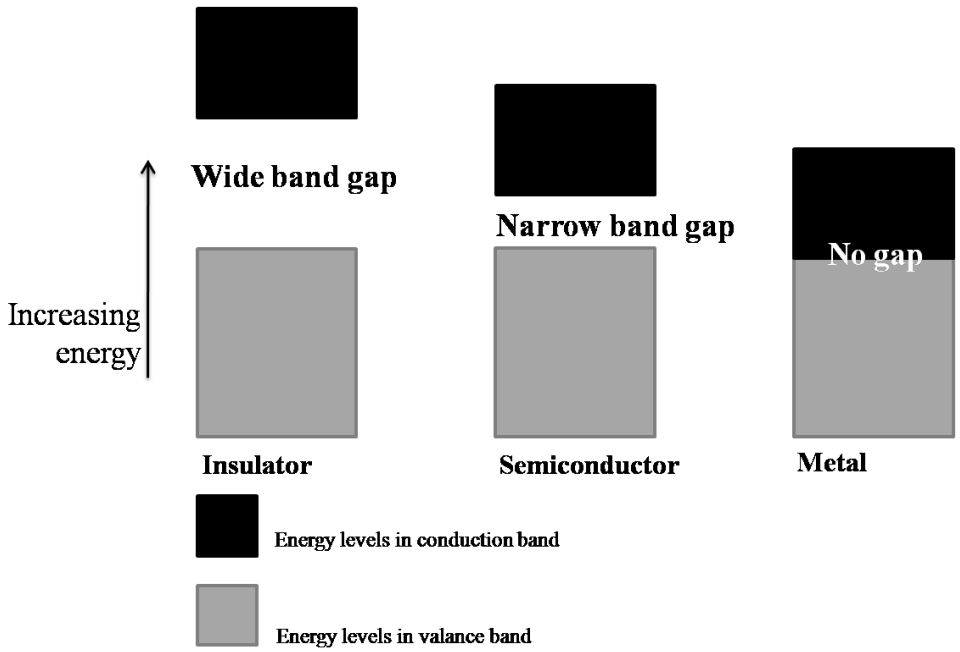

Figure 1.2. Simple band picture explaining the difference between an insulator, a semiconductor and a metal [24]

Figure 1.3 shows the formation of a band structure as conjugation increases from thiophene to polythiophene. The number of π bonding and anti-bonding orbitals increases with addition of thiophene rings. As the π-system is extended by linking a string of π-aromatic molecules together, a molecular system with well-defined

HOMO and LUMO energies is converted to a system with continuous energy bands since the energies of the molecular orbitals no longer have discrete energies. The valence band consists of filled π bonding orbitals and the conduction band consists of empty π anti-bonding orbitals. The energy difference between these two bands is called the bandgap, which is the energy required to promote an electron from the valence band to the conduction band. The energy difference decreases as the conjugation length increases along with an increase in the number of energy levels.

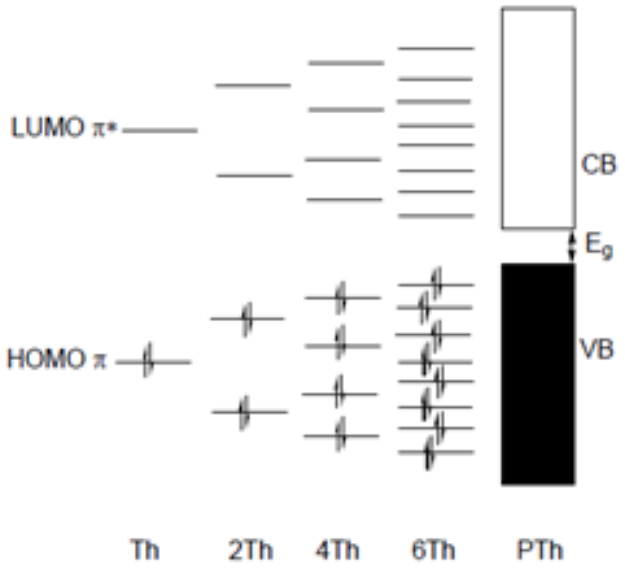

Figure 1.3. The formation of a band structure as conjugation increases from thiophene to polythiophene

1.3. Conductivity in π-Conjugated Organic Materials

The mechanism of conductivity in the conjugated polymers based on the existence of positive or negative charge carriers and the motion of those charge carriers along the π-backbone of a polymer chain. The charge carriers, either positive (p-type) or negative (n-type) are created on the polymer backbone via the oxidation or reduction process of the polymer, respectively.

The simplest conducting polymer is trans-polyacetylene; the conjugated nature of the polymer chain allows it to have two possible electronically extreme states (Figure 1.4). Unlike all the other conducting polymers, the two resonance forms of trans-polyacetylene are degenerate, i.e. their ground states are thermodynamically equivalent [25]. All other organic conducting polymers have non-degenerate ground states for example; polypyrrole has both benzenoid and quinoid configurations (Figure 1.4), of which the quinoid structure generally has a slightly higher energy, and thus being less favorable, than the benzenoid structure.

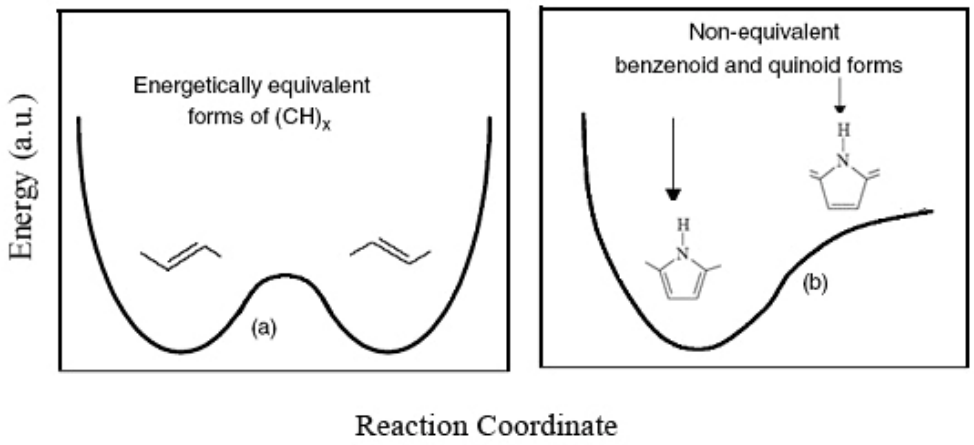

Figure 1.4. (a) Degenerate polyacetylene; and (b) non-degenerate polypyrrole [25]

The mechanism of conduction in non-degenerate ground state conjugated polymers was illustrated in Figure 1.5. When a conjugated polymer is oxidized, electrons are removed from the valence band and "holes", that is, radical cations are created. The radical cation is partially delocalized over several structural units and is called the polaron. Charge neutrality is maintained by the diffusion of counterions into the polymer. Upon oxidation in these systems, the energy level from which the electron is removed is raised in energy and now lies in the region of the band gap. This deformation causes the formation of two new electronic states which appear within the valence and conduction band of the polymer. Further oxidation can either convert the polaron into a spinless bipolaron (C), or introduce another polaron (D). Both polarons and bipolarons are mobile and can move along the polymer chain in an

electric field, and thus conduct electrical current. The conversion between neutral, polaronic, and bipolaronic species is reversible, using either chemical or electrochemical means to oxidize or reduce the polymer.

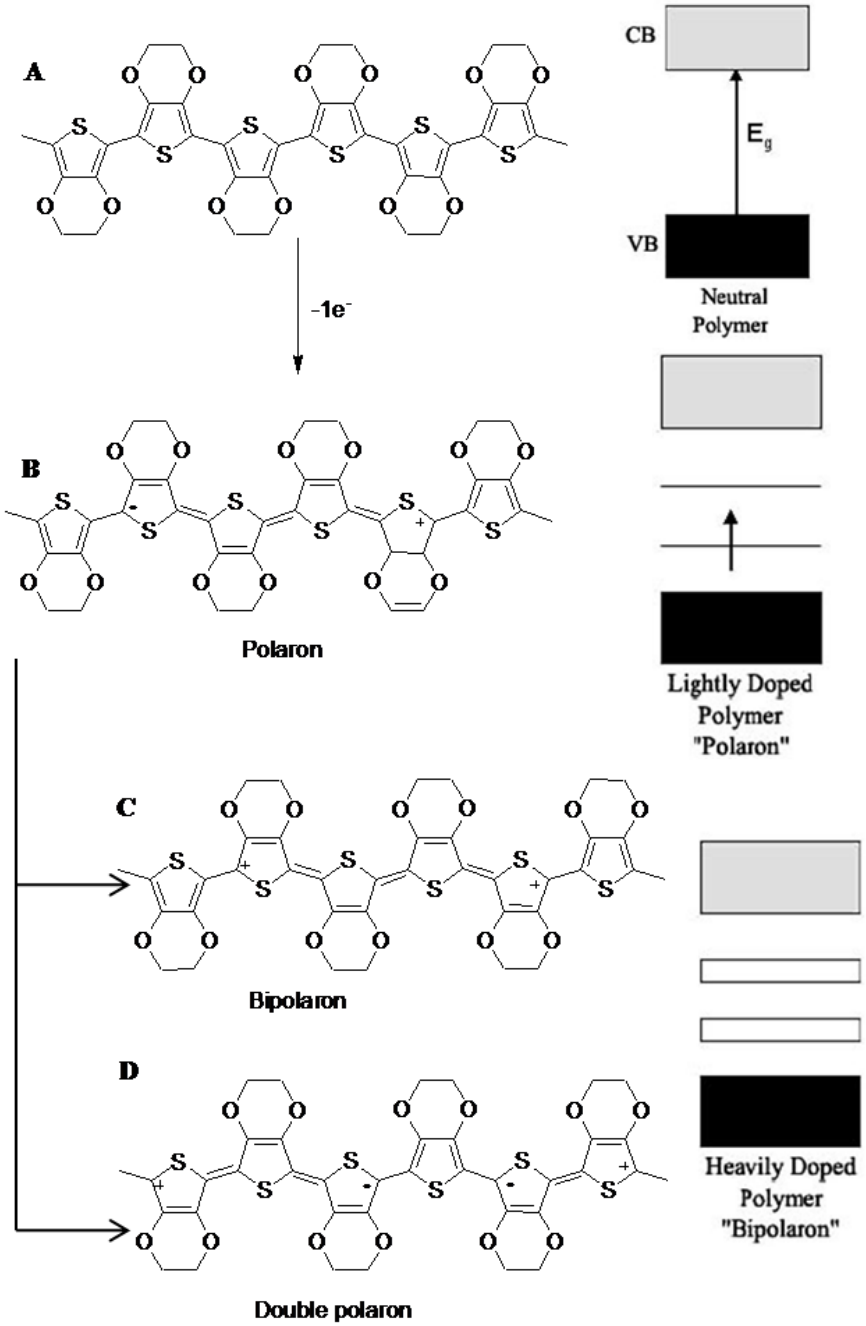

Figure 1.5. Charge carries in PEDOT and its corresponding energy bands in the mid-gap.

1.4. Doping Types in Conducting Polymers

Conjugated polymers are insulating or poorly conducting due to their energy gaps. These systems only become highly conductive through doping process which is the charge injection process into a conjugated polymer chain. The polymer can be doped to either partially fill the conduction band by adding electrons (n-type doping) or partially vacate the valance band by oxidation (p-type doping). As shown in Figure 1.6, reversible charge injection by "doping" can be accomplished in many different ways. Chemical, photochemical, interfacial or electrochemical means could be exploited in various possible applications [27].

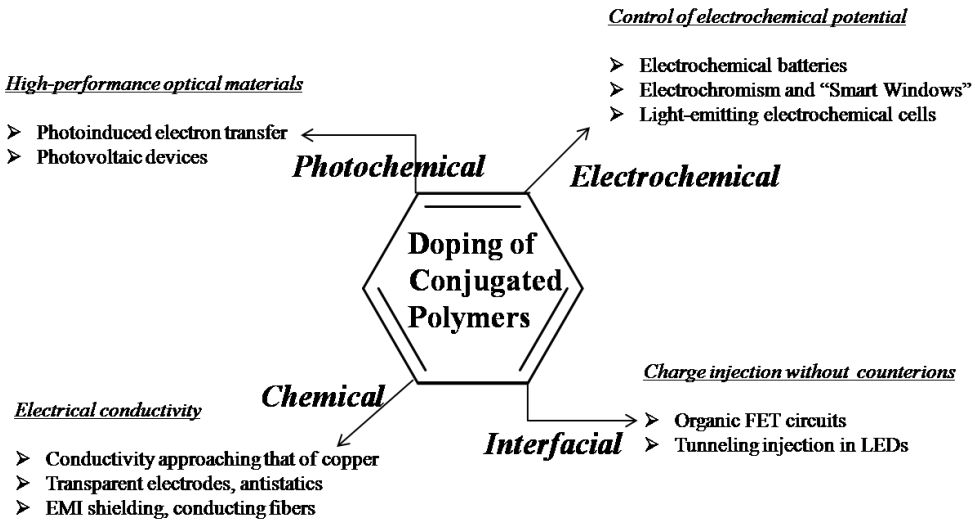

Figure 1.6. Doping mechanisms and related applications

A chemical or other oxidation of the conducting polymer essentially a removal of electrons from the valence band, leads to the presence of positive charges on the polymer backbone. Doping of the conducting polymers can be accomplished chemically by subjecting the polymer in a solution with a solution or vapor of the dopant.

For instance, trans-$(CH)_x$ was oxidized using an oxidizing agent iodine [28,29]:

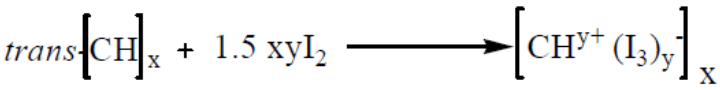

The p-doping can also be accomplished by electrochemical oxidation. When a positive potential is applied to a conducting polymer, for instance a trans-(CH)x film deposited on an inert electrode, the dopant anion (ClO_4^-) moves into the polymer towards delocalized charge sites on the polymer, and p-doping occurs. This p-doping is also termed as anionic doping [30]:

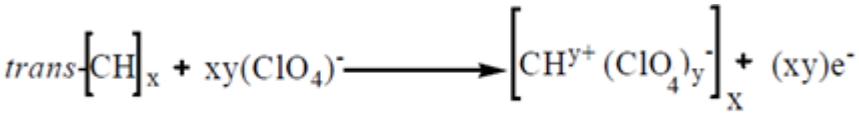

The n-doping, i.e. partial reduction of the backbone π-system of an organic polymer, was also discovered using trans-$(CH)_x$ by treating it with a reducing agent such as sodium naphthalide [29,30]:

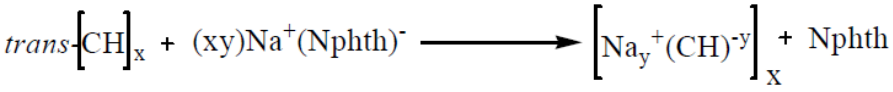

The n-doping can also be carried out by electrochemical reduction. A negative potential is applied in solution to a conducting polymer, for instance a trans-(CH)x film deposited on an inert electrode, the dopant cation (Li^+) would move from the solution to the polymer. This would be termed cationic, or n-type doping [31]:

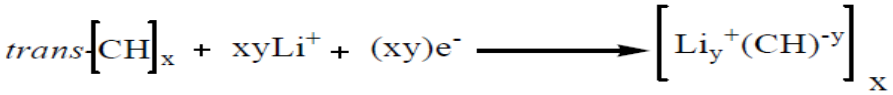

1.5. Polymerization Methods

Chemical and electrochemical polymerization techniques are mainly used to synthesize conducting polymers. The most immediate feature of electropolymerization is its rapidity. Although the several hours and tedious work-up is required by chemical methods, the growth of a polymer film requires only a few seconds via electrochemical methods, Another advantage of using electrochemical polymerization method is that the synthesized polymer is directly obtained in its oxidized form. In contrast, polymer generated chemically is in its neutral (insulating) form and can be chemically or electrochemically doped to their conducting form.

1.5.1. Chemical Polymerization

Two common chemical methods are used in the polymerization of thiophene based monomers: (1) oxidation of monomers in the presence of excess ferric chloride or other transition metal, (2) metal catalyzed coupling reaction [31].

In 1980, Yamamoto et al. described the Ni-catalyzed polycondesation of 2,5-dibromothiophene to unsubstituted PTh (Figure 1.7a). 2,5-dibromothiophene reacted with magnesium metal in tetrahydrofuran to yield 2-magnesiobromo-5-bromo-thiophene. The Ni-catalyzed reaction of 2,5-dibromothiophene with thienyl Grignard reagent afforded PTh [32]. The same year, Lin and Dudek described another example of the transition metal catalyzed route using transition metal acetylacetonates as catalysts [33].

The $FeCl_3$ mediated polymerization of thiophene in chloroform is the most widely used oxidative route to 3- or 3,4-substituted PThs [32]. High molecular weight polymers with polydispersities ranging from 1.3 to 5 have been produced using $FeCl_3$ as an oxidant.

Unsubstituted PTh is an insoluble and infusible material. Therefore it is difficult to process unsubstituted PTh as a material for electronic applications. Introduction of side chains at position 3 or at both positions 3 and 4 enhances the solubility. However, polymerization of 3-substituted thiophenes can lead to three different types of coupling of thiophene ring along the polymer main chain. These couplings are namely head to tail (HT), head to head (HH) and tail to tail (TT). The presence of head to head coupling leads to obtain irregular polythiophenes. This irregular polymer chain causes a steric repulsion between the side groups and increases twist of the thiophene units with a loss in conjugation. This resulted in increased band gap (blue shift in absorption) and decreased conductivity [32].

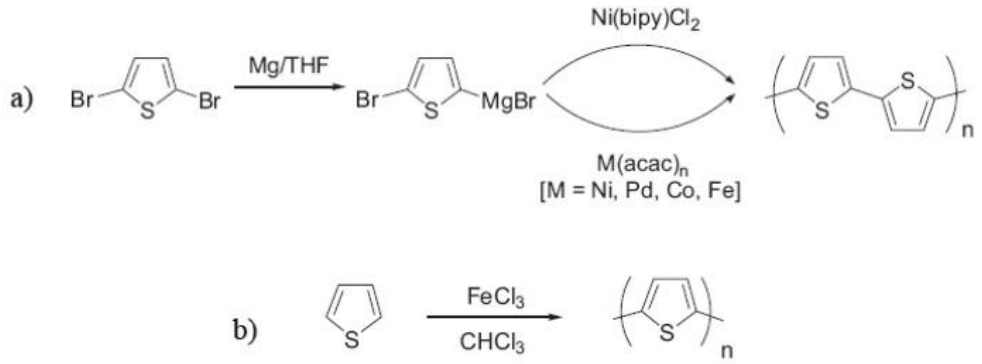

Figure 1.7. Synthesis of polythiophene via a) metal catalyzed coupling and b) chemical oxidation

Several approaches have been developed to synthesize less sterically hindered, regioregular HT polythiophenes. The McCullough method was the first synthetic approach for the regioselective polymerization that was achieved by selective metalation at 5-position of 3-alkylthiophene derivatives (Figure 1.8) [34].

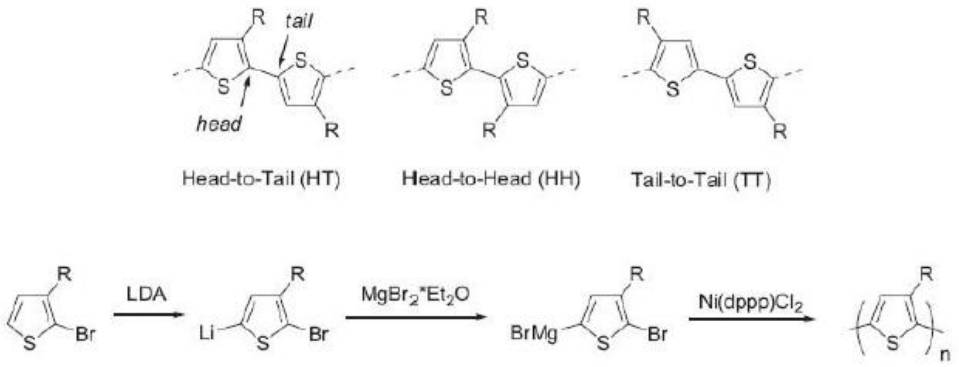

Figure 1.8. McCullough method for the synthesis of regioregular poly(alkylthiophenes) [34]

1.5.2. Electrochemical Polymerization

In electrochemical polymerization, an inert electrode, such as gold, platinum or ITO coated glass slide is polarized positively in an electrolytic solution containing the monomer. An applied potential induces oxidation of monomers to polymers.

The electrochemical polymerization method is fast, simple and requires only small amount of monomer to yield both electrode-supported and free standing films. Electrochemical polymerization basically involves electrogenerated radical cations as the reactive species. Polymer formation proceeds then through a series of radical coupling reactions and electrochemical reoxidation according to general $E(CE)_n$ mechanism [35]. Figure 1.9 showed the proposed mechanism for the electropolymerization of heterocyclics by anodic coupling. The first electrochemical step (E) consists of the oxidation of the monomer to its resonance stabilized radical-cation. Since the electron-transfer reaction is much faster than the diffusion of the monomer from the bulk solution, it follows that a high concentration of radicals is continuously maintained near the electrode surface. The second step involves the coupling reactions.

The coupling proceeds either by the combination of two radical cation to form a dication or the radical cation couple with a molecule to form a radical cation dimer which loses another electron to form dication. The resulting dicationic dimer rapidly loses two protons to produce a neutral dimer. The rearomatization is the driving force for this chemical step (C). Due to the applied potential, the dimer, which is more easily oxidized than the monomer occurs in its radical form and undergoes a further coupling with a monomeric radical. Subsequent electrochemical and chemical reactions follow the general E(CE) pathway, leading to the formation of a long polymer chain.

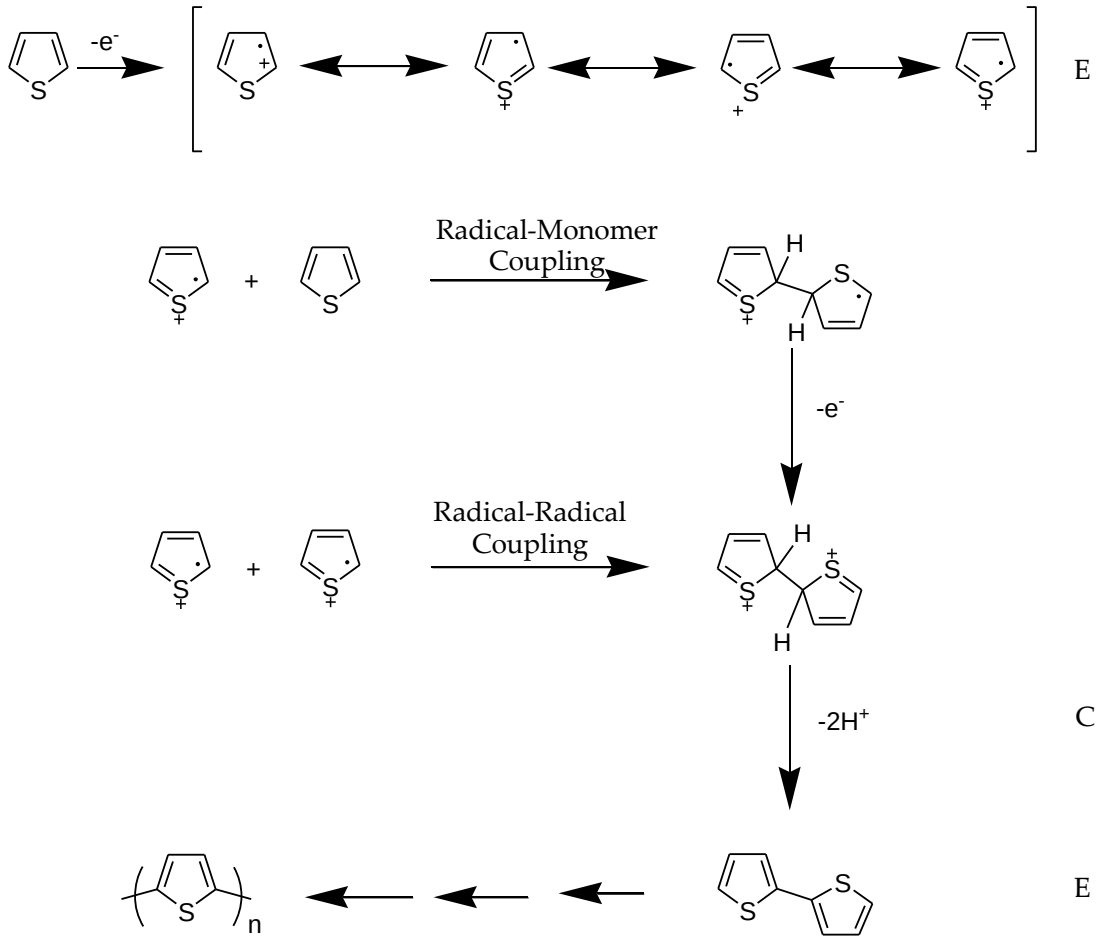

Figure 1.9. Mechanism of oxidative polymerization of thiophene

1.6. Band Gap

Π-Conjugated polymers offer a broad range of attractive features for use in a variety of device architectures, such as a strong overlap with the solar spectrum (PVDs), ease of oxidation and reduction (ECDs) as well as the potential for high electron and hole mobility (PVDs, TFTs and LEDs), and a potentially transparent oxidized state (ECDs). The electronic and optoelectronic properties of the π-conjugated system depend on band gap. Therefore various strategies have been developed to control the magnitude of band gap. Although introduction of a flexible long chain into monomer backbone increases the solubility of polymers, a decrease in the band gap can be achieved using different synthetic approaches. These approaches have been developed to control the factors that affect band gap.

1.6.1. Factors effecting band gap

The various structural variables should be taken in consideration in order to control the band gap of conducting polymers. Factors that affect the band gap in conducting polymers are bond length alternation ($E^{\Delta r}$), the mean deviation from planarity (E^{Θ}), the aromatic resonance energy (E^{res}), the inductive and mesomeric electronic effects of substituents (E^{sub}) and the interchain interactions (E^{Int}) [36].

$$Eg = E^{\Delta r} + E^{\Theta} + E^{res} + E^{sub} + E^{Int}$$

These factors affect the band gap in conducting polymers has been reviewed in Figure 1.10.

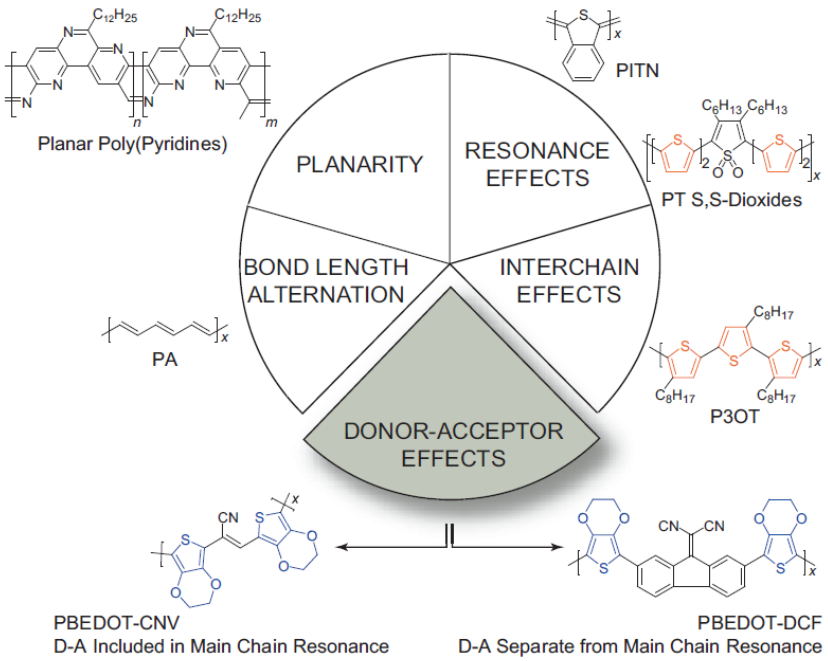

Figure 1.10. Overview of methods for the modification of band gap [37]

Bond length alternation is defined as the difference between single and double bond lengths for polyacetylene. However this definition cannot be used for polyaromatics such as PTh that differ from polyacetylene by their non-degenerate ground state. The two limiting mesomeric forms aromatic and quinoid are no energetically equivalent [38]. For polyaromatics, Bredas et al. stated that bond length alternation is the maximum difference between the lengths of C-C bond inclined relative to the chain axis and C-C bond parallel to the chain axis [39]. The band gap decreases as the contribution of the aromatic geometry decreases or quinoid geometry increases.

Figure 1.11. The nondegenerate ground state resonance of polythiophene

The existence of single bonds between the aromatic cycles causes interannular rotations in conjugated polymer (Figure 1.12). The rotational distortion around the single bonds leads to reduction in the effective conjugation along the polymer backbone with the decline in the extent of overlap. Therefore any deviation from coplanarity will result in an increase of Eg [40].

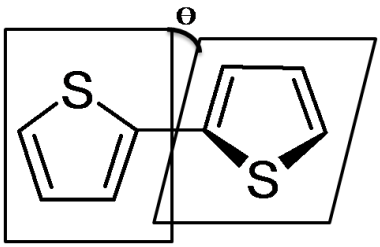

Figure 1.12. Interannular rotation in conjugated polymer

The band gap of conjugated polymer generally decreases with decrease in the resonance energy per electron. This aromatic results in a competition between π-electron confinement within the rings and delocalization along the chain.

The character and position of substituent on the polymer backbone has a great effect on the magnitude of band gap. Electron donating groups increase the energy of HOMO and electron withdrawing group lower the energy of LUMO. The introduction of electron-donating substituent onto the polymer backbone leads to decrease the band gap by raising the energy of the valence band ("HOMO" of the conjugated chain). Interaction between individual molecules affects their orientation and organization in the solid state. The intermolecular or interchain coupling leads to decrease Eg.

1.6.2. Band gap control in π-conjugated polymers

The optical and electrochemical properties of the conducting polymers are based on the magnitude of band gap. Finding an effective synthetic methodology to adjust the energy levels of the HOMO and LUMO is one of the challenges for synthetic chemists. Two different strategies can be used to design and synthesize polymers with Eg less than 2 eV. The first approach based on increasing the stability of quinoid form of a conjugated polymer with reducing bond length alternation. The second approach is based on building a polymer chain with alternating electron rich (donor) and electron deficient (acceptor) units [40].

1.6.2.1. Low band gap conducting polymers with increased quinoid character

The first truly low band gap polymer, namely, polyisothianaphthene (PITN) was reported by Wudl and Heeger [41]. The fusion of the benzene and thiophene rings across the 3 and 4 positions of the thiophene ring leads to a 10 electron system. This arrangement induces a competition for aromaticity in the monomer since only one of the two rings can be aromatic [42].

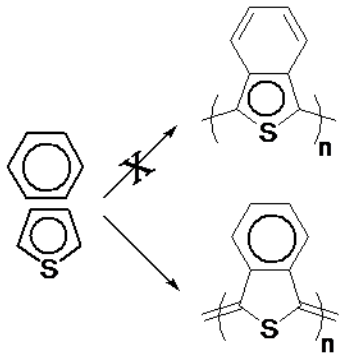

Figure 1.13. Mesomeric forms of polyisothianaphthene

The two limiting mesomeric forms, aromatic and quinoid structures are not energetically equivalent. The aromatic resonance energy of benzene (1.56 eV) is higher than that of thiophene (1.26 eV). Quinoid geometry is imposed on the

polythiophene backbone since benzene has a greater tendency to remain aromatic. The quinoid state of PITN lowers the band gap of the system by decreasing bond length alternation. The synthesis of polythiophene based polymer, PITN with a band gap of 1.1 eV proved that increasing quinoid character of polyaromatic lowers the band gap [37]. The fused benzene ring also increases the effective conjugation of the polymer. The increased quinoid character in the electronic structure of the polymer and the enlarged effective conjugation decrease the band gap of PITN [41].

Several modification of the structure of isothianaphthene was performed in order to achieve further reduction of the band gap and improve the solubility of the polymers. Introduction of the electron donating methylenedioxy unit on the phenyl ring decreases the oxidation potential from 1.4 V vs Ag/Ag^+ for ITN to 0.65 V [43]. Halogen substitution on the phenyl ring leads to positive shift of the onset potential of p-doping [44].

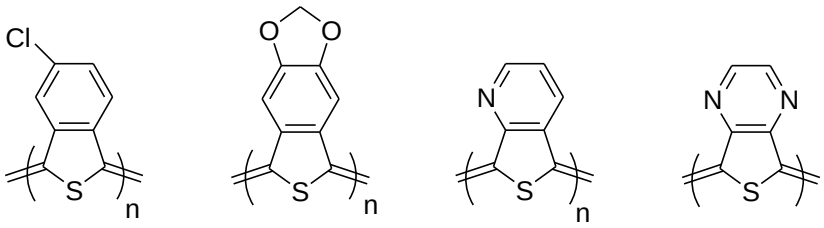

Figure 1.14. Overview of some synthesized PITN derivatives

Introduction of a pyridine and pyrazine ring onto the polythiophene backbone increases the quinoid character in the electronic structure of the polymer and also the effective conjugation along the polymer. Insertion of nitrogen atom into the six-membered ring of ITN stabilizes the aromatic contribution to the ground state geometry of PITN since the aromatic resonance energy of pyridine (0.3483) and pyrazine (0.2930) is lower than that of benzene (0.3920).

1.6.2.2. Low band gap conducting polymers with alternating donor-acceptor moieties along the chain

The introduction of adequate quinoid structures into the aromatic-type backbone can decrease the bond length alternation and may reduce the band gap accordingly. Hence, polyisonaphthothiophene was synthesized; it showed lower band gap than thiophene. Kertesz suggested that copolymer of thiophene and isonaphthothiophene would realize a small band gap of 0.54 eV [45]. This approach leads us to combine monomer units with different electronic properties and incorporate fused rings into conjugated systems. A combination of electron rich (donor) and electron deficient (acceptor) moieties into the polymer chain is the most successful approach to synthesize low band gap polymers. Alternation on the polymer backbone cause intramolecular charge transfer (ICT) from the donor to the acceptor, an absorption band at lower energy is generated. The strength of intramolecular charge transfer can be tuned through a careful design and selection of the donor and acceptor moieties. The logic behind the donor-acceptor-donor (D-A-D) approach is that the high HOMO of the donor and the low level of the LUMO are incorporated into the resulting monomer and thus polymer electronic structure increases double bond character leads to broadening of valence and conduction bands and induces small band gap. Thus, the new donor-acceptor material has a reduced bandgap (Eg) relative to either of its parent components (Figure 1.15) [37].

Electron donor segments in the conjugated polymers are generally constituted by electron rich heteroaromatic rings such as thiophene or pyrrole units. The use of fused aromatics as an acceptor unit, containing benzene-fused heteroaromatic rings with nitrogen atom(s) is one of the effective ways to design these systems. The structure of D-A-D interaction in the polymer backbone resulted in much more red-shifted absorption spectra and low band gaps of ~1.0 eV have been obtained.

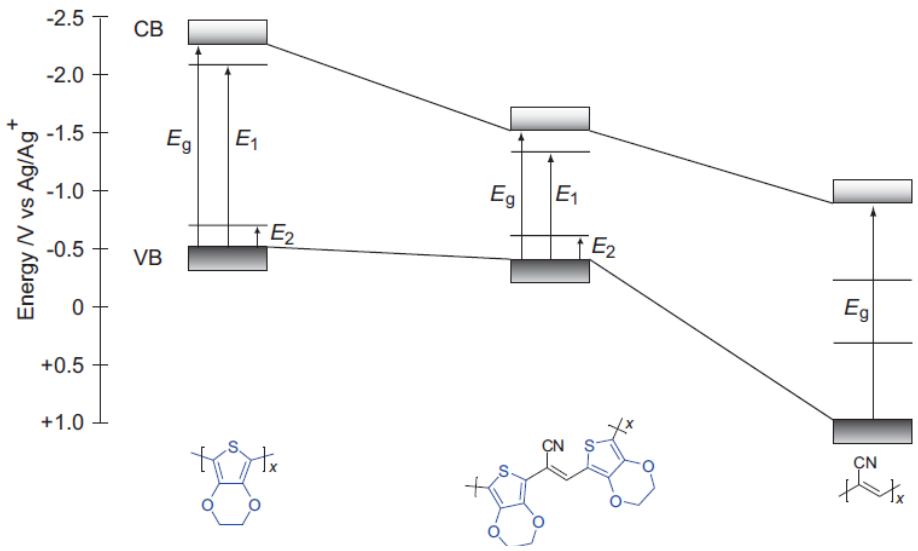

Figure 1.15. The donor-acceptor approach, alternating donor and acceptor moieties results in a polymer that has the combined optical properties of the parent donor or acceptor monomers [37].

1.6.3. Structural Design and Synthetic Methodology for Low Band Gap Materials

Π- Conjugated monomers with a well-defined chemical structure have been examined to analyze the relationships between structure and electronic/optoelectronic properties of the resulting polymers. Systematic analyses of the results led to design and synthesize new precursor structures with specific properties. Thiophene based π-conjugated polymers have been receiving a great deal of interest due to their suitable electronic properties associated with environmental stability and their synthetic flexibility in modifying the monomer structure. The delocalized electronic structures of π-conjugated polymers which are responsible for their unusual electronic properties tend to yield relatively stiff chains with little flexibility and with relatively strong interchain interaction which make them insoluble. The inherent insolubility of the conducting polymer that limits the characterization and processing is avoided by introducing the flexible side chain.

Functionalized thiophene polymers were synthesized by attaching alkyl groups to the 3- and/or 4-positions of the thiophene ring. The evolution of the electrochemical and optoelectronic properties of polythiophene and its derivative as a function of chain length was analyzed. While introduction of relatively long alkyl chains to thiophene has increased the solubility of the resulting polymers, it causes a slight change in the optoelectronic properties of the polymer [47]. The substituent also contributes to decrease the oxidation potential of the monomer since their electron donating nature stabilizes the radical cation formed upon oxidation. Oxidation potential of thiophene is higher than that of alkyl substituted derivatives.

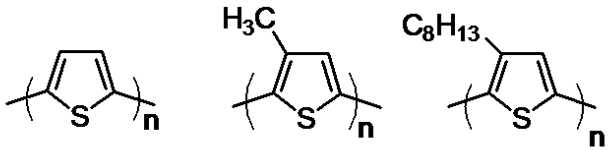

	I	II	III
λmax	480 nm	500 nm	440 nm
Eg	2.0 eV	1.97 eV	2.10eV

The electronic band gap of polymer, defined as the onset of the π-π* transition, was 2.0 eV for the unsubstituted polythiophene (**I**). While poly(3-methylthiophene) (**II**) showed a band gap 1.97 eV, poly(3-hexylthiophene) showed a slightly higher band gap of 2.10 eV. The repulsive interaction between the flexible chains reduces the extent of conjugation which increases the band gap. Basically, attaching substituent group to the 3- position of thiophene has a positive effect on polymer properties since the occurrence of α-β coupling during the polymerization decreases.

3,4-disubstituted thiophenes were synthesized to increase selectivity and the reactivity of the monomers. However, substitution in both 3- and 4- positions would reduce the mean conjugation length due to the steric interaction between substituents

on adjacent monomer units. The uses of alkoxy groups (**I**) as a substituent instead of alkyl group not only reduces the bandgap of the polymer but also do not cause a steric twist of the polymer. Ethylenedioxy thiophene (x=2, **II**) which incorporates as a cyclic substituent in the 3 and 4 positions of thiophene, eliminates the steric problems typically found with 3,4 disubstitution. The band gap is lowered by ca. 0.4 eV to 1.6 eV when compared to polythiophene. Polythiophene itself is red in the neutral state and blue in the oxidized state. Combining a narrow optical band gap an especially low oxidation potential when compared to its unsubstituted PTh parent, neutral deep blue PEDOT shows relatively stable and highly transmissive sky blue oxidized state.

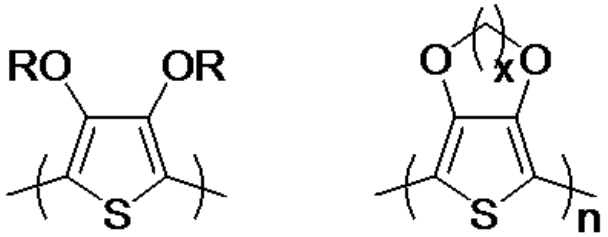

I **II**

Increasing the conjugation length of the monomer raises the energy of the HOMO and stabilizes the radical cations forms upon oxidation resulting in a decrease in oxidation potential. The simplest example of this mehod is shown in the synthesis of polythiophene from bithiophene (**I**). Oxidation potential of the polymer is lowered by 0.4 V vs Ag/Ag^{+} when compares to polythiophene to polybithiophene, thus indicating a higher mean conjugation length in polybithiophene. Polymers based on EDOT also have been synthesized from extended conjugation monomers. While EDOT polymerizes at 1.1 V vs Ag/Ag+, the dimer 2,2'-bis(EDOT) (**II**) polymerizes at 0.51 V [48].

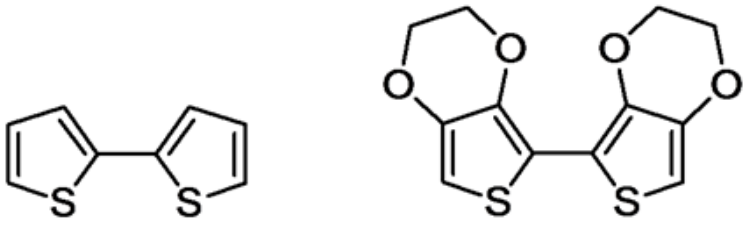

I **II**

Insertion of vinylene unit between two thiophene rings constitutes a monomer with an extended π-conjugation [49]. Electrochemical polymerization of dithienylethylene (**I**) produced the polymer with a band gap of 1.80 eV. Replacing thiophene by 3,4-ethylenedioxy thiophene (**II**) leads to conducting polymers showing an optical band gap of 1.48 eV. The presence of electron rich EDOT units lowers the band gap by raising the valence band. The band gap of poly(**III**) which consists in rigidification of the precursor by covalent bridging of the thiophene rings with the central double bond (**III**) is lower than that of the unsubstituted thiophene and EDOT derivatives. This steady decrease of band gap from thiophene (2.0 eV) to poly(**III**) (1.40 eV) suggests that the grafting of alkyl chains on the rigid backbone limit the rotational disorder associated with the interannular rotations around single bonds in polythiophene.

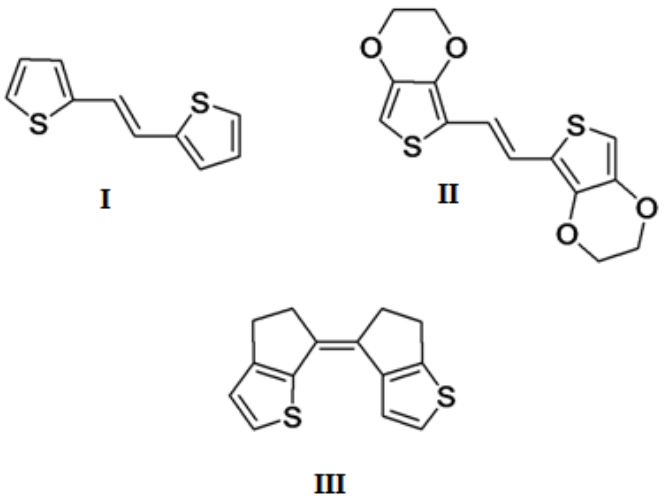

I **II**

III

Extended conjugation monomers that use a combination of heterocycles, substituted fused aromatics/heteroaromatics have been synthesized to produce polymers with a wide variety of optical and electrical properties. Research over the last decade aimed almost exclusively to manipulate band gap via synthesizing polymers having alternating donor and acceptor moieties. By controlling both the electron donating and electron accepting abilities of the monomer, it is expected that the corresponding polymers will have easily accessible oxidation and reduction potentials and lowered band gaps. The use of fused aromatics as an acceptor unit, containing benzene-fused heteroaromatic rings with nitrogen atom(s) is one of the effective ways to design these systems. Many electron-accepting moieties, including quinoxaline and 2,1,3-benzothiadiazole, thienopyrazine have been used in π-conjugated D-A-D type polymers. Thiophene, 3,4- ethylenedioxythiophene (EDOT) and their derivatives have mostly been used as the electron-donating moieties in constructing D-A-D architecture.

1.7. Chromism

Chromism is a reversible color change or variation in light transmission as a result of a chemical or physical external stimulus. The stimulus that causes changes can be any external force such as light, heat, or electrical current. Chromic materials include inorganic compounds, organic small molecules and conducting polymers and the property can result from many different mechanisms. There are also several types of chromism, like thermochromism, photochromism, halochromism, solvatochromism, piezochromism and electrochromism [50]. With the exception of electrochromism, the other major types of chromism in conjugated polymers can be defined as conformation-induced chromism.

Thermochromism is the reversible color change of a substance induced by temperature change. A large variety of substances, organic, inorganic, organometallic, supramolecular and polymeric systems exhibit this phenomenon [51].

Photochromism can be defined as a reversible change of a single chemical species between two states having distinguishable absorption spectra, such a change being induced in at least one direction by the action of electromagnetic radiation [52]. Halochromism is the reversible color change due to a change in pH of a solution. Piezochromism is the reversible color change caused by mechanical grinding [53]. Solvatochromism is the reversible color changed induced by solvents. This often is deriven from changes in polarity of various solvents [54].

1.7.1. Electrochromism

Electrochromism is defined as the reversible change in transmittance and/or reflectance that is associated with an electrochemically induced oxidation–reduction reaction [55]. The switching of redox states generates different electronic absorption bands. Electrochromism not only includes changes in the visible region, but also in the ultraviolet (UV), infrared (IR), and even the microwave regions of the spectrum [56-58]. The color change is commonly between a transparent ("bleached") state where the chromophore only absorbs in the UV region and a colored state, or between two colored states. In some cases the electrochromic materials may exhibit several colors and may be termed as polyelectrochromic [59]. By virtue of their numerous applications, electrochromic materials are currently attracting a great deal of interest. Commercial applications of these materials include anti-glare rear-view mirrors, electrochromic strips as battery state of charge indicators and electrochromic sunglasses [60]. Moreover electrochromic materials have been demonstrated as potential candidates for smart optical attenuation systems which could be useful in architectural windows for conservation of energy.

The important characteristics of electrochromic materials are the switching times, the contrast ratios, coloration efficiency, electrochromic memory and long term stability. The contrast ratio is defined as the difference in transmittance in the visible spectrum between the two different colored states. The electrochromic memory is the ability of the material to remember its color without applied current.

The long term stability is the ability of the material to retain its electrochromic properties over a large number of switching cycles. Electrochromic materials have been known since 1969 [50]. Starting from the first discovery in inorganic materials, this phenomenon has been investigated by many scientists. Basically three classes of electrochromic materials are known; metal oxide films, molecular dyes and conducting polymers. Among electrochromic materials, oxides of many transition metal, especially the high band gap semiconductor tungsten trioxide (WO_3) have been studied most widely. Electrochromism in WO_3 is introduced by reference to the simple reaction in equation:

$$WO_3 + xM^+ + xe^- \rightarrow M_xWO_3$$

(transparent) (blue)

where $M^+ = H^+$, Li^+, Na^+ or K.

Tungsten trioxide which is a transparent thin film, has all tungsten sites in oxidation state W^{VI}. Upon electrochemical reduction, W^V sites are generated to give the electrochromic effect. The coloration mechanism is generally accepted that the injection and extraction of electrons and metal cations (Li^+, H^+, etc.) give the electrochromic effect [61].

Another type of material that shows electrochromism are organic small molecules that are produced by diquaternization of 4,4'-bipyridyl, 1,1'-disubstituted-4,4'-bipyridilium salts, commonly known as viologens' [62]. Figure 1.16 shows the three common redox states of viologens with the two successive electron transfer reactions. Upon one-electron reduction, a highly colored radical cation is formed. The dication is the most stable redox state and is colorless.

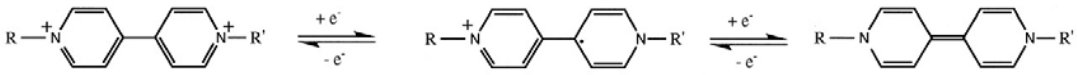

Figure 1.16. The three common redox states of viologens

The color of the violegen depends on the nitrogen substituent. Substituent allows the color choice of the radical via controlling the molecular orbital energy levels. For example, alkyl groups promote a blue/violet color whereas green color is obtained in the presence of cyano group as a substituent.

1.8. Electrochromism in Conducting Polymers

Electrochromism can be exploited in a series of optical devices with potential use in various applications, such as in information display and storage, in the automotive industry (as rear-view mirrors), and in architecture (as smart windows to control luminosity and save energy through the control of sunlight transmission [63].

Among organic molecules, conducting polymers have emerged as one of the most promising electrochromic materials as replacement for inorganic materials in electronic devices, since they offer additional advantages, such as, low processing cost, enhanced mechanical properties, no dependence with angle of vision and the flexibility in tailoring specific electronic properties through the modification of polymer's chemical structure. The π - π * transition can be adjusted across the electromagnetic spectrum from the UV, through the visible and into the near-infrared by adjusting the electronic character of the π system along the neutral polymer backbone [64].

The redox switching of conjugated polymers is accompanied by changes in electronic transitions. Figure 1.17 shows the principle of electrochromism in conjugated polymers [24]. In the neutral state the polymer exhibits single broad transition from the valence band to the conduction band (π to π*).

The energy difference between these two levels is the band gap (Eg), and it is measured as the onset of the π to π* absorption in the neutral state of the polymer. Upon oxidation, removal of an electron from the valence band, leads to the formation of polaron. This results in state with an unpaired electron whose energy state is higher than the valence band. Accordingly, there occurs the lowering of the corresponding antibonding level in the conduction band; leading to formation of new two intragap states. This should lead to possible four new transitions. However, since the oscillator strength of transitions **a** and **b** (Figure 1.17 b) are much greater than transitions **c** or **d**, two low energy transitions are expected as the signature for a polaron. Upon oxidation, the absorbance of the main inter-band peak (π to π*) decreases along with a formation a new peak at lower energy region of the spectrum. Further oxidation of the polymer will create more polarons by the removal of electrons from the valence band. The unpaired electron of the polaron will be removed to form a dication. Thus, bipolaron will be formed (Figure 1.17 c). Since the bipolaron levels are unoccupied, only transitions from valence band are possible.

The signature of a bipolaron is one broad low energy transition. This is because of the stronger nature of the transition **e** with respect to transition **f**. Yet, basically conducting polymers change color by the creation and destruction of polarons and bipolarons.

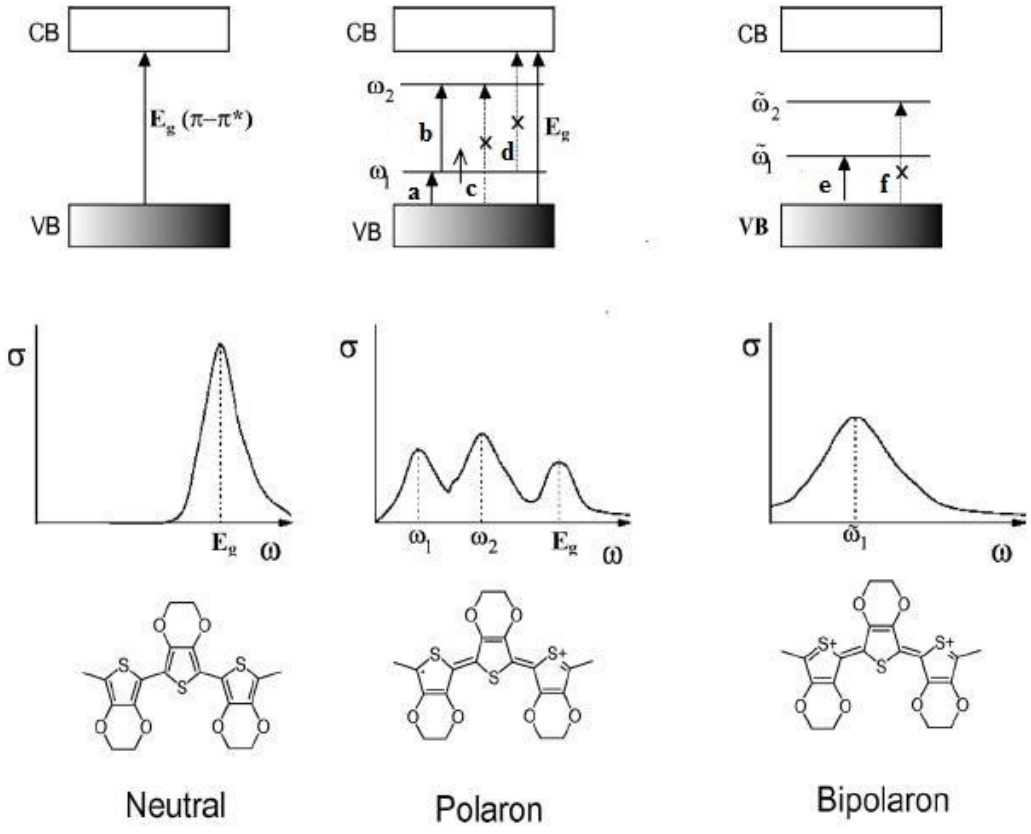

Figure 1.17. Polaron and bipolaron in non-degenerate ground state polymers: band diagrams for (a) neutral, (b) polaron, (c) bipolaron [24]

All conducting polymers are potentially electrochromic, redox switching giving rise to new optical absorption bands in accompaniment with simultaneous transport of counter ions in and out of the polymer matrix. The optical absorption band is shifted towards the lower energy part of the spectrum by oxidative p-doping process. The color change or contrast between oxidized (doped) and neutral (undoped) forms of the polymer vary significantly with the bandgap.

Thin films of conducting polymers with Eg greater than 3 eV (~400 nm) are colorless and transparent in the neutral form, while in the doped form they are generally absorbing in the visible region. Those with Eg equal to or less than 1.5 eV (~800 nm) are highly absorbing in the neutral form but, after doping, the free carrier

absorption is relatively weak in the visible region as it is transferred to the near infrared. Polymers with intermediate gaps have distinct optical changes throughout the visible region and can be made to induce many color changes.

Among the conducting polymers, polythiophenes is the one of the first to be investigated both in terms of electropolymerization mechanism and optical properties. Polythiophene is blue (~730 nm) in the doped (oxidized) state and red (~470 nm) in the undoped form [65]. Poly(3,3-diethyl-3,4-dihyrdo-2H-thieno[3,4-b][1.4]dioxepine) (PProDOT-Et_2) is purple-blue in the neutral state, and upon electrochemical oxidation switches to a transmissive sky blue in the oxidized state. The neutral state of PProDOT-Et_2 has a strong π-π^* absorption in the visible region and a band gap of 1.7 eV (λ_{max}=580 nm). Upon oxidation, a new absorption band appeared in the near IR region (~900 nm) [66].

1.9. Application Areas of Conducting Polymers

The ability to tailor both the electronic and optoelectronic properties of conducting polymers makes these compounds excellent materials for a large extent of applications. The majority of applications take advantage of properties of these materials resulting from electroactivity. Combining the electrical properties of semiconductors with the properties of polymer, that is, low cost, chemical and thermal stability, versatility of chemical synthesis, ease of processing, and flexibility have emerged as the materials to replace metals and semiconductors in the electronic and optoelectronic industry.

Π-Conjugated polymers with low band gap, broad absorption spectra and ambipolar charge transporting (p- and n-doping) ability are used for light emitting diodes and photovoltaic applications [67-69]. Due to their high optical contrast, fast switching time, p- and n-doping ability, π-conjugated polymers have been used as active layers in electrochromic devices [70-73].

1.9.1. Absorption/Transmission ECDs

An electrochromic device that allows electrochemically driven modulations of light transmission and reflections, save energy by reducing heat loss and avoiding overheating of buildings, and also providing comfortable levels of daytime light. Such electrochromic device is usually called as “smart window”.

Studies in electrochromic devices started with inorganic compounds such as tungsten trioxide (WO_3) and iridium dioxide (IrO_3). In the recent years, conducting polymers have received much attention for electrochromic applications since conducting polymers are potentially electrochromic materials and are more processable than inorganic electrochromic materials. Other advantages of using conducting polymers over inorganic compounds; outstanding coloration efficiency, fast switching ability, multiple colors with the same material and fine tuning of the band gap through chemical structure modification.

The most appropriate design for electrochromic windows for practical applications is similar to that found in a rechargeable battery, comprising five active layers (Figure 1.18). The working electrode (electrochromic electrode) is separated by a suitable solid or liquid electrolyte from a charge balancing counter electrode and the color changes occur by charging and discharging the electrochemical cell with applied potential of a few volts. Upon application of a voltage, simultaneously intercalation of ions into the electrochromic film occurs, inducing the color change. After the resulting pulse of current has decayed and the color change has been affected, the new redox state persists. Electrochromic device keeps its color under open circuit condition so it is called as “smart window”.

The electrochromic electrode of these devices, which can work either in the reflective or transmissive mode, is constituted by a conductive, transparent glass coated with electrochromic material. The counter electrode can be of any material (such as gold) that provides a reversible electrochemical reaction in device operating

in the reflective mode (like electrochromic displays); by contrast, the electrode material must be transmissive to the wavelength range of interest in absorption/transmission ECDs.

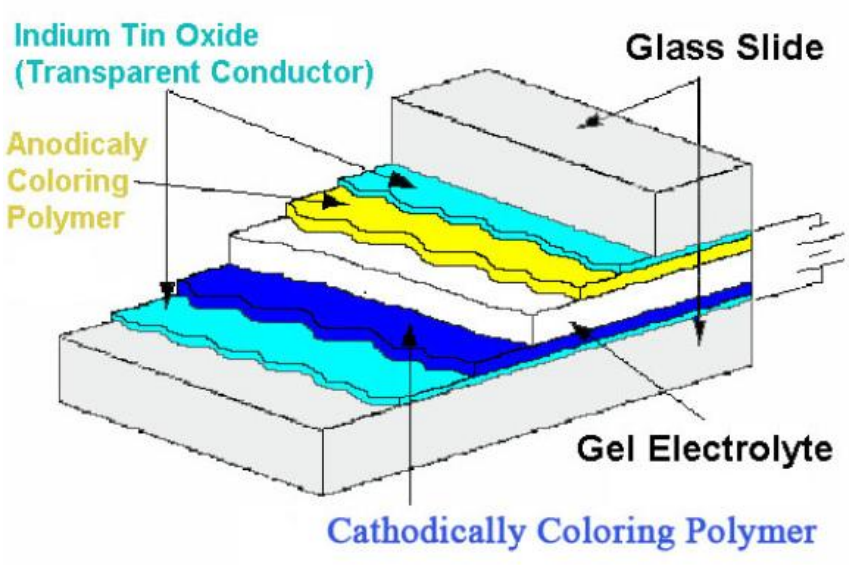

Figure 1.18. Schematic illustration of dual type absorptive/transmissive type ECD configuration [74]

An absorption/transmission ECD switches reversibly between a state of high optical density (colored) and a more transmissive state (ideally transparent) on application of electrical bias. To take the advantage of the full contrast in an EC cell, the color changing materials are sandwiched between two transparent substrates.

1.9.2. Light Emitting Diodes

Although efficient light generation is achieved in inorganic semiconductors with direct band gaps, the discovery of electroluminescence (EL) in a thin poly(p-phenylenevinylene) (PPV) have aroused much interest towards polymeric light emitting diodes (PLEDs) in 1990 [75]. The main advantages of PLEDs over conventional luminescent materials are the tuning of wavelength emitted by

chemical modification, low operating voltage, flexibility, easy processing, low cost, possibility of making large area device and output colors in whole visible spectrum.

The basic structure of PLED consists of a positive hole-injecting electrode with a high work function such as ITO or conducting polymer, a negative electron-injecting electrode with a low work function such as Al, In, Mg or Ca. The undoped form of the polymer with the mobile charge carriers (electrons and holes) supported by the delocalized π-bonding along the polymer chain is sandwiched between these two electrodes [76]. The electrons are injected from the cathode into the π* band of the semiconducting polymer and holes are injected into the π band from the anode. Driven by the applied electric field, the oppositely charged carriers move through the polymer film over a certain distance and couple to form neutral bound excited states (excitons), which then decay with photon emission (Figure 1.19).

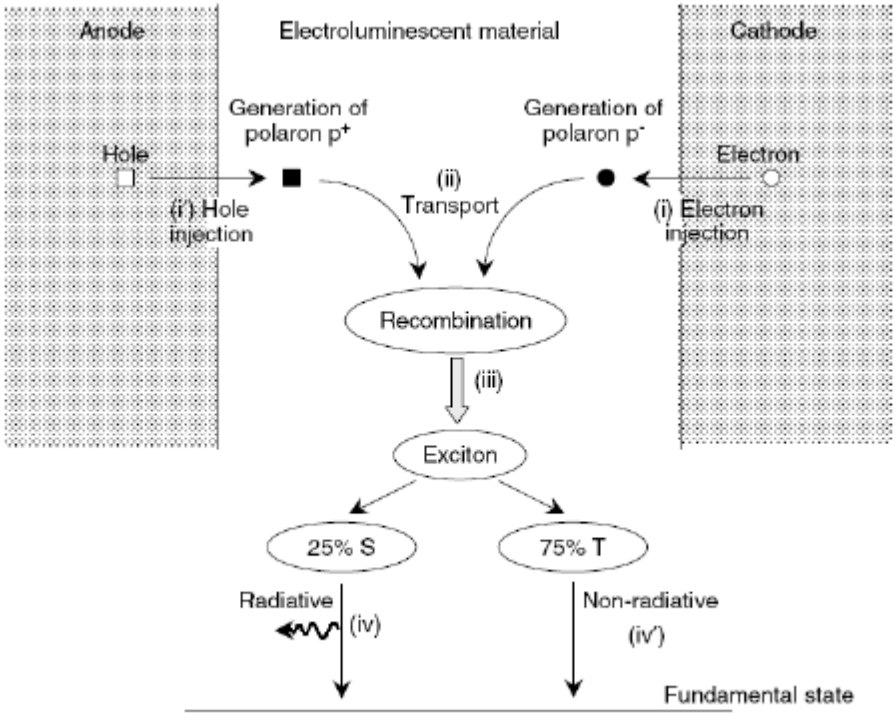

Figure 1.19. Schematic representation of polymer light emitting diode [76]

1.9.3. Solar Cell

Photovoltaic device (PVD or solar cell) offers great technological potential as a renewable, alternative source for electrical energy. The demand for inexpensive renewable energy source is the driving force for new approaches in the production of low cost polymer photovoltaic devices. A photovoltaic device provides a source of electrical current under the influence of light or similar radiation. In essence, a photovoltaic device (PVD or solar cell) converts sunlight into electrical power [77].

In π-conjugated polymers, photon absorption results in the generation of an exciton which is an excited state. This quasi-particle diffuses inside the material as long as recombination processes (of the electron–hole pair which make up the exciton) do not take place. If the diffusion length is sufficiently long so that the exciton meets an internal field (for example, located at an acceptor–donor interface), hole and electron separation occurs and these charges are collected at their respective electrodes.

A great effort has been devoted for developing materials and morphological structures in order to facilitate efficient harvesting of the solar spectrum and improve charge photogeneration, and indeed encouraging progress of power-conversion efficiencies of above 5% [78]. To increase cell efficiencies, it will be necessary to develop new semiconducting polymers exhibiting high absorption coefficients and broader solar absorptions. Extending the energy bandgap (Eg) to 1000 nm will allow 53% of the available photons to be absorbed, providing a considerable gain in photocurrent. From this point of view, there is interest in developing low bandgap conjugated polymers for light harvesting up to longer wavelengths. Nevertheless, an increase in power conversion efficiency (PCE) does not solely rely upon an improved current density; a high open circuit voltage (Voc) and a reasonable fill factor (FF) are also required. The inefficient performance of low band polymers is often associated with their lower hole mobility, unwanted highest occupied molecular orbital (HOMO)/lowest unoccupied molecular orbital (LUMO) energy levels, or poor solubility.

CHAPTER 2

EXPERIMENTAL

2.1. Materials and Methods

The molecular structure of compounds was characterized using Nuclear Magnetic Resonance Spectrometer (NMR). ^{1}H-NMR and ^{13}C-NMR spectra of the compounds were recorded on a Bruker Spectrospin Avance DPX-400 Spectrometer at 400 MHz and 100 MHz, respectively. Chemical shifts (δ) were reported in ppm relative to tetramethylsilane as the internal standard. Deuterochloroform ($CDCl_3$) was used as the solvent.

Purification of the synthesized compounds was done by column chromatography. Merck Silica Gel (70 -230 mesh) was used as the solid absorbent packed into a glass column. TLC was used to monitor the reaction and determine the eluent for the column chromatography. Commercial aluminum sheets were precoated with silica gel 60 F 254 (Merck) to allow visualizing the spots under a UV light (l = 254 and 366 nm).

Electroactivity and redox behaviors of the π-conjugated monomers were examined potentiodynamically using a Voltalab PST050 potentiostat. Electropolymerization of the monomers was performed in a three-electrode cell consisting of ITO-coated glass slide as the working electrode, platinum wire as the counter electrode, and Ag wire as the pseudo reference electrode.

Electrochromic measurements; spectroelectrochemistry and switching studies of the polymer film deposited on ITO-coated glass slide were carried out in an appropriate solvent/supporting electrolyte system in the absence of monomer using Varian Cary 5000 spectrophotometer. Applied potential was controlled using a Solartron 1285 potentiostat/galvanostat. A Conica Minolta CS-100 spectrophotometer was used to perform colorimetry measurements.

2.2. Syntheses of π-Conjugated D-A-D Type Monomers

2.2.1. Preparation of Donor Moieties

In order to prepare the Stille reagent, tributyltin substituted thiophene, 3-hexylthiophene and EDOT were prepared in high yield by lithiation with n-butyl lithium and subsequent quenching with tributyltin chloride.

2.2.1.1. Tributyl(thiophen-2-yl)stannane (1)

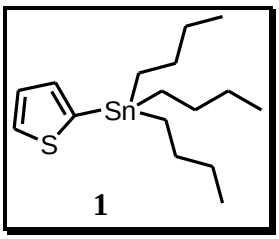

1

A solution of thiophene (1g, 0.95 mL) in 30 mL of anhydrous THF under argon was cooled to -30°C in a dry ice/o-xylene cooling bath. To the stirred precooled solution, 5.76 mL of 2.5 M n-butyllithium were added dropwise and the mixture was stirred at this temperature under argon for 2 h. Then tributylstannyl chloride (3.48 mL) was added, and the mixture was stirred at -30 °C for 1.5 h. The solvent was evaporated under vacuum after stirring the mixture at room temperature for 12 h. The residue was poured into saturated aqueous sodium hydrogen carbonate and extracted with dichloromethane.

The organic phase was separated and washed with saturated aqueous brine and then dried over an anhydrous sodium sulfate. The solvent was removed at a reduced pressure. The title compound was obtained as oil which was used without any further purification for the next step.

2.2.1.2. Tributyl(4-hexylthiophen-2-yl)stannane (2)

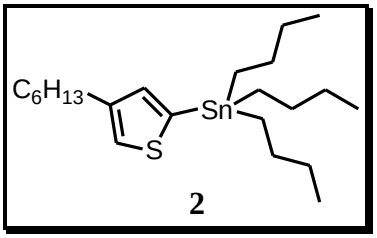

2

A solution of 3-hexylthiophene (2 g, 2.13 mL) in anhydrous THF (30 mL) under argon was cooled to -78°C in a dry ice/acetone cooling bath. To the stirred precooled solution 5.2 mL of 2.5 M n-butyllithium were added dropwise via syringe. After the solution was stirred for 1.5 h at -78 °C under argon, a 3.5 mL of tributylstannyl chloride were added slowly. After stirring at -78 °C for 4 h, the solution was warmed to room temperature and stirred overnight. The solvent was removed at a reduced pressure. The residue was poured into saturated aqueous sodium hydrogen carbonate and extracted with dichloromethane. The organic phase was separated and washed with saturated aqueous brine and then dried over an anhydrous sodium sulfate. The solvent was removed at a reduced pressure to give the product as colorless oil.

2.2.1.3. Tributyl(2,3-dihydrothieno[3,4-*b*][1,4]dioxin-7-yl)stannane (3)

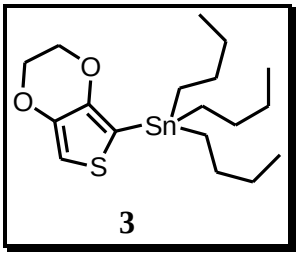

3

A 2.0 g (1.5 mL) sample of 2,3-dihydrothieno[3,4-*b*][1,4]dioxine in 150 mL of anhydrous THF was treated dropwise with 5.7 mL of 2.5 M n-butyllithium at -78 °C under argon. After the solution was stirred for 1.5 h at -78 °C, 3.97 mL of tributylstannyl chloride were added to the solution. The solution was stirred at -78 °C under argon for 4 h. Then the solution was warmed to room temperature. The solvent was removed by rotary evaporation after the solution was stirred overnight. After the removal of the solvent at a reduced pressure, the residue was poured into saturated aqueous ammonium chloride and extracted with dichloromethane. The organic phase was separated and washed with saturated aqueous brine and then dried over an anhydrous magnesium sulfate. The solvent was removed at a reduced pressure to afford tributyl(2,3-dihydrothieno[3,4-*b*][1,4]dioxin-7-yl)stannane as a yellow liquid. The compound was used for the next reactions as obtained, with no further purifications.

2.2.2. Syntheses of Quinoxaline Derivatives

2.2.2.1. 4,7-Dibromobenzo[*c*][1,2,5]thiadiazole (5)

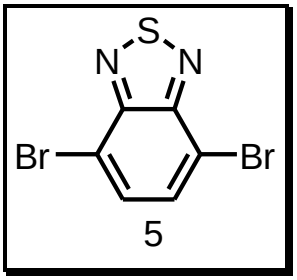

5

To a 250 ml two-necked round bottom flask benzo[*c*][1,2,5]thiadiazole (5 g, 36.7 mmol) and 75 ml of HBr (47%) were added. A solution of Br_2 (17.6 g, 110.16 mmol) in 50 ml of HBr were added dropwise with stirring at room temperature. After the addition was completed, the reaction mixture was heated at reflux with stirring for 6 h. The mixture was cooled to room temperature. Then the mixture was filtered and the orange solid residue was treated with $NaHSO_3$ to consume completely any excess Br_2. The crude was dissolved in dichloromethane and extracted with brine. The combined organic layers were dried over anhydrous sodium sulfate, filtered and concentrated under vacuum. The solid was then washed once with cold diethyl ether and dried under vacuum, affording 4,7-dibromobenzo[*c*][1,2,5]thiadiazole (5) (9.53g, 88%). ^{1}H-NMR (400MHz, $CDCl_3$): δ (ppm) 7.65 (s, 2H). ^{13}C-NMR (100 MHz, $CDCl_3$): δ(ppm) 152.75, 132.13, 113.70.

2.2.2.2. 3,6-Dibromobenzene-1,2-diamine (6)

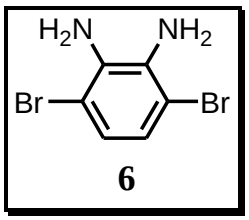

6

4,7-Dibromobenzo[*c*][1,2,5]thiadiazole (500 mg, 1.7 mmol) and EtOH (30 mL) were added to a 100 mL two-necked round bottom flask. The mixture was cooled to 0^{o}C in an ice bath and $NaBH_4$ powder (2.57 g, 68.0 mmol) was slowly added. When gas evolution stopped, the reaction was warmed to room temperature and stirred for 20 h. After evaporation of the solvent, 50 mL of water was added, and the mixture was extracted with diethyl ether. The combined organic layers was washed with brine and dried over anhydrous sodium sulfate. Evaporation of the solvent gave 3,6-dibromobenzene-1,2-diamine as a pale yellow solid (307 mg, 67%). ^{1}H-NMR (400MHz, $CDCl_3$): δ (ppm) 6.75 (s, 2H), 3.83 (s,4H). ^{13}C-NMR (100 MHz, $CDCl_3$): δ (ppm) 133.74, 123.37, 109.70.

2.2.2.3. 1-(2,3-Dihydrobenzo[b][1,4]dioxin-6-yl)-2-(2,3-dihydrobenzo[b][1,4] dioxin 7-yl) ethane-1,2-dione (8)

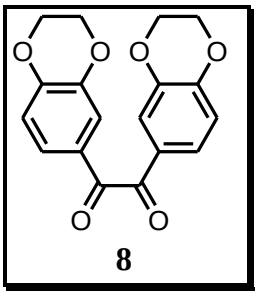

8

Benzo-1,4-dioxane was subjected to Friedel–Crafts acylation with oxalyl chloride to give 1,2-dione. To a suspension of $AlCl_3$ (0.98 g, 7.4 mmol) in dichloromethane (15 mL), a solution of benzo-1,4-dioxane (1 g, 7.4 mmol) and oxalyl chloride (0.47 g,3.7 mmol) in dichloromethane (15 mL) was added dropwise at 25^{o}C.

The violet mixture was stirred at room temperature for 4 h. The resulting mixture was then poured into 100 mL ice. The yellow organic phase was washed with saturated solution of sodium hydrogen carbonate and brine, and then dried over magnesium sulfate. After evaporation of the solvent, yellow solid was chromatographed over a bed silica using dichloromethane as the eluent. The solid recrystallized from ethanol yielded 1-(2,3-dihydrobenzo[*b*][1,4]dioxin-6-yl)-2-(2,3-dihydrobenzo[*b*][1,4]dioxin-7-yl)ethane-1,2-dione (750 mg, 62.5%). ^{1}H-NMR (400 MHz, $CDCl_3$): δ (ppm) 7.50 (s, 2H), 7.43 (d, 2H), 6.77 (d, 2H), 4.24 (s, 8H).

2.2.2.4. 5,8-Dibromo-2-(2,3-dihydrobenzo[b][1,4]dioxin-6-yl)-3-(2,3-dihydro benzo[b] [1,4]dioxin-7-yl)quinoxaline (9)

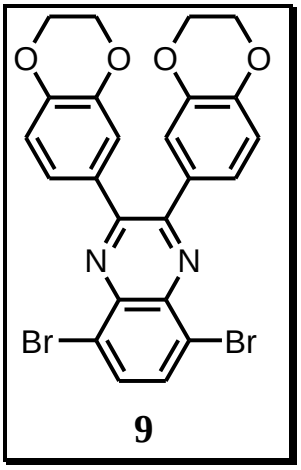

9

To a solution of 3,6-dibromobenzene-1,2-diamine (150 mg, 0.56 mmol) in 150 mL of ethanol at room temperature, 1-(2,3-dihydrobenzo[*b*][1,4]dioxin-6-yl)-2-(2,3-dihydrobenzo[*b*][1,4]dioxin-7-yl)ethane-1,2-dione (184 mg, 0.56 mmol) was added. After stirring for 4 h at 85°C with a catalytical amount of paratoluenesulfonic acid, the mixture was cooled. The precipitate was collected by filtration, washed with cold ethanol, and dried under vacuum. Yield: 125 mg, 40.2%. ^{1}H-NMR (400 MHz, $CDCl_3$): δ (ppm) 7.78 (s, 2H), 7.33 (s, 2H), 7.00 (d, 2H), 6.70 (d, 2H), 4.23 (s, 8H). ^{13}C-NMR (100 MHz, $CDCl_3$): δ (ppm) 153.15, 145.20, 143.61, 130.04, 132.67, 131.41, 123.80, 123.48, 119.19, 117.09, 64.58, 64.27.

2.2.2.5. General Procedure for the Synthesis of 14, 15, 16 via Stille coupling

2-(2,3-Dihydrobenzo[b][1,4]dioxin-6-yl)-3-(2,3-dihydrobenzo[b][1,4]dioxin-7-yl) quinoxaline substituted compunds were all synthesized by Stille coupling reactions. To a solution of 5,8-dibromo-2-(2,3-dihydrobenzo[b][1,4]dioxin-6-yl)-3-(2,3-dihydrobenzo[b][1,4]dioxin-7-yl) quinoxaline (400 mg, 0.72 mmol) in 100 mL of anhydrous THF, tributylstannane derivative (2.88 mmol) were added. After purging the solution with argon for 30 min, dichlorobis(triphenylphosphine)palladium(II) (84 mg, 0.12 mmol) was added at room temperature. The mixture was refluxed for 16 h under argon atmosphere. Solvent was evaporated under vacuum. The residue was purified by column chromatography on silica gel.

2.2.2.5.1. 2-(2,3-Dihydrobenzo[*b*][1,4]dioxin-6-yl)-3-(2,3-dihydrobenzo[*b*][1,4] dioxin-7-yl)-5,8-di(thiophen-2-yl)quinoxaline (14)

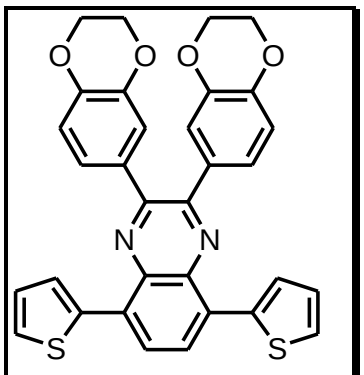

14

The crude product was purified by column chromatography over silica gel, eluting with 7:1 (chloroform/hexane) and give yellow solid (198 mg, 49%). ^{1}H-NMR (400 MHz, $CDCl_3$): δ (ppm) 8.05 (s, 2H), 7.78 (d, 2H), 7.45 (d, 2H), 7.36 (s, 2H), 7.10 (d, 4H), 6.78 (d, 2H), 4.25 (s, 8H).

2.2.2.5.2. 5,8-Bis(4-hexylthiophen-2-yl)-2-(2,3-dihydrobenzo[*b*][1,4]dioxin-6-yl)-3-(2,3-dihydrobenzo[*b*][1,4]dioxin-7-yl)quinoxaline (15)

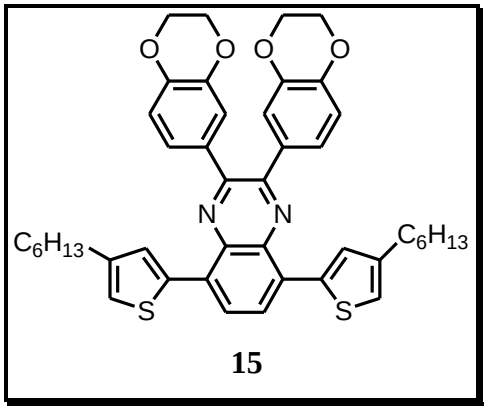

15

The crude product was purified by column chromatography over silica gel, eluting with 1:1 (chloroform/hexane) and gave orange solid (375 mg, 71%). ^{1}H-NMR (400 MHz, $CDCl_3$): δ (ppm) 7.97 (s, 2H), 7.37 (d, 2H), 7.10 (d, 4H), 7.05 (s,2H), 6.75 (d,2H), 4.20 (s, 8H), 2.60 (t, 4H), 1.65 (p, 4H), 1.37 (m, 12H), 0.81 (t, 6H). ^{13}C-NMR (100 MHz, $CDCl_3$): δ (ppm) 150.90, 144.90, 143.75, 143.06, 138.87, 137.28, 132.62, 132.51, 128.25, 126.89, 124.30, 123.94, 119.64, 117.24, 64.85, 64.56, 32.03, 31.87, 30.88, 29.39, 22.94, 14.41.

2.2.2.5.3. 2-(2,3-dihydrobenzo[*b*][1,4]dioxin-6-yl)-3-(2,3-dihydrobenzo[*b*][1,4] dioxin-7-yl)-8-(2,3-dihydrothieno[3,4-*b*][1,4]dioxin-5-yl)-5-(2,3-dihydrothieno [3,4-*b*][1,4]dioxin-7-yl)quinoxaline (16)

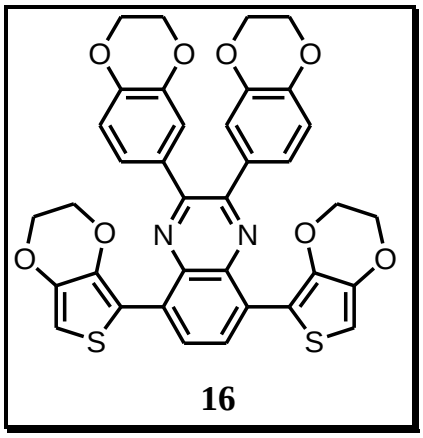

16

The crude product was purified by column chromatography over silica gel, eluting with 3:1 (dichloromethane/hexane) and gave red solid (307 mg, 62%). ^{1}H-NMR (400 MHz, $CDCl_3$): δ (ppm) 8.47 (s, 2H), 7.41 (s, 2H), 7.10 (d, 2H), 6.73 (d, 2H), 6.45 (s, 2H), 4.30 (s, 8H), 4.25 (s, 8H).

2.2.2.6. 10,13-Dibromodibenzo[*a,c*]phenazine (10)

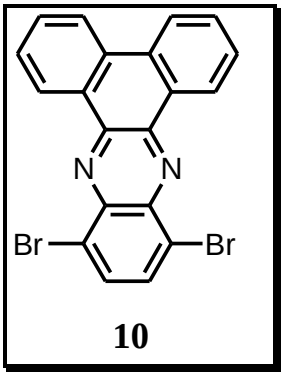

10

Condensation reaction of 3,6-dibromobenzene-1,2-diamine (150 mg, 0.56 mmol) with phenanthrene-9,10-dione (117 mg, 0.56 mmol) was performed in 30 mL ethanol with a catalytical amount of paratoluenesulfonic acid. At the end of the reaction

yellow colored cloudy mixture was observed. Filtration of the reaction mixture followed by washing with cold ethanol afforded the product as a yellow solid (198 mg, 81%). ^{1}H-NMR (400 MHz, $CDCl_3$): δ (ppm) 9.50 (d, 2 H), 8.57 (d, 2H), 8.0 (s, 2H), 7.7- 7.8 (dd, 4H).

2.2.2.7. General Procedure for the Synthesis of 17, 18 via Stille coupling

10,13-Dibromodibenzo[*a,c*]phenazine (100 mg, 0.23 mmol) and tributylstannane derivative (0.95 mmol) were dissolved in anhydrous THF (100 mL), the solution was purged with argon for 30 min and dichlorobis(triphenylphosphine)palladium(II) (40mg, 0.057mmol) was added at room temperature. The mixture was refluxed for 12 h under argon atmosphere. Solvent was evaporated under vacuum and the crude product was purified by column chromatography over silica gel.

2.2.2.7.1. Synthesis of DAD monomer based on dibenzo [a,c] phenazine and 3-hexylthiophene

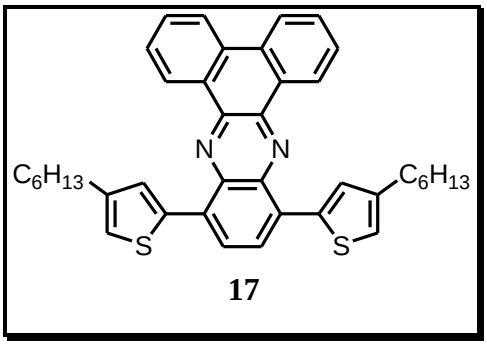

17

The crude product was purified by column chromatography over silica gel, eluting with 1:1 (dichloromethane/hexane) and gave orange solid (79 mg, 56%). ^{1}H-NMR (400 MHz, $CDCl_3$): δ (ppm) 9.60 (d, 2H), 8.50 (d, 2H), 8.13 (s, 2H), 7.65-7.8 (dd, 4H), 7.10 (s, 4H), 2.71 (t, 4H), 1.7 (p, 4H), 1.4 (m, 12H), 0.8 (t, 6H). ^{13}C-NMR (100 MHz, $CDCl_3$): δ (ppm) 141.87, 140.73, 137.76, 137.61, 131.44, 130.66, 129.63, 129.34, 127.05, 126.77, 125.95, 124.90, 122.89, 121.90, 30.79, 29.67, 29.65, 28.14, 21.66, 13.12.

2.2.2.7.2. Synthesis of DAD monomer based on dibenzo [a,c] phenazine and EDOT

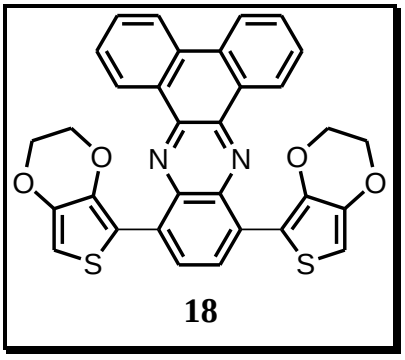

18

The crude product was purified by column chromatography over silica gel, eluting with 3:1 (dichloromethane/hexane). Chromatography followed by evaporation in vacuum and recrystallization (chloroform/hexane), afforded dark red solid (105 mg, 81.4 %). ^{1}H-NMR (400 MHz, $CDCl_3$): δ (ppm) 9.57 (d, 2H), 8.67 (s, 2H), 8.50 (d, 2H), 7.65-7.8 (dd, 4H), 6.6 (s, 2H), 4.39 (m, 4H), 4.27 (m, 4H). ^{13}C-NMR (100 MHz, $CDCl_3$): δ (ppm) 141.57, 141.23, 140.44, 138.72, 132.37, 130.73, 130.21, 128.97, 128.23, 128.08, 128.03, 122.88, 113.45, 103.01, 65.03, 64.43.

2.2.2.8. 1,10-Phenanthroline-5,6-dione (12)

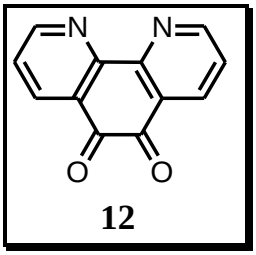

12

20 mL of cold concentrated sulfuric acid (98%) were added into a mixture of 1,10-phenanthroline (2.00 g, 0.01 mol) and potassium bromide (3.00 g, 0.025 mol) at 0^{o}C in a three-necked, round bottomed flask with reflux condenser. 10 mL of fuming nitric acid (65%) were added dropwise to the mixture by keeping the temperature under 30^{o}C. After the addition of nitric acid was completed, the mixture was heated

to 40°C for 3 h. Then temperature was increased to 80–90°C and the mixture was kept at this temperature about 1 h. To remove bromine from the reaction mixture, the reflux condenser was removed and mixture stirred at the same temperature about 3 h. The mixture was cooled and poured into a mixture of ice and water. Saturated sodium hydroxide solution was added dropwise to adjust pH at 6–7. The solution was extracted with dichloromethane. The combined organic layers were washed with brine and dried over magnesium sulfate. The drying agent was filtered off and solvent was evaporated under vacuum. Yellow needles of 1,10-phenanthroline-5,6-dione was obtained via recrystallization from methanol. Yield: 1.75 g, 83.3%. ^{1}H-NMR (400 MHz, $CDCl_3$): δ (ppm) 9.13 (d, 2H), 8.42 (dd, 2H), 7.50 (q, 2H). ^{13}C-NMR (100 MHz, $CDCl_3$): δ (ppm) 178.69, 156.40, 152.94, 137.30, 128.10, 125.60.

2.2.2.9. 3-(2,3-Dihydrothieno[3,4-b][1,4]dioxin-5-yl)-6-(2,3-dihydrothieno[3,4-b][1,4] dioxin-7-yl)benzene-1,2-diamine (20)

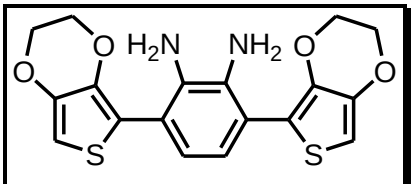

20

To a solution of 4,7-dibromobenzo[*c*][1,2,5]thiadiazole (300 mg, 1.03 mmol) and tributyl(2,3-dihydrothieno[3,4-b][1,4]dioxin-7-yl)stannane (1.77 g, 4.11 mmol) in anhydrous THF (100 mL), dichlorobis(triphenylphosphine)palladium(II) (108 mg) was added. The mixture was refluxed for 16 h. After cooling, the reaction mixture was concentrated under reduced pressure. Hexane was added to the residue. Then the resulting precipitates were filtered off and washed with hexane. Further purification was performed by column chromatography using $CHCl_3$ as the eluent. The resulting compound (250 mg, 0.60 mmol) was reduced by refluxing with zinc dust (796 mg, 12.18 mmol) in 9 mL of acetic acid for 15 min. After that the reaction mixture was filtered and the residue was washed with diethyl ether. The filtrate was washed with

5% NaOH. The combined organic layers were washed with brine and dried over magnesium sulfate. The solvent was removed under vacuum to give the title compound as oil which was used without any further purification for the next step.

2.2.2.10. Synthesis of DAD monomer based on 1,10-phenanthroline

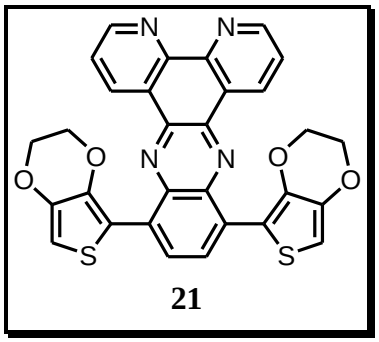

21

Condensation reaction of 1,10-phenanthroline-5,6-dione and 3-(2,3-dihydrothieno[3,4-b][1,4]dioxin-5-yl)-6-(2,3-dihydrothieno[3,4-b][1,4] dioxin-7-yl)benzene-1,2-diamine was performed in ethanol. At the end of the reaction a violet cloudy mixture was observed. Filtration of the reaction mixture was followed by washing with cold ethanol. The residue was purified by column chromatography over silica gel, eluting with 1:1 (dichloromethane/ hexane) gave violet solid. ^{1}H-NMR (400 MHz, $CDCl_3$): δ (ppm) 9.71 (dd, 2 H, J=8.1, 1.8 Hz), 9.20 (dd, 2 H, J=4.4, 1.8 Hz), 8.64 (s, 2H), 7.75 (dd, 2H, J=8.1, 4.4 Hz), 6.60 (s, 2H), 4.39 (m, 4H), 4.27 (m, 4H).

2.2.3. Thienopyrazine Derivative

2.2.3.1. 2,5-Dibromo-3,4-dinitrothiophene (23)

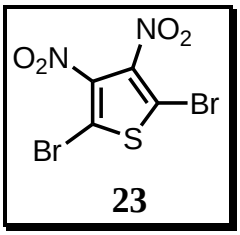

23

Concentrated sulfuric acid (18.58 mL) and fuming sulfuric acid (30% SO_3, 18.58 mL) were mixed in a flask equipped with a mechanical stirrer and cooled with an ice bath. 2,5- Dibromothiophene (10 g, 41 mmol) was then added maintaining a temperature below 20^{o}C. Nitric acid (6.5 mL) was then added dropwise, by keeping the temperature under 30^{o}C. Once the addition was complete, the mixture was allowed to react for an additional three hours and then poured on 150 g ice. Following the melting of the ice, the solid residue was recovered by vacuum filtration and washed well with water to produce a light yellow powder. Recrystallization with methanol gave pure material (11.2 g, 82%).^{13}C-NMR (100 MHz, CDCl3): δ (ppm) 139.6, 112.4.

2.2.3.2. 2,5-Bis(4-hexylthiophen-2-yl)-3,4-dinitrothiophene (24)

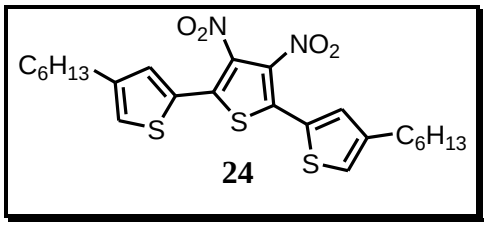

24

2,5-Dibromo-3,4-dinitrothiophene (400 mg, 1.20 mmol) and tributyl(4-hexylthiophen-2-yl)stannane (2.20 g, 4.82 mmol) were dissolved in anhydrous THF (100 ml). The solution was purged with argon for 30 min and dichlorobis(triphenyl phosphine)palladium(II) (84 mg, 0.12 mmol) was added at room temperature.

The mixture was refluxed for 16 h under argon atmosphere. Solvent was evaporated under vacuum and the crude product was purified by column chromatography over silica gel, eluting with 1:2 (dichloromethane/hexane) and give yellow needle (422mg, 69%). ^{1}H-NMR (400MHz, $CDCl_3$): δ (ppm) 7.26 (d, 2H, *J*=1.3 Hz), 7.07 (brs, 2H), 2.51 (t, 4H, *J*=7.7 Hz), 1.53 (p, 4H), 1.25 (m, 12H), 0.79 (t, 6H, *J*=6.6 Hz). ^{13}C-NMR (100 MHz, $CDCl_3$) : δ (ppm) 143.9, 134.4, 132.9, 131.2, 136.7, 125.0, 30.5, 29.3, 29.2, 27.8, 21.5, 13.0.

2.2.3.3. 2,5-Bis(4-hexylthiophen-2-yl)thiophene-3,4-diamine (25)

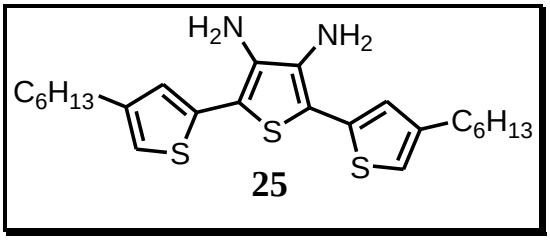

25

2,5-Bis(4-hexylthiophen-2-yl)-3,4-dinitrothiophene (200 mg, 0.39 mmol) and tin(II) chloride dihydrate (1.87 g, 9.87 mmol) were dissolved in 50 mL ethyl acetate and stirred at reflux for 2 h. The mixture was added to a solution of sodium carbonate (50 ml, 0.25 M), stirred vigorously with dichloromethane (50 ml). The resulting mixture was filtered over celite. The organic phase was washed with water and dried over magnesium sulfate. The solvent was evaporated under vacuum.Yield: 156 mg, 89%. ^{1}H-NMR (400MHz, $CDCl_3$): δ (ppm) 6.85 (s, 2H), 6.77 (s, 2H), 3.25 (brs, 4H), 2.52 (t, 4H, *J*=7.7 Hz), 1.56 (p, 4H), 1.25 (m, 12H), 0.82 (t, 6H, *J*=6.8 Hz). ^{13}C-NMR (100 MHz, $CDCl_3$): δ (ppm) 143.0, 134.4, 132.0, 124.2, 117.5, 109.8, 30.6, 29.5, 29.3, 28.0, 21.5, 13.0.

2.2.3.4. 5,7-Bis(4-hexylthiophen-2-yl)-2-(2,3-dihydrobenzo[b][1,4]dioxin-6-yl)-3-(2,3-dihydrobenzo[b][1,4]dioxin-7-yl)thieno[3,4-b]pyrazine (26)

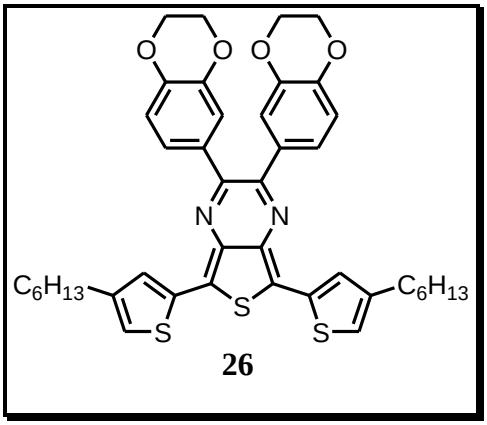

26

2,5-Bis(4-hexylthiophen-2-yl)thiophene-3,4-diamine (100 mg, 0.22 mmol) and 1-(2,3-dihydrobenzo[b][1,4]dioxin-6-yl)-2-(2,3-dihydrobenzo[b][1,4]dioxin-7-yl)etha ne -1,2-dione (50 mg, 0.22 mmol) were dissolved in 10 mL ethanol with a catalytic amount of paratoluenesulfonic acid. After the reaction was completed, the solvent was removed under vacuum. The residue was purified by column chromatography over silica gel, eluting with 3:1 (dichloromethane/hexane) and give green solid (113 mg, 69%). ^{1}H-NMR (400MHz, $CDCl_3$): δ (ppm) 7.36 (d, 2H, *J*=1.0 Hz), 7.24 (d, 2H, *J*=2.0 Hz), 6.93 (dd, 2H, *J*=8.4, 2.0 Hz), 6.89 (d, 2H, *J*=1.0 Hz), 6.71 (d, 2H, *J*=8.4 Hz), 4.23 (m,8H), 2.56 (t, 4H, *J*=7.6 Hz), 1.60 (p, 4H), 1.27 (m, 12H), 0.83 (t, 6H, *J*=6.9 Hz). ^{13}C-NMR (100 MHz, $CDCl_3$): δ (ppm) 150.89, 143.68, 142.42, 142.32, 136.27, 133.41, 131.67, 124.71, 123.44, 122.72, 120.57, 117.90, 115.73, 63.56, 63.28, 30.69, 29.41, 29.40, 27.99, 21.60, 13.08.

2.3. Electrochemical Method

Characterization of conducting polymers was performed using the electroanalytical tools such as potentiostatic (controlled potential) and galvanostatic (controlled current) methods. Electroactivity of the monomers and redox properties of the resulting polymers were examined via cyclic voltammetry and square wave potential steps (chronocoulometry).

Cyclic voltammetry is the most useful potentiostatic method since the synthesis of the desired polymer on an electrode's surface allows for rapid characterization of CPs via both electrochemical and optical studies. This section will detail fundamentals of cyclic voltammetry and opto-electrochemical techniques: spectroelectrochemistry, switching and colorimetry studies.

2.3.1. Electrochemical cells

Electrochemical polymerization was carried out in a one-compartment three electrode cell (Figure 2.1). The cell was consisted of an indium-tin oxide coated glass slide working electrode, a platinum wire as a counter electrode, and a silver wire pseudo-reference electrode in an appropriate supporting electrolyte/solvent system.

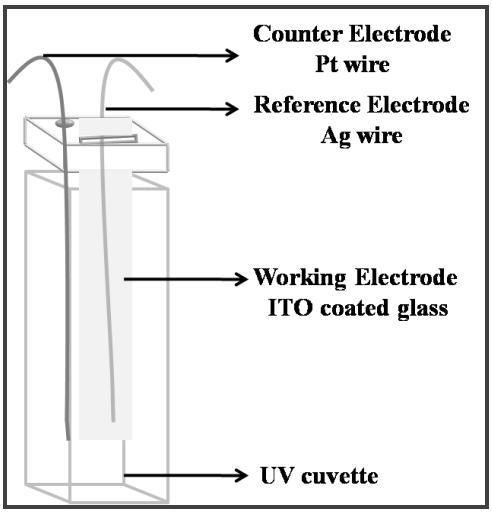

Figure 2.1. A three electrode electrochemical cell set up

All three electrodes were connected to the Solartron 1285 potentiostat that applied the desired potential between a working electrode and a reference electrode. Electrochemically inert and non-nucleophilic solvent should be used in order to avoid decomposition of the solvent at the applied potential. Solvent with high dielectric constant allows the movement of doping ions into or out of the conducting polymer during charge and discharge.

Common solvents were used in electrochemical studies; acetonitrile, benzonitrile, tetrahydrofuran, propylene carbonate, and methylene chloride. Acetonitrile is the most widely preferred solvent since its greater volatility and inertness lead to less solvent retention within the conducting polymer matrix. Also the use of acetonitrile offers a wide potential window required for both p-and n-type doping.

2.3.2. Cyclic Voltammetry

Cyclic voltammetry is one of the most popular potentiostatic methods that can be performed for qualitative analysis of electrochemical processes, particularly those occurring during the synthesis and redox reactions of conducting polymers. This method consists of cycling the potential of working electrode at a constant rate and measuring the resulting current at the electrode. Therefore, the obtained voltammogram is a plot of current density as a function of potential (Figure 2.2).

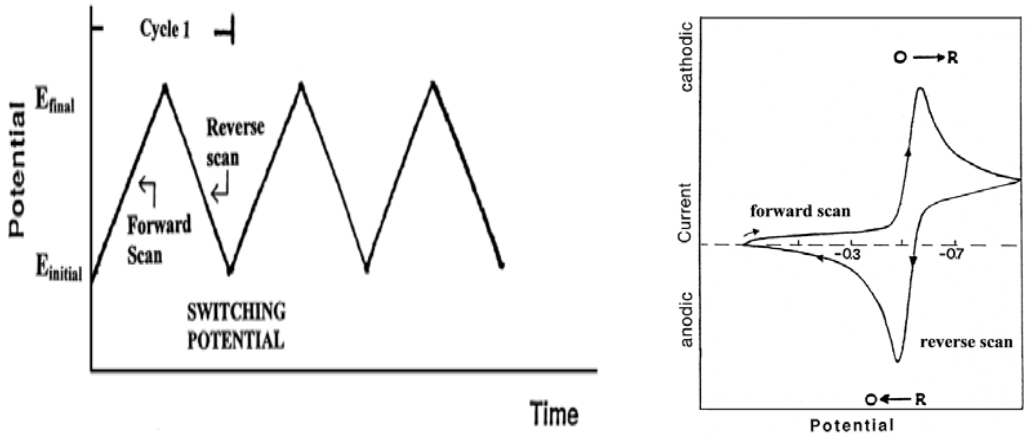

Figure 2.2. Typical (a) Potential−time excitation signal in CV (b) cyclic voltammogram of a reversible $O + ne^- \leftrightarrow R$ redox process [79]

As shown in Figure 2.3, the electrochemical polymerization of electron rich monomer is carried out by starting at a low potential where no redox process takes place and scanning in the anodic direction. Upon continued cycling in the anodic direction, electroactive monomer in diffusion layer is oxidized and leads to the

current to peak. This current response decreases as the concentration of electroactive monomer diminishes in the diffusion layer. Oxidation of monomer is immediately followed by chemical coupling which results in the formation of dimer and consequently oligomers. Once these oligomers reach a length where they become insoluble in the electrolyte solution, they deposited onto the electrode surface. Upon scanning the potential in the reduction direction, the electroactivity of the deposited polymer is monitored. The reduction of the polymer from its oxidized state to neutral state occurs at a lower potential. Upon consecutive cycle formation, a new oxidation peak at a lower potential than the oxidation potential of the monomer is appeared to the re-oxidation of the polymer.

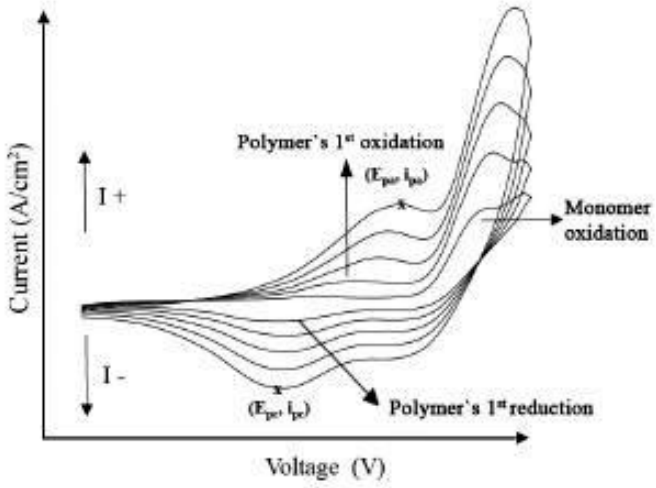

Figure 2.3. Cyclic voltammogram of a representative electroactive monomer

The surface area of the working electrode increases due to the deposition of the electroactive material onto the surface of the electrode as the number of cycle increases. The electrode acts as the new electrode upon subsequent scanning since deposition onto the surface of the electrode affects its area.

This increment in current may be attributed to increase in the area of the electrode as illustrated in the Randles-Sevcik equation:

$$ip = (2.69x10^5)n^{1.5}AD^{0.5}C^b v^{0.5}$$

where n is the number of electrons transferred, A is the electrode surface area (cm^2), D is the diffusion constant (cm^2s^{-1}), C^b is the bulk concentration ($molcm^{-3}$) and υ is the scan rate (Vs^{-1}) [80]. Thus, in diffusion controlled system, peak current is proportional to surface area, A.

The redox properties of the conducting polymer are examined in a monomer free medium using cyclic voltammetry. In monomer free system, there is no diffusion from solution and also the surface area of polymer deposited electrode is constant. The redox properties of the polymer cannot be characterized using the Randles-Sevcik equation given above.

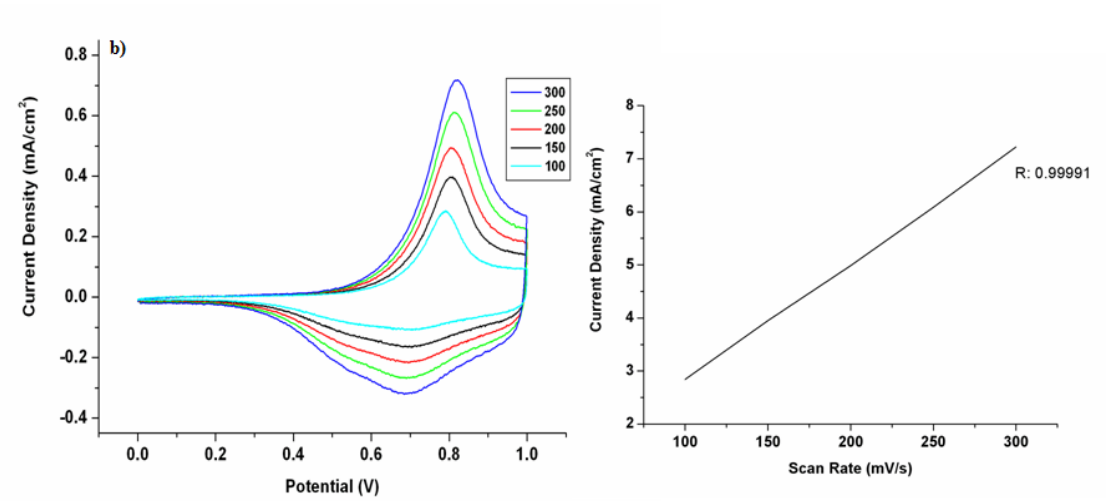

Figure 2.4. Cyclic voltammogram of a representative type of electroactive monomer at scan rates of 100, 150,200, 250 and 300 mV/s.

According to the theory of immobilized redox centers, the peak current for the polymer is given by;

$$i_p = n^2 F^2 \Gamma \nu / 4RT$$

where Γ is the total amount of electroactive species present at the electrode surface [81]. Therefore the peak current will be linearly dependent on the scan rate (Figure 2.4). The peak current intensities of the polymer gradually increase as a linear function of scan rate which indicates that the electrochemical processes are reversible and non-diffusion-controlled.

2.4. Optical Methods

Spectroelectrochemistry, electrochromic switching and colorimetry are the methods that have been used to describe the electrochemical behaviors of conjugated polymers. These techniques allow us to examine the changes in optical transitions upon doping, but also the energy of the band gap, along with the color and relative transmissivity of the polymer film as sensed by the human eye.

2.4.1. Spectroelectrochemistry

Spectroelectrochemistry is an important and routine method used in the characterization of electrochromic polymers. The redox switching of conjugated polymers is accompanied by changes in electronic transitions. These electronic transitions can be probed by the use of UV-Vis-Near Infrared (NIR) spectroscopy. Spectroelectrochemistry experiments provide information about the material's band gap and intraband states (polaron and bipolaron bands) that are created upon doping as well as give some insight into a polymer color through the location of the absorption maxima.

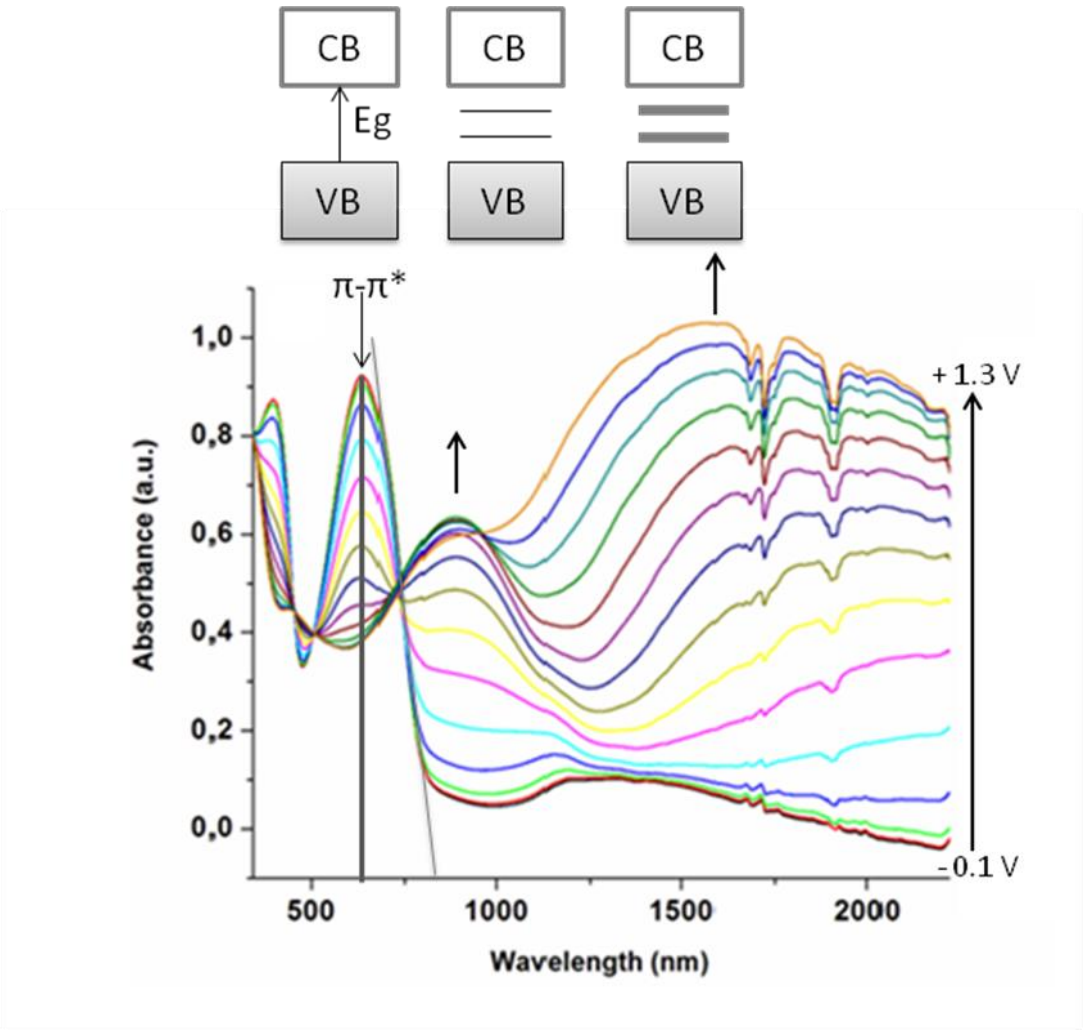

Figure 2.5. p-Doping spectroelectrochemistry of a representative electrochromic conducting polymer

Figure 2.5 shows the expected transitions for a conjugated polymer. In the neutral state the polymer exhibits one transition from the valence band to the conduction band (π to π *). The energy difference between these two levels is the band gap (Eg), and it is measured as the onset of the π-π* absorption in the neutral state of the polymer. On applied voltage, reduction in the intensity of the π-π* transitions along with evolution of new absorption bands were observed. These transitions are attributed to polaron and bipolaron charge carrier bands.

To examine the optical properties, the polymer film was deposited onto ITO-coated glass slides. Then the polymer film was washed with monomer-free electrolyte solution and placed into cuvette for UV-vis-NIR spectroelectrochemistry studies. A series of spectra was collected while the polymer film was switched from neutral state to oxidized state by increasing the potential stepwise.

2.4.2. Electrochromic Switching

The ability of a polymer to switch rapidly and demonstrating a striking color change are essential properties for an electrochromic polymer. Electrochromic switching is proven to be one of the most efficient and easiest ways to monitor these properties.

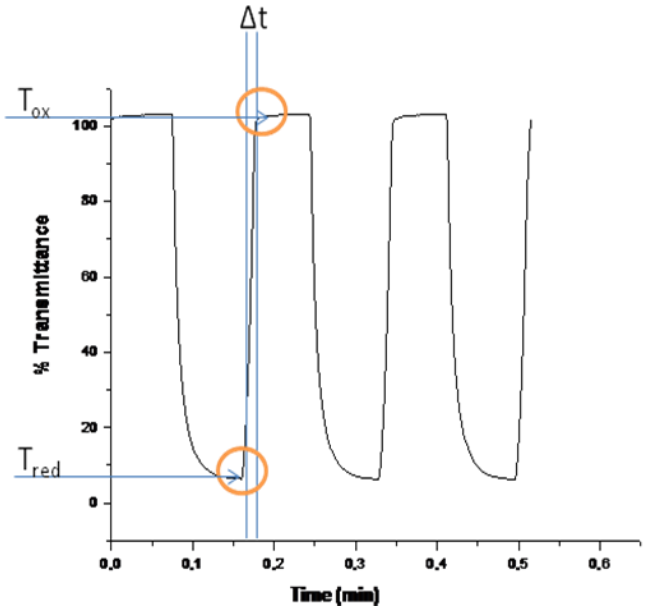

Figure 2.6. Switching studies of a representative electrochromic conducting polymer

Electrochromic switching studies were carried out to monitor absorbance changes with time during repeated potential stepping between reduced and oxidized states. In this double potential step experiment, the potential was set at an initial potential for a set period of time, and was stepped to a second potential for a set period of time,

before being switched back to the initial potential again. During the experiment, the % transmittance (%T) of the polymer was measured using a UV–vis spectrophotometer. The optical contrast was measured as the difference between %T in the reduced (T_{red}) and oxidized (T_{ox}) forms and is noted as % ΔT (Figure 2.6). The rate of change in transmittance upon oxidation/reduction provides a direct indication of the switching ability of a material. Switching rate (Δt) was often reported as the time required for the oxidation/reduction process of the polymer film.

2.4.3. Colorimetry

Colorimetry is performed to define color precisely for electrochromic polymers since specific and reproducible color states are required for any commercial electrochromic material. Colorimetry provides a more precise way to define color than spectroelectrochemistry studies. Rather than measuring the absorption bands, colorimetry measures the human eye's sensitivity to light across the visible region and gives a mathematical function to describe color.

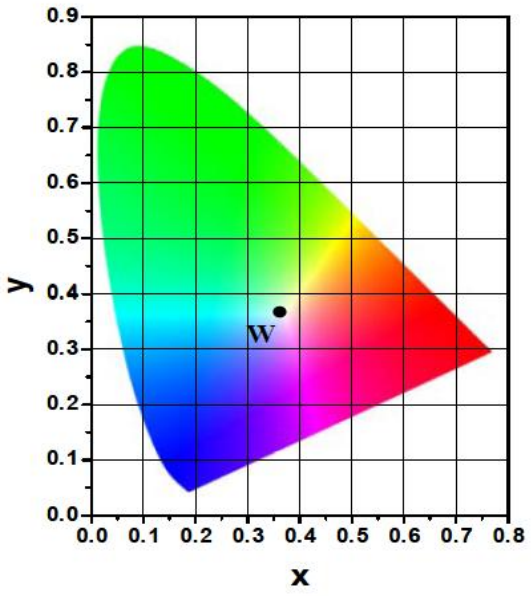

Figure 2.7. CIE 1931 Yxy color space [82]

This technique records three values as regards to color: the hue (dominant wavelength), which is the wavelength where maximum contrast occurs, saturation (purity), which is the color's intensity, and brightness (luminance), which is the relative lightness of the color. The colorimetry analysis is based on the Commission Internationale de l'Eclairge (CIE 1931) Yxy color space which is a quantitative scale to define and compare colors (Figure 2.7). The CIE color space defined color matching functions take into account the manner in which "the human eye perceives color". When studying a color, its hue will vary depending on the illumination and surroundings. Illumination affects the hue due to the color of light. Color is the product of wavelengths that are either absorbed or reflected by the surface of an object when strongly illuminated. Color measurements were performed via Minolta CS-100 Spectrophotometer.

2.5. Electrochromic Devices

The persistent changes in optical properties of the conducting polymers induced by the electrochemical redox process enable the use of them as electroactive layers for the manufacturing of electrochromic devices (ECDs).

The possibility of reversible doping/undoping process accompanied by the spectral change regulates the light transmission through window. Hence, the energy efficiency of buildings and vehicles can be improved. An electrochemical device is a two-electrode electrochemical cell in sandwich configuration of two thin polymer films deposited on transparent indium tin oxide coated glass (ITO), and separated by a gel electrolyte (Figure 2.8).

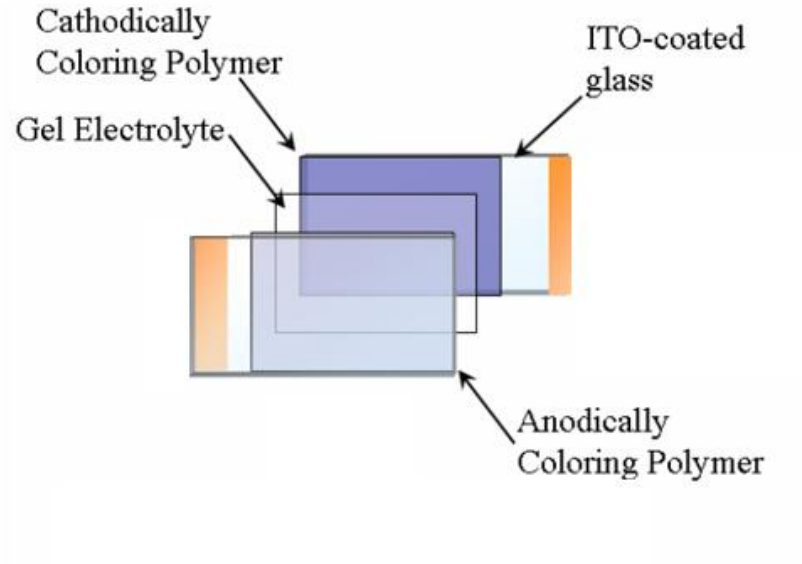

Figure 2.8. ECDs

2.5.1. Device Construction

Figure 2.9 is a schematic representation of an electrochromic device operating at absorptive/transmissive mode. A simple two-electrode circuit is used to construct an electrochromic device for practical investigations. Electroactive species; the anodically coloring and cathodically coloring materials are deposited onto transparent ITO electrodes. These electrodes are arranged facing each other separated by a gel electrolyte to provide ionic conduction. Before assembling the devices, cathodically coloring polymer is fully oxidized and anodically coloring polymer is fully reduced. ECD operates by reversibly switching the device between a highly absorptive, colored state and a highly transparent, bleached state. The colors of the device are additive in that they are a combination of those exhibited by both materials.

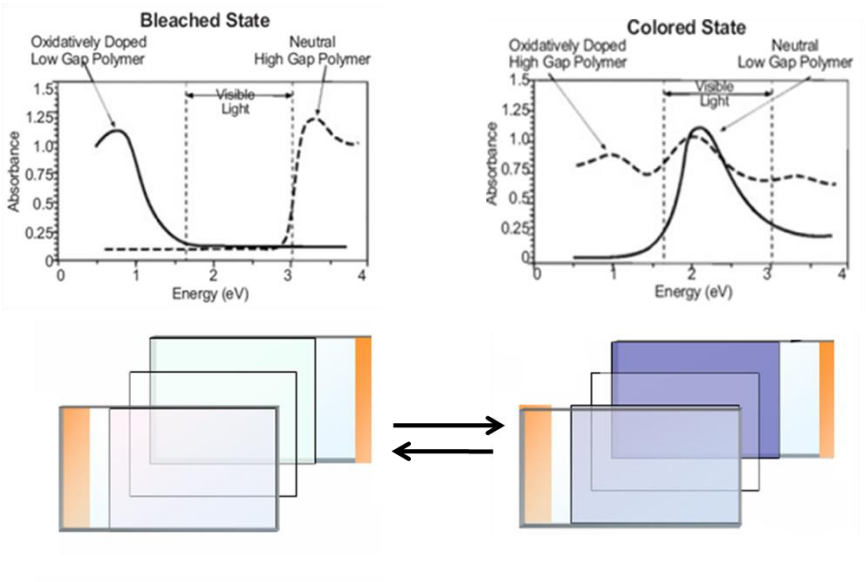

Figure 2.9. Schematic representation of a typical absorptive/transmissive electrochromic device [83]

2.5.2. Preparation of Gel Electrolyte

A gel electrolyte based on PMMA and $TBAPF_6$ was plasticized by PC to form a highly transparent and conductive gel. To allow an easy mixing of the gel components, ACN is used as a high vapor pressure solvent. The composition of the casting solution by weight ratio of $TBAPF_6$: PMMA: PC: ACN was 3:7:20:70. Gel preparation begins by dissolving the electrolyte salt in ACN, followed by the addition of PMMA. This polymeric component is not easily dissolved, thus vigorous stirring and mild heating (60° C) for a period of about two hours is required. When all of the PMMA has dissolved, PC was introduced to the reaction medium. The mixture was stirred and heated until the highly conducting transparent gel was produced.

2.5.3. Characterization of ECDs

2.5.3.1. Spectroelectrochemistry

A typical spectroelectrochemical experiment is carried out to examine the optical properties of electrochromic devices. Spectroelectrochemical analyses of the devices are performed by sequentially stepping the applied potential. In order to apply voltage across the device, the counter and the reference electrodes are connected to one another creating short cut, working electrode is connected to anodically coloring polymer layer. The alternation of the color is observed upon stepwise increase of the potential while measuring the absorbance as a function of wavelength. The baseline is collected using the device that is assembled consisting of two bare ITOs sandwiched together with gel electrolyte.

2.5.3.2. Switching Studies

Switching studies are performed to examine the time required for switching between the two extreme states of the ECD. The device's stability during repeated cycles is evaluated by a square-wave potential step method coupled with optical spectroscopy.

2.5.3.3. Open Circuit Memory

The optical memory of an electrochromic device is the ability of the material to retain its absorption state after the electric field is removed. The ability of an ECD to maintain its color is examined by polarizing it in the redox states by an applied pulse for 1 s and then holding at open circuit conditions for 200 s. The optical spectrum as a function of time at open circuit conditions is monitored.

CHAPTER 3

RESULTS AND DISCUSSION

3.1. Donor-Acceptor-Donor Type π-Conjugated Monomers

3.1.1. Quinoxaline Derivatives

Donor-acceptor-donor (DAD) approach was used to design π-conjugated monomers. Syntheses of donor-acceptor-donor type of π-conjugated monomers were performed to examine the effects of the donor/acceptor units' strength on the electrochemical and optoelectrochemical properties of the resulting monomer and polymer. Effects of electron donor strength on these properties were examined by changing the density of electron-rich unit (donor). Thiophene, 3-hexylthiophene and EDOT were incorporated together with the acceptor structures to probe the effect of increasing the electron density along monomer backbone. The use of the stronger electron donating unit decreases the oxidation potential of the monomer and the band gap of the resulting polymer.

The first row of Table 3.1 shows a series of quinoxaline derivatives where alternation on the monomers were completed by inserting benzo-1,4-dioxane on the acceptor unit (**9**). Another series of donor-acceptor-donor type π-conjugated monomer with increased rigidity were prepared using dibenzo[*a*,*c*]phenazine acceptor (**10**) unit as shown in Table 3.1. Insertion of 1,10-phenanthroline-5,6-dione in acceptor unit allows to examine how the number of imine units affects acceptor strength, thus the

electrochemical and spectroelectrochemical properties of the resulting monomer (**21**) and polymer changed. Palladium catalyzed Stille cross-coupling reaction of an organotin reagent with an organic electrophile is a well-known synthetic method for generating a carbon-carbon bond and it was used for the synthesis of target monomer. Stille coupling reaction was preferred for the formation of carbon-carbon between acceptor and donor units since the reaction takes place in mild conditions. Also protection -deprotection reactions are not necessary due to the high tolerance of the organotin compounds towards a wide variety of functional groups. Thiophene, 3-hexylthiophene and EDOT were treated with n-BuLi followed by Bu_3SnCl in order to prepare the organotin reagents. Synthetic approaches that were used to prepare the acceptor units and the D-A-D type π-conjugated monomers involved bromination, nitration, reduction and condensation reactions.

Table 3.1. Donor-Acceptor-Donor Type Quinoxaline Derivatives

Acceptor Unit \ Donor Unit	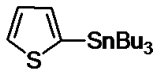 1	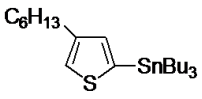 2	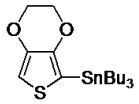 3
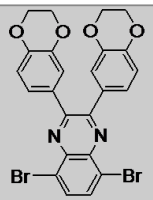 9	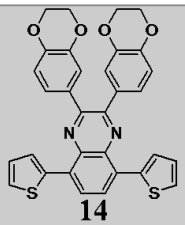 14	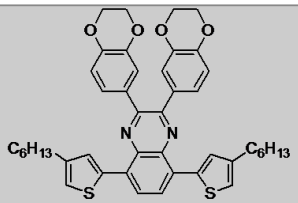 15	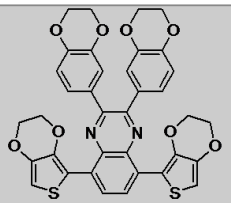 16
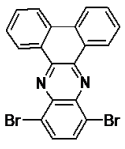 10		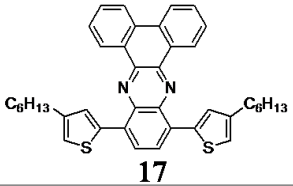 17	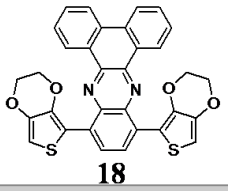 18
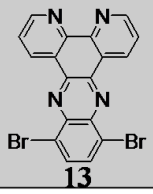 13			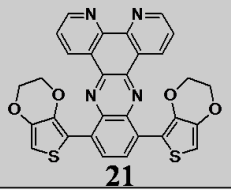 21

3.1.2. Thienopyrazine Derivative

To comply with the donor-acceptor-donor approach, a new low band gap polymer which contains a 3-hexyl thiophene substituted thieno(3,4-*b*)pyrazine core was synthesized (Figure 3.1). An advantage of the thieno(3,4-*b*)pyrazine core in monomer structure was investigated. Insertion of thiophene ring into monomer backbone leads to a decrease in the steric hindrance between adjacent rings. The effective π-conjugation length along the polymer backbone increases due to the coplanarity of the adjacent rings.

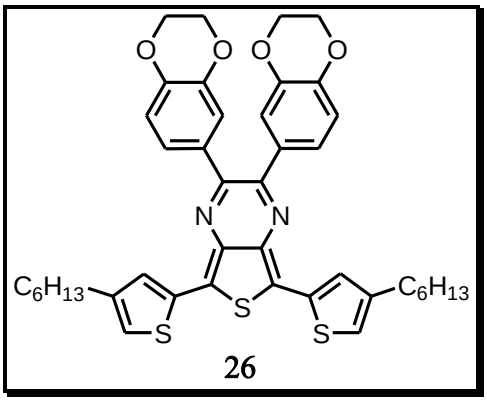

Figure 3.1. Donor-Acceptor-Donor Type Thienopyrazine Derivative

3.1. 3. Donor Moieties

The major advantage of the DAD approach is that the band gap of the resulting polymer will be manipulated by changing the strength of donor and acceptor moieties. The use of thiophene and its derivatives as the donor unit has proven to be one of the effective ways for the development of electropolymerizable π-conjugated materials with low band gaps. Electron-rich nature of donor unit raises the energy of the highest occupied molecular orbital thus the band gap value is lowered. Donor strength of these units is given as EDOT > 3-hexylthiophene > thiophene as also supported by their oxidation potentials.

Palladium catalyzed Stille coupling route in which tributyltin substituted compounds coupled with dibromide compounds was used to prepare the donor-acceptor-donor monomer. The stannyl intermediate of donor units; tributyltin substituted thiophene [84], 3-hexylthiophene [84] and EDOT [85] were prepared in high yield by lithiation with n-butyl lithium and subsequent quenching with tributyltin chloride as shown in Scheme 3.1.

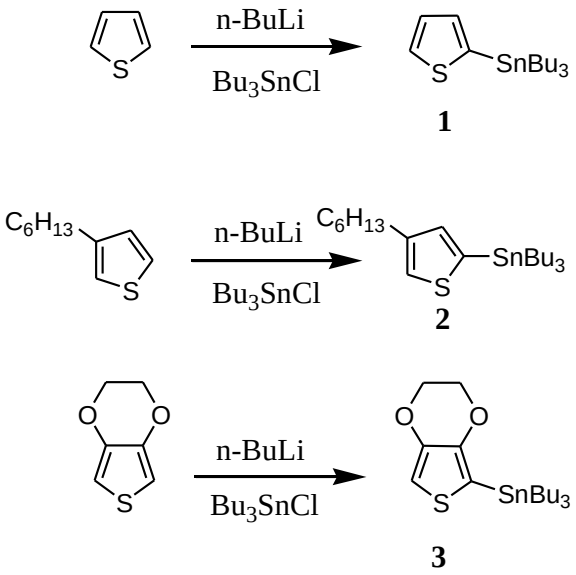

Scheme 3.1. Preparation of organotin compounds

3.1.4. Acceptor Moieties

3.1.4.1. Synthesis of 5,8-dibromo-2-(2,3-dihydrobenzo[*b*][1,4]dioxin-6-yl)-3-(2,3-di hydrobenzo[*b*][1,4]dioxin-7-yl)quinoxaline (9)

Benzo-1,4-dioxane substituted dibromoquinoxaline can be prepared in three steps as shown in Scheme 3.2. Bromination of commercially available benzo[*c*][1,2,5]thiadiazole with Br_2 in 48% hydrobromic acid at 150^{o}C was achieved in very high yields [86]. Subsequent reduction of 4,7-dibromobenzo[*c*][1,2,5]thiadiazole was done using excess amount of $NaBH_4$ in EtOH at 0˚C [87].

Friedel–Crafts acylation of benzo-1,4-dioxane with oxalyl chloride gave 1,2-dione [88]. Then, the condensation reaction between **6** and **8** was carried out in the presence of catalytic amount of paratoluenesulfonic acid (PTSA) and ethanol to give the corresponding dibromoquinoxaline [89].

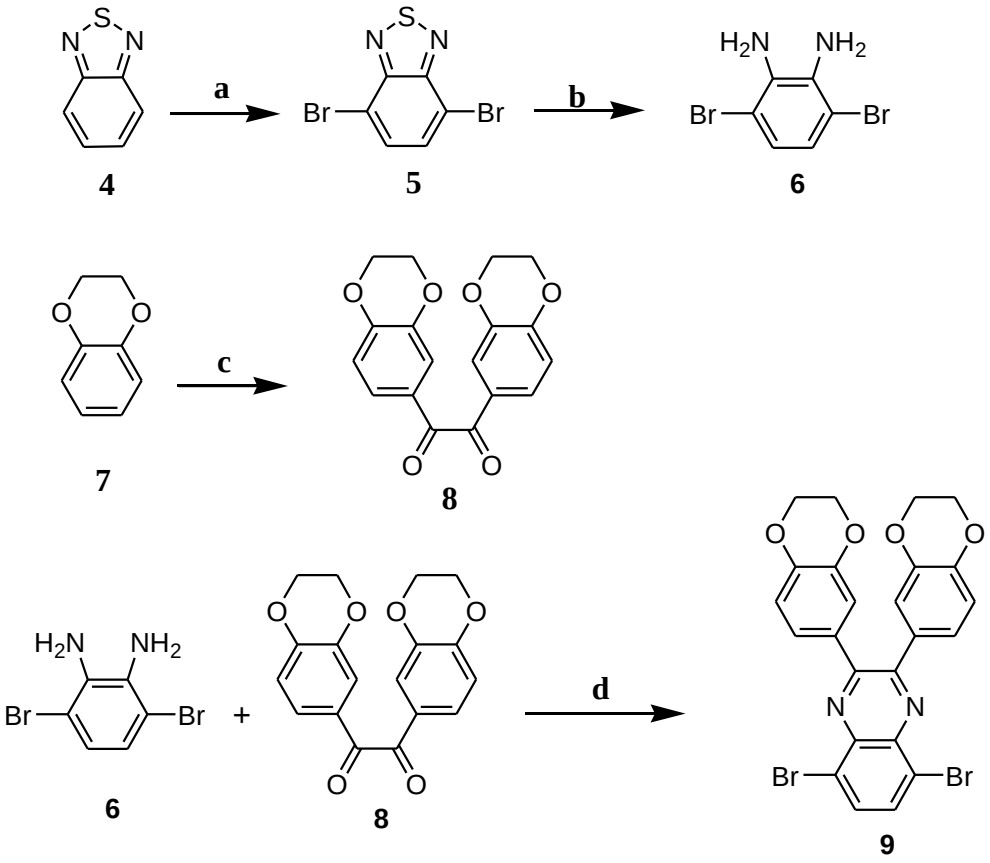

a) Br_2/HBr,150^oC,6h **b)** $NaBH_4$, EtOH, 0^oC **c)** oxalyl chloride, $AlCl_3$, CH_2Cl_2 **d)** PTSA, EtOH, 4h, 85^oC.

Scheme 3.2. Synthetic route to dibromoquinoxaline (**9**).

Sulfur extrusion from 4,7-dibromobenzo[*c*][1,2,5]thiadiazole followed by a ring closure reaction with an appropriate 1,2-dione were utilized to synthesize the quinoxaline derivative. The sulfur extrusion was easily performed by reduction with $NaBH_4$. Substitution of electron donating or electron withdrawing groups on the

benzo[*c*][1,2,5]thiadiazole unit has no a significant effect on the reduction process. Therefore, reduction of 4,7-dibromobenzo[*c*][1,2,5]thiadiazole was accomplished in high yield using $NaBH_4$ as the reducing agent. ^{1}H-NMR spectrum revealed that amine protons resonated at 3.83 ppm as a singlet. The characteristic aromatic proton, attached to the carbon atom neighbor to the Br-connected carbon resonated at 6.75 ppm as singlet.

Ethylenedioxy substituted benzene was converted to benzil in an intermolecular Friedel-Crafts acylation using oxalyl chloride and $AlCl_3$. Identification of the 1,2-dione (**8**) was done using NMR spectroscopy. The characteristic aromatic proton, attached to the carbon atom that is neighbor to the carbonyl connected carbon resonated at 7.43 ppm as a singlet. Aliphatic protons of the $–OCH_2CH_2O-$ units resonated at 4.24 ppm. In the ^{13}C-NMR spectrum of **8**, it was observed that $–OCH_2CH_2O-$ unit carbons resonated at 64.31ppm. Carbon atoms of carbonyl units resonated at 194.5 ppm.

3.1.4.2. Synthesis of 10,13-dibromodibenzo [a,c] phenazine (10)

Benzo[*c*][1,2,5]thiadiazole was brominated with Br_2 in HBr at 150^{o}C to give the corresponding dibrominated compound in very high yields [87]. One-pot reduction of 4,7-dibromobenzo[*c*][1,2,5]thiadiazole (**5**) with excess amount of $NaBH_4$ gave 3,6-dibromo-1,2- phenyl-diamine (**6**) [87]. Ring closure reaction of the resulting diamine with phenanthrene-9,10-dione to form the aromatic diimine(**10**) was performed in ethanol with a catalytic amount of PTSA (Scheme 3.3) [89].

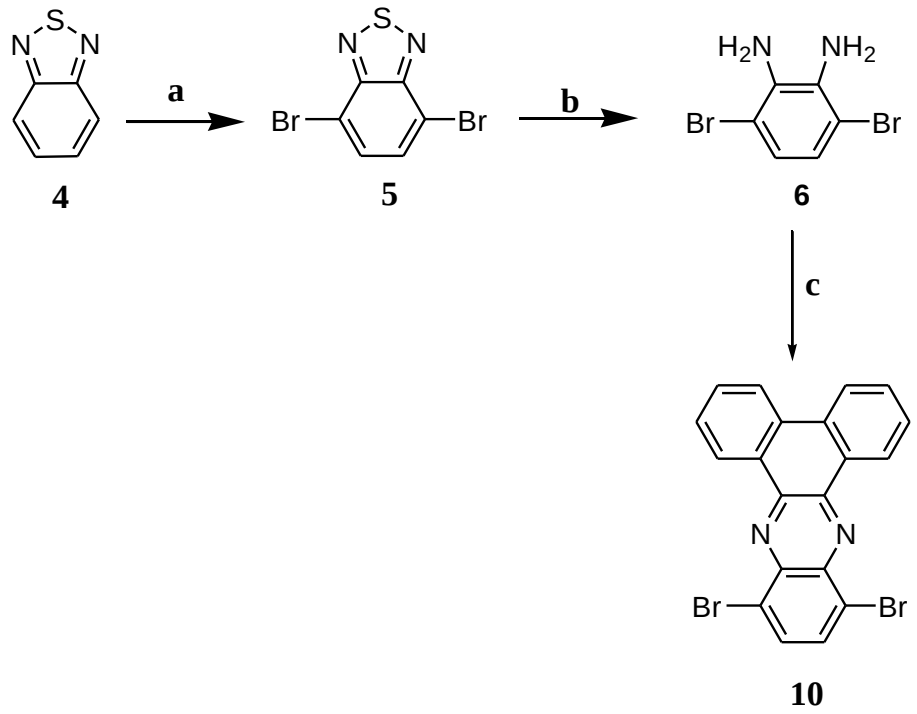

a) Br_2/HBr, 150^oC, 6h **b)** $NaBH_4$, EtOH, 0^oC **c)** phenanthrene-9,10-dione, PTSA, EtOH, 4h, 85^oC.

Scheme 3.3. Synthetic route to dibromoquinoxaline (**10**)

3.1.4.3. Synthesis of 10,13- dibromodipyrido[3,2-a:2,3-c]phenazine

4,7-Dibromobenzo[*c*][1,2,5]thiadiazole (**5**) was synthesized by a procedure similar to that described previously [87]. Treating the resulting compund with $NaBH_4$ yield 3,6-dibromobenzene-1,2-diamine [87]. The dicarbonyl compound 1,10-phenanthroline-5,6-dione (**12**) was prepared from 1,10-phenanthroline by oxidation with H_2SO_4/HNO_3 in the presence of potassium bromide [90]. Condensation reaction of diamine (**6**) and 1,10-phenanthroline-5,6-dione (**12**) was performed in ethanol to give the corresponding dibromoquinoxaline (**13**).

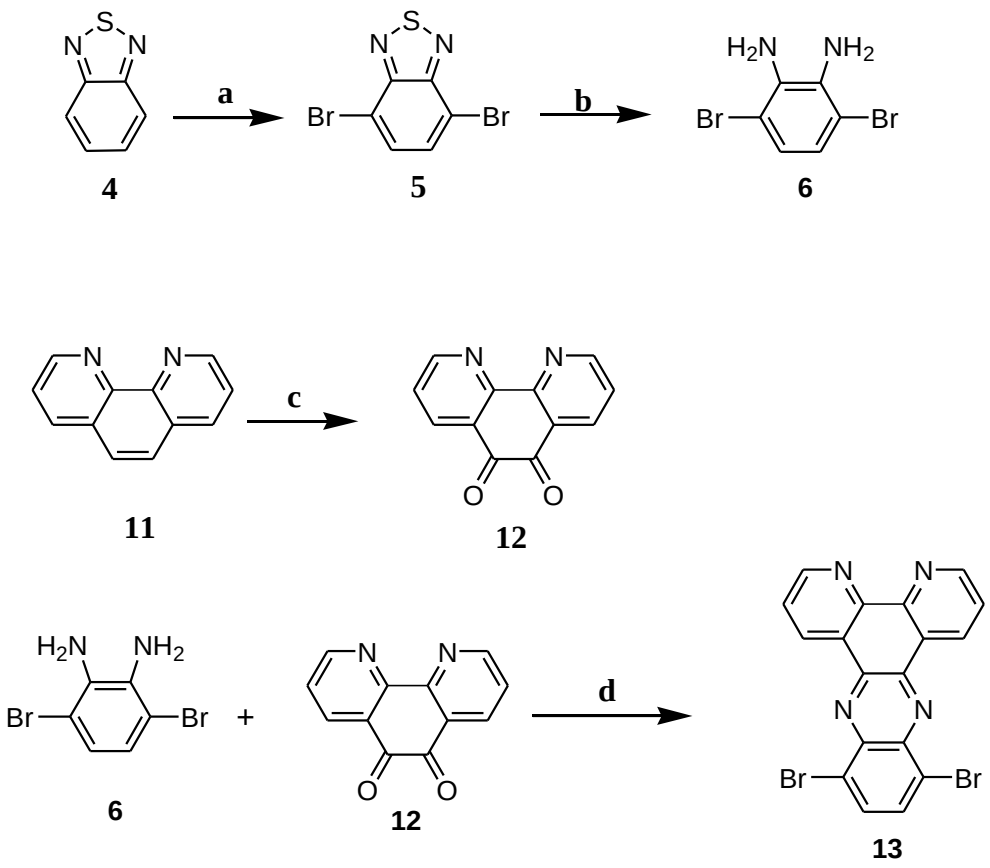

a) Br_2/HBr,150^{o}C,6h **b)** $NaBH_4$, EtOH, 0^{o}C **c)** H_2SO_4/HNO_3, KBr **d)** PTSA, EtOH, 4h, 85^{o}C.

Scheme 3.4. Synthetic route to dibromoquinoxaline (**13**)

The oxidation of 1,10-phenanthroline is accomplished by H_2SO_4/HNO_3 and KBr. In the literature there are many studies that were performed to examine the effect of sulfate, nitrate and halogen ions (bromide, chloride ions) on the rate of nitration reaction [91]. The results indicated that sulfate and nitrate ions do not affect the rate of reaction. Bromide ions have the highest catalyst effect.

3.1.4.4. Characterization of Acceptor Moieties

A series of dibromoquinoxalines were prepared in a multistep procedure as described previously. The electron accepting capacity of the acceptor moieties were altered to understand the structure–property relationships in this new series of π-conjugated monomers. Increasing the planarity in π-conjugated polymers and enhancing the strength of the acceptor unit result in lowering the energy gap of the polymer. The structures of the acceptor units were tailored by extending conjugation over fused ring systems, changing the nature and the position of the heteroatom. Electron accepting strength of the three heterocycle cores in this study follow the trend 1,10-phenanthroline (**13**) > phenanthrene (**10**) > ethylenedioxy benzene (**9**) substituted quinoxaline as evidenced by NMR spectra and monomer oxidation potential.

Examination of ^{1}H-NMR chemical shifts in the aromatic region showed that the ethylenedioxy benzene substituted quinoxaline is a less effective electron-acceptor than the other (Figure 3.2).

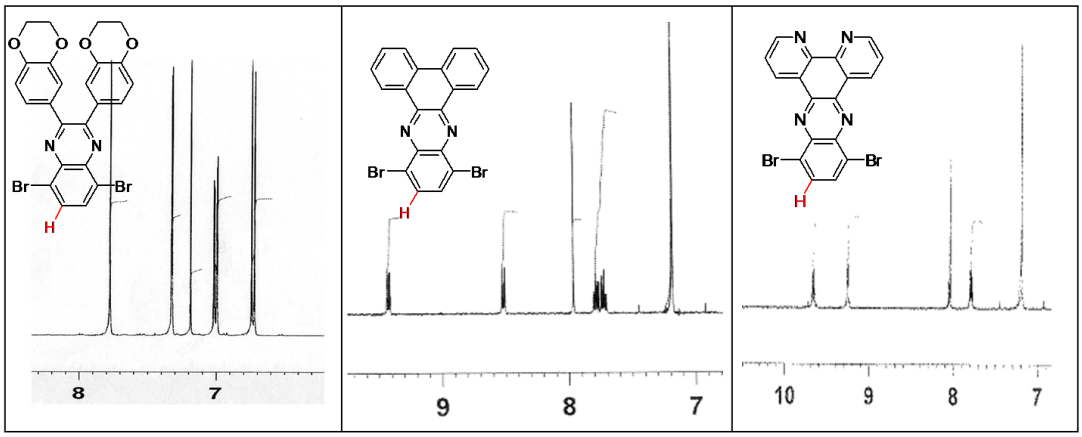

Figure 3.2. Aromatic chemical shifts of π-conjugated monomers

Chemical shift of the proton is related to electron density in the compound. The aromatic protons (H-) of 1,10-phenanthroline substituted quinoxaline resonate at a lower magnetic field strength than the other due to its strong electron-accepting property with high π-character density.

By increasing the electron-withdrawing imine (C=N) groups in the compounds from 2 to 4, the chemical shift moves downfield by 0.20 ppm to 8.05 ppm.

3.2. Syntheses of Donor-Acceptor-Donor Type Quinoxaline Derivatives

Palladium catalyzed Stille coupling reaction was used to attach donor moieties to the acceptor quinoxaline unit to give the target compounds [92]. Access to the monomers, namely 2-(2,3-dihydrobenzo[b][1,4]-dioxin-6-yl)-3-(2,3-dihydrobenzo[b][1,4]dioxin-7-yl)-5,8-di(thiophen-2-yl)quinoxaline (**14**), 5,8-bis(4-hexylthiophen-2-yl)-2-(2,3-dihydrobenzo[b][1,4]dioxin-6-yl)-3-(2,3-dihydrobenzo[b][1,4]dioxin-7-yl)quinoxali-ne(**15**) and 2-(2,3-dihydrobenzo[b][1,4]-dioxin-6-yl)-3-(2,3-dihydrobenzo[b][1,4] dioxin-7-yl)-5-(2,3-dihydrothieno[3,4-b] [1,4]dioxin-5-yl)-8-(2,3-dihydrothieno[3,4-b][1,4]dioxin-7-yl)quinoxaline (**16**), was afforded by Pd-catalyzed cross coupling reaction of the dibromoquinoxaline derivative with tributyl(thiophen-2-yl)stannane, tributyl(4-hexylthiophen-2-yl)stannane and tributyl(2,3-dihydrothieno[3,4-b][1,4]dioxin-5-yl)stannane in refluxing THF under argon (Scheme 3.5).

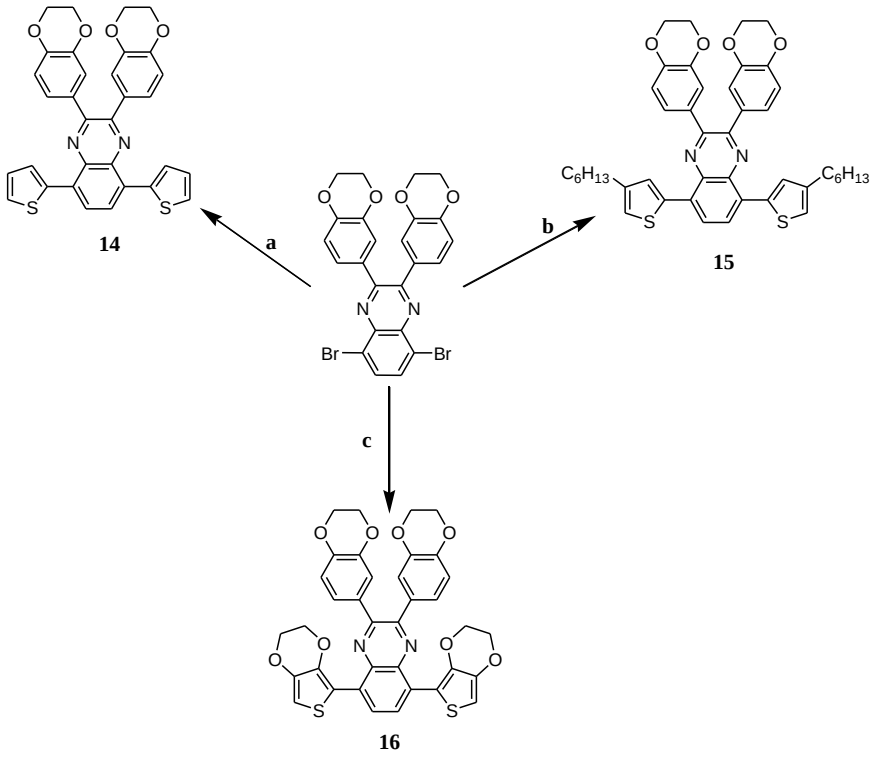

a) tributyl(thiophen-2-yl)stannane, $PdCl_2(PPh_3)_2$, **b)** tributyl(4-hexylthiophen-2-yl)stannane, $PdCl_2(PPh_3)_2$ **c)** tributyl(2,3-dihydrothieno[3,4-b][1,4]dioxin-7-yl)stannane, $PdCl_2(PPh_3)_2$.

Scheme 3.5. Syntheses of Quinoxaline Derivatives

The structure elucidation of π-conjugated monomers was done using NMR spectroscopy. Chemical shifts of the aromatic protons (H-) that were attached to the carbon atom of benzene ring were examined specifically. In Figure 3.3, π-conjugated monomers were ranked from the least shielding of the resonance of the aromatic protons (H-) to the most. Shielding/deshielding effects can be examined with respect to the relative electron density around the aromatic protons (H-). Electron-donating ethylenedioxy units lead to the aromatic protons (H-) resonated at 8.47 ppm as a singlet. These protons were more effectively shielded since the σ-electron density around them is high. By decreasing the donor strength from EDOT to thiophene, the chemical shift moves high field by 0.42 ppm to 8.05 ppm.

This resonance at high field further illustrating the point that thiophene is a poorer electron-donor than EDOT.

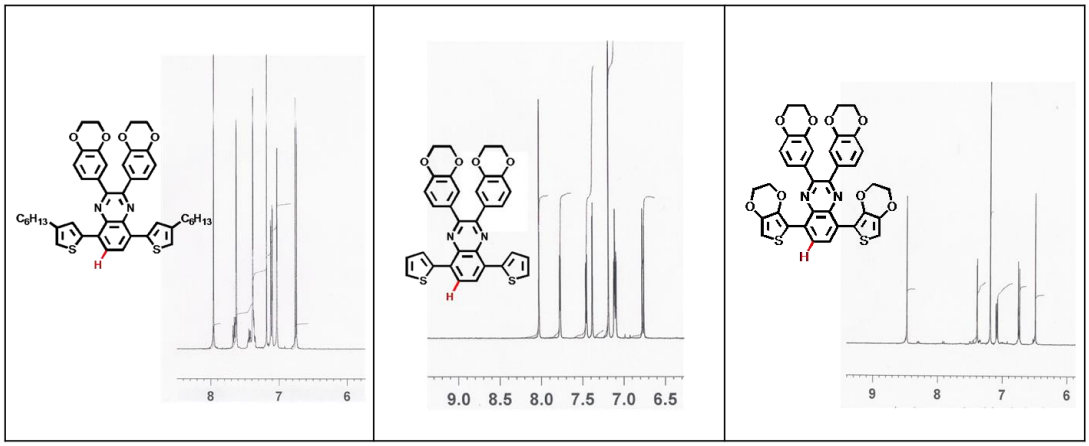

Figure 3.3. Aromatic chemical shifts of π-conjugated monomers

The coupling reaction of tributyltin substituted compound with dibromoquinoxaline catalyzed by palladium takes place under mild conditions in high yields. Mechanism of the coupling reaction that was proposed by Stille consists of three-step catalytic cycle. 10,13-Bis(2,3-dihydrothieno[3,4-*b*][1,4]dioxin-5-yl)dibenzo[*a,c*]phenazine substituted molecules were synthesized by Stille coupling reactions as outlined in Scheme 3.6. Pd(II) is reduced by the stannane to Pd(0) that is responsible for the oxidative addition process. The first step of cycle is the oxidative addition of dibromoquinoxaline (R-Br) to the active palladium (0)-complex. The resulting palladium (II)-ligand2-Br-R-complex undergoes transmetalation process with tributyltinstanne ($R'SnBu_3$) to form R-palladium-(II)-ligand2-R' and tributyltin bromide. The final step of cycle is the reductive elimination in which the R-R' product is obtained and the active palladium-(0) complex is regenerated [94].

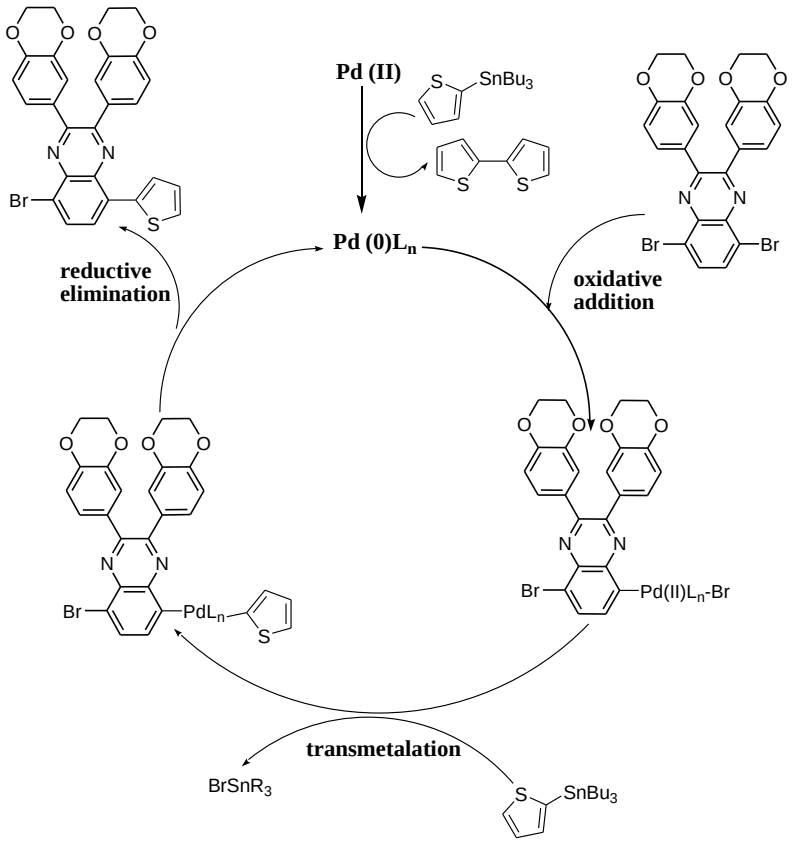

Scheme 3.6. General aryl-aryl coupling mechanism

The target monomer **17** was obtained as a result of the reaction between dibromoquinoxaline with tributyl(4-hexylthiophen-2-yl)stannane in the presence of $Pd(PPh_3)_2Cl_2$ as the catalyst (Scheme3.7). At the end of the reaction, the crude product was purified by column chromatograpy on silica gel, eluting with 1:1 (DCM/Hexane). The desired product was isolated as orange crystalline solid.

The coupling of dibromoquinoxaline with tributyl(2,3-dihydrothieno[3,4-b][1,4]dioxin-7-yl)stannane in the presence of catalytic $Pd(PPh_3)_2C1_2$ in THF gave the target molecule, **18**. After the purification of the crude product by column chromatography on silica gel, eluting with 3:1 (DCM/Hexane) and then recrystallization ($CHCl_3$/hexane), the desired product was isolated as dark red solid.

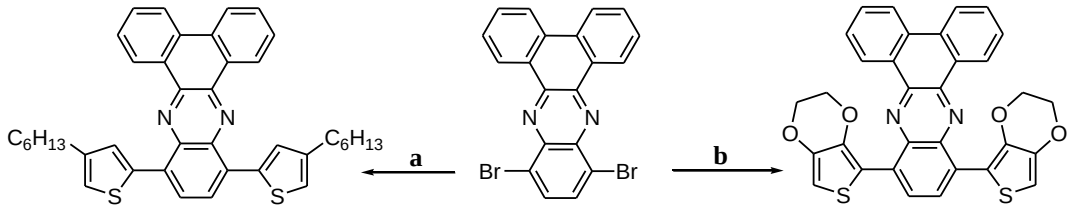

17 **18**

a) tributyl(4-hexylthiophen-2-yl)stannane, $PdCl_2(PPh_3)_2$ **b)** tributyl(2,3-dihydrothieno[3,4-b][1,4]dioxin-7-yl)stannane, $PdCl_2(PPh_3)_2$.

Scheme 3.7. Syntheses of Quinoxaline Derivatives.

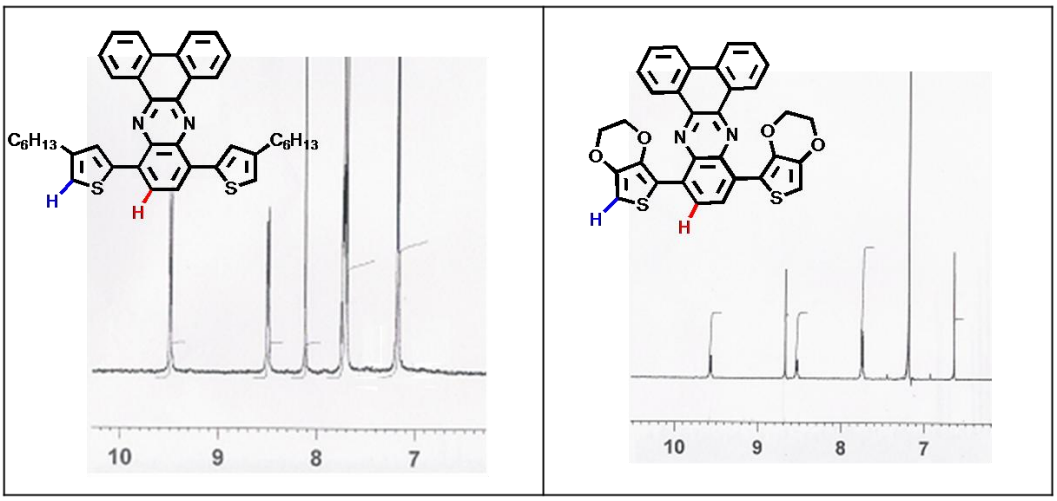

Figure 3.4. Aromatic chemical shifts of π-conjugated monomers

Identification of the target monomers was accomplished by NMR spectroscopy. It was observed that the characteristic aromatic proton (H-) in EDOT-substituted compound resonates at 8.67 ppm as a singlet (Figure 3.4). On the other hand the same proton (H-) in 3-hexyl-substituted compound resonated at 8.65 ppm as singlet. Chemical shifts of the aromatic protons (H-) that were attached to the carbon atom of thiophene ring appeared at 8.62 ppm for the 3-hexyl-substituted compound.

The EDOT-substituted compound with a proton resonance at 6.60 ppm that indicates the circulating σ-electrons of ethylenedioxy unit on thiophene shifts the signal up field.

3.3. Synthesis of DAD monomer based on 1,10-phenanthroline

Synthetic route that was used for the synthesis of the other quinoxaline derivatives modified to synthesize this 1,10-phenanthroline containing monomer. Although the dibromoquinoxaline acceptor unit (**13**) was prepared following bromination, reduction and condensation steps, the resulting compound has low solubility in the common solvents such as THF and DMF were usually used in Stille coupling reaction. To overcome these drawbacks, firstly D-A-D type π-conjugated monomer backbone was prepared [94]. Subsequent reduction of this compound gave donor substituted-diamino compound that undergo condensation reaction with dicarbonyl compound 1,10-phenanthroline-5,6-dione [95]. Condensation reaction produced target monomer, **21**.

The general synthetic strategy towards the π-conjugated monomer (**21**) is outlined in Scheme 3.8. Bromination of benzo[*c*][1,2,5]thiadiazole (**4**) was achieved using a mixture of HBr/Br_2. 3, 4-Ethylenedioxy thiophene was converted to its stannyl derivative (**3**) by treatment with n-BuLi followed by Bu_3SnCl. A Stille coupling between 4,7-dibromobenzo[*c*][1,2,5] thiadiazole (**5**) and 2-tributylstannyl-3,4-ethylenedioxythiophene (**3**) gave the compound **19**. Zinc was used to reduce the resulting compound to diamine compound (**20**). The dicarbonyl compound 1,10-phenanthroline-5,6-dione (**12**) was synthesized by a procedure similar to that described previously. Condensation reaction of diamine (**20**) and 1,10-phenanthroline-5,6-dione (**12**) was performed in ethanol. At the end of the reaction violet colored cloudy mixture was observed. Reduction of D-A-D π-conjugated monomer backbone was carried out as described using Zn metal as the reducing agent. $NaBH_4$ is not preferred for this reduction process since steric hindrance resulted from the substitution of donor moieties on 2,1,3-benzothiadiazole unit lowers the yield. Filtration of the reaction mixture was followed by washing

with cold ethanol. The residue was purified by column chromatography over silica gel, eluting with 1:1 (dichloromethane: hexane) gave violet solid. Identification of the target monomer was accomplished by NMR spectroscopy. Chemical shifts of the aliphatic protons belonging to EDOT appeared at 4.32 ppm and 4.22 ppm. Aromatic proton of EDOT resonated at 6.60 ppm as singlet.

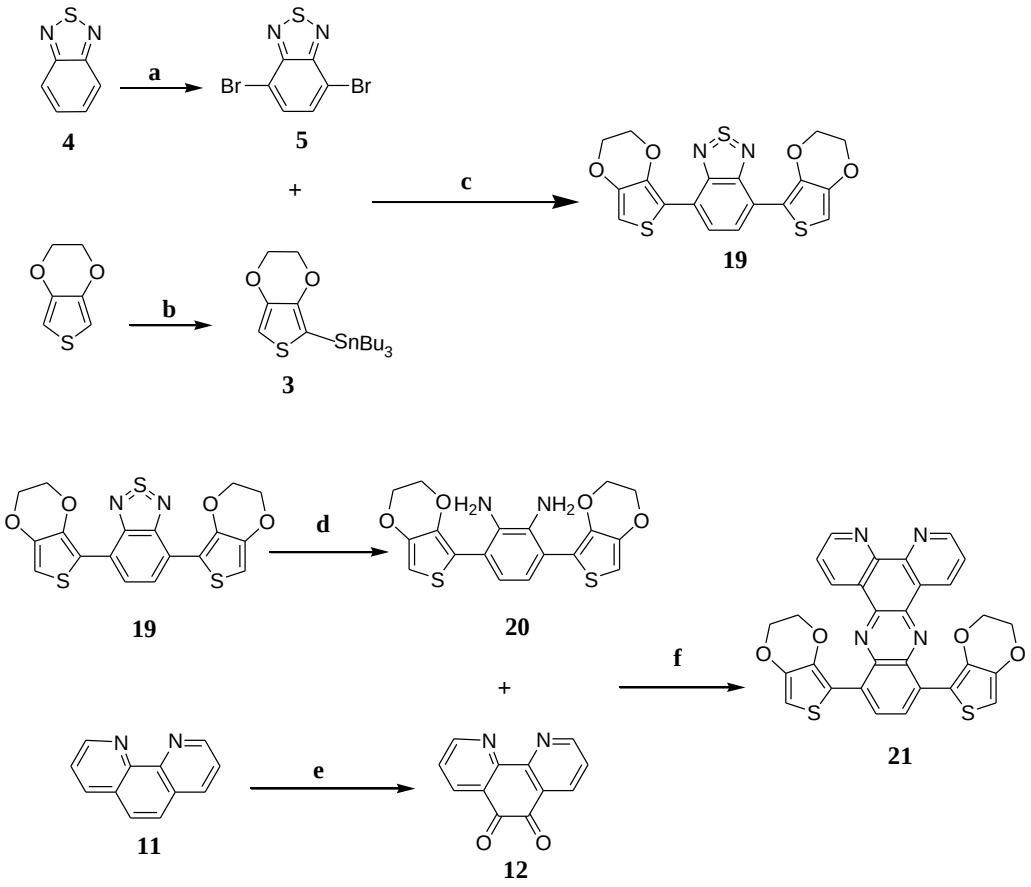

a) Br_2/HBr,150^oC,6h **b)** n-BuLi, Bu_3SnCl, -78^oC **c)** tributyl(2,3-dihydrothieno[3,4-b][1,4]dioxin-7-yl)stannane, $Pd(PPh_3)_2Cl_2$, THF **d)** Zn, CH_3COOH, 15 min. **e)** H_2SO_4/HNO_3, KBr **f)** PTSA, EtOH, 4h, 85^oC.

Scheme 3.8. Synthetic route to quinoxaline derivative (**21**)

3.4. Synthesis of Thienopyrazine Derivative

3.4.1. 5,7-bis(4-hexylthiophen-2-yl)-2-(2,3-dihydrobenzo[b][1,4]dioxin-6-yl)-3-(2,3-dihydrobenzo[b][1,4]dioxin-7-yl)thieno[3,4-b]pyrazine

The general synthetic strategy towards the thieno[3,4-b]pyrazine containing ethylenedioxy phenyl units on electron-withdrawing moiety of π-conjugated terthienyl system is outlined in Scheme 3.9. 2,5-Dibromo-3,4-dinitrothiophene (**23**) was prepared starting from 2,5-dibromothiophene (**22**) [96]. Nitration of 2,5-dibromo thiophene was performed by dropwise addition of nitric acid to the solution of 2,5-dibromothiophene, concentrated sulfuric acid and fuming sulfuric acid. The Stille coupling reaction of 2,5-dibromo-3,4-dinitrothiophene (**23**) with tributyl(4-hexylthiophen-2-yl)stannane (**2**) gave a dinitro compound (**24**). For the palladium-catalyzed Stille coupling reaction, tetrahydrofuran (THF) was used as the solvent and $Pd(PPh_3)_2Cl_2$ was used as the catalyst. Reduction of the resulting dinitro compund (**24**) to the diamine compund (**25**) was performed in the presence of tinchloride as the reducing agent and ethylacetate as the solvent [96]. Through the condensation reaction between the diamine compound (**25**) and 1-(2,3-dihydrobenzo[b][1,4]dioxin-6-yl)-2-(2,3-dihydrobenzo[b][1,4]dioxin-7-yl)ethane-1,2-dione (**8**), π-conjugated terthienyl system was obtained. Column chromatography (dichloromethane/hexane, 3:1) gave **26** as a green solid.

Preparation of diamine involved nitration of 2,5-dibromothiophene and subsequent reduction of the dinitro group to amino groups. Synthesis of 2,5-dibromo-3,4-dinitrothiophene depends on the use of fuming H_2SO_4 and HNO_3. Only the mononitro product is synthesized unless the fuming acids are used. The use of concentrated sulfuric acid increases the rate of nitration reaction via increasing the concentration of the nitronium ion. Nitro aromatic compound was reduced using $SnCl_2$ as the reducing agent. The nitrogen atom is reduced from an oxidation state of +V to –III and the tin atom is oxidized from +II to +IV hence four equivalents of tin is needed per nitro group.

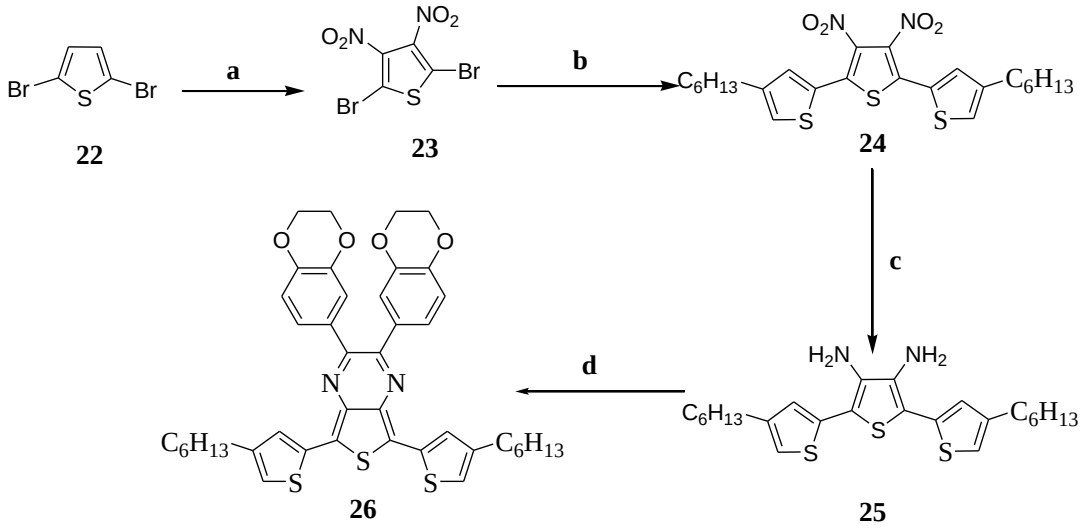

a) conc. and fuming H_2SO_4, conc. HNO_3, 3 h **b)** tributyl(4-hexyltiophen-2-yl)stannane, $Pd(PPh_3)_2Cl_2$, THF **c)** $SnCl_2$, EtOAC, 2 h **d)** 1-(2,3-dihydrobenzo[b][1,4]dioxin-6-yl)-2-(2,3-dihydrobenzo[b][1,4]dioxin-7-yl)ethane-1,2-dione , EtOH, PTSA, 6 h.

Scheme 3.9. Synthetic route to thienopyrazine derivative (**26**)

3.5. Characterization of Conducting Polymers

3.5.1. Ethylenedioxy Benzene Substituted Quinoxaline Derivatives

3.5.1.1. Electrochemistry

As typical conjugated molecules containing thiophene and its derivatives with unblocked 2 or 5 positions, these monomers (**14**, **15**, and **16**) oxidatively were polymerized to form redox-active, electrode-confined films on ITO. Multiple cyclic voltammograms for the repeated scanning electropolymerization of **14**, **15** and **16** were shown in Figure 3.5.

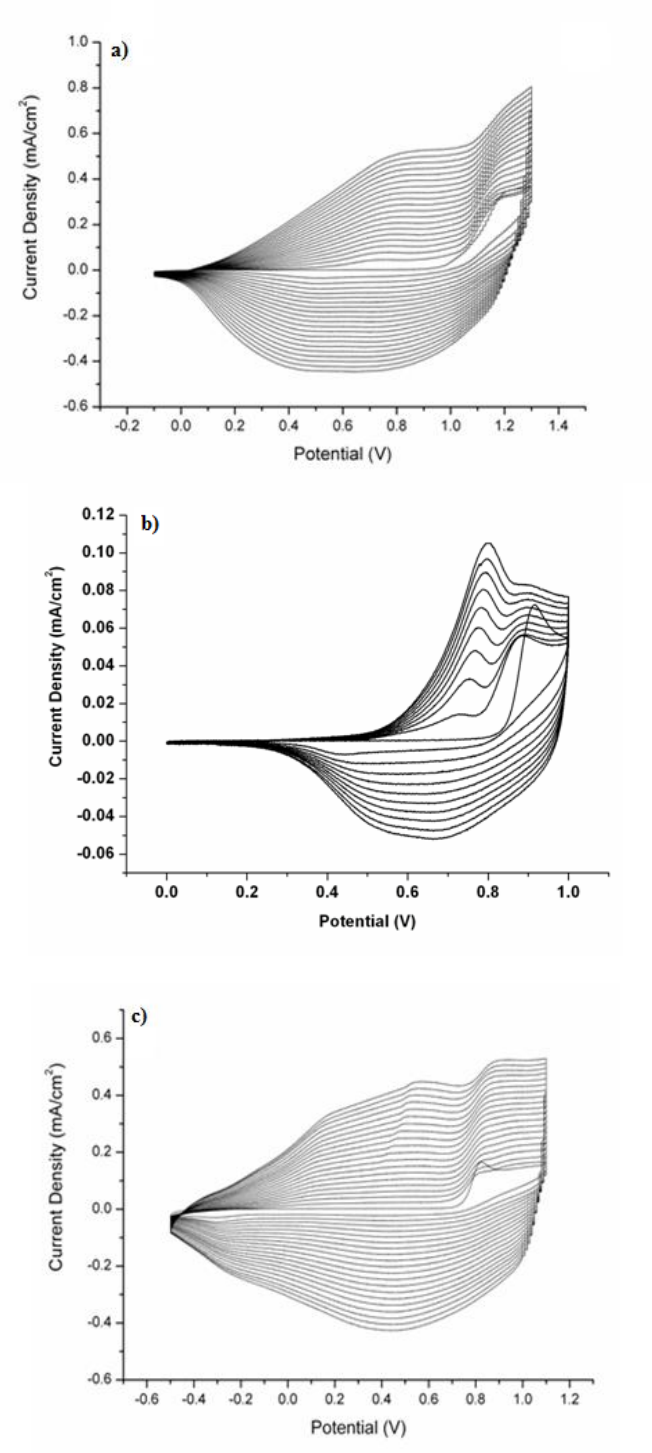

Figure 3.5. Repeated potential scan electropolymerization of a) 14 c) 16 in 0.1 M $TBABF_4$/ACN/DCM, b) 15 in 0.1 M $NaClO_4$/ACN at 100 mV/s on the ITO electrode.

Cyclic voltammetry of **14** and **16** were carried out in ACN/DCM (90/10,v/v) solvent mixture using $TBABF_4$ (0.1 M) as the supporting electrolyte. Repeated potential scan electropolymerization of **15** was performed in 0.1 M $NaClO_4$/ACN supporting electrolyte/solvent system. During the first anodic scan, a single peak was observed which corresponds to irreversible monomer oxidation at a bare ITO glass electrode. The onset of oxidation starts at + 1.0 V for **14** and at 0.97 V for **15** vs Ag wire pseudo-reference electrode. The oxidation wave for **16** is shifted to +0.7 V due to the presence of electron donating group on donor moiety. The oxidation potential of **16** is lower than that of **14** and **15** measured under the described conditions, thus indicating that the HOMO level of **16** is higher than that of **14** and **15**.

The electron-rich character for the three heterocycle compounds follows the trend EDOT>3-hexylthiophene>thiophene as evidenced by their oxidation potentials. On the anodic scans, polymer oxidations were evolved at about + 0.55 V for **P16**, + 0.7 V for **P14** and + 0.80 V for **P15**. Reduction of the polymers evolved a peak at + 0.67 V for **P15**, +0.60 V for **P14**, +0.43 V for **P16** vs same reference electrode (Scheme 3.10).

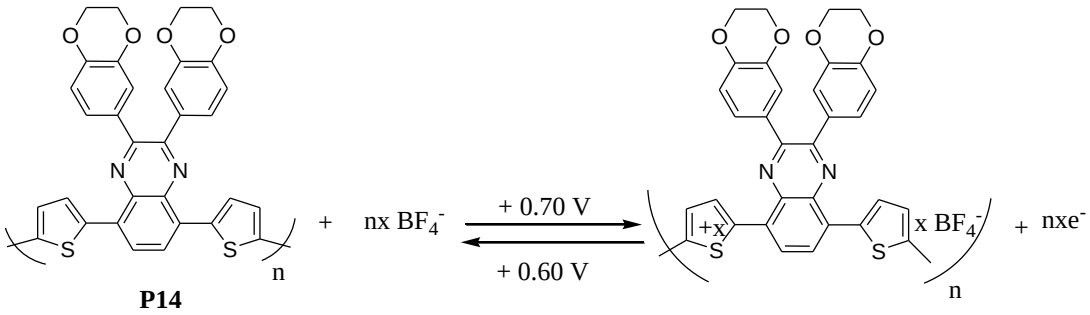

P14

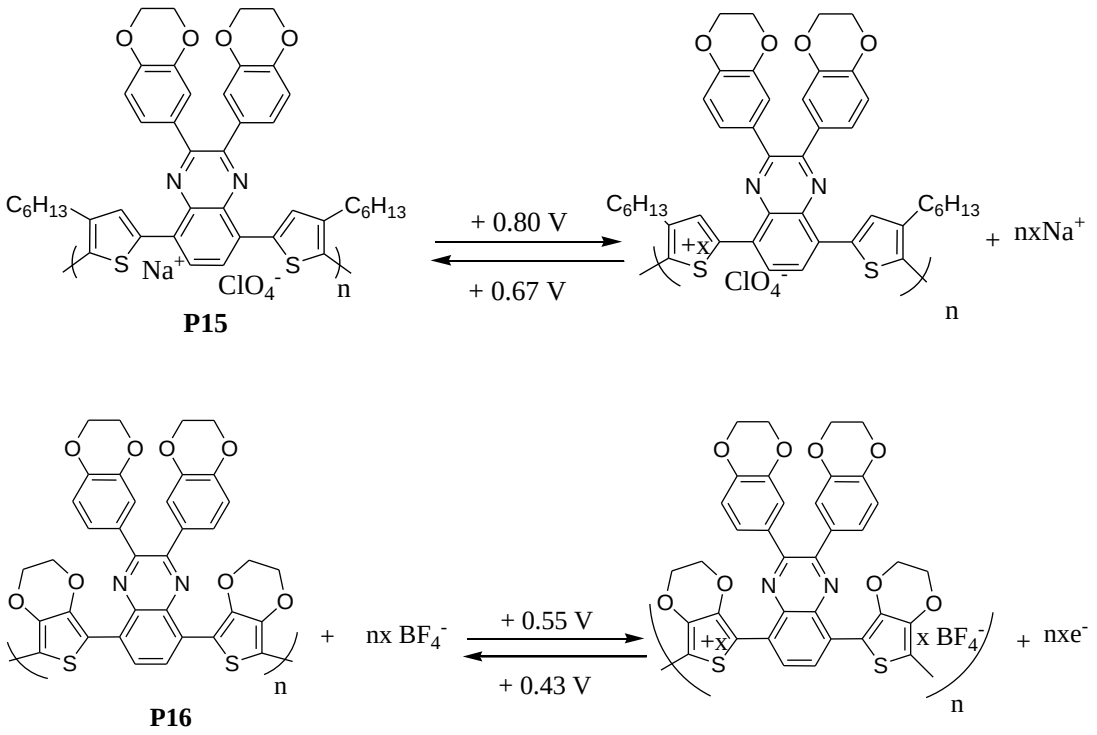

Scheme 3.10. p-Doping of P14, P15 and P16.

The scan rate dependence of the anodic and cathodic peak currents was studied in a monomer-free electrolyte solution (Figure 3.6). A linear relationship between the peak current and scan rate demonstrates that the films were well adhered and the electrochemical processes were reversible and non-diffusion-controlled.

P16 film gives rise to an electrochemically active cycle in the reduction region. A sharp reversible peak corresponding to reversible n-doping of **P16** appears at -1.35 V and the corresponding n-dedoping peak appears at -1.14 V vs Ag wire. In contrast with the n-doping/dedoping process, the current associated with the p-doping in the oxidation process of **P15** is very small. The results suggest that **P16** is a good n-type conjugated polymer (Figure 3.6).

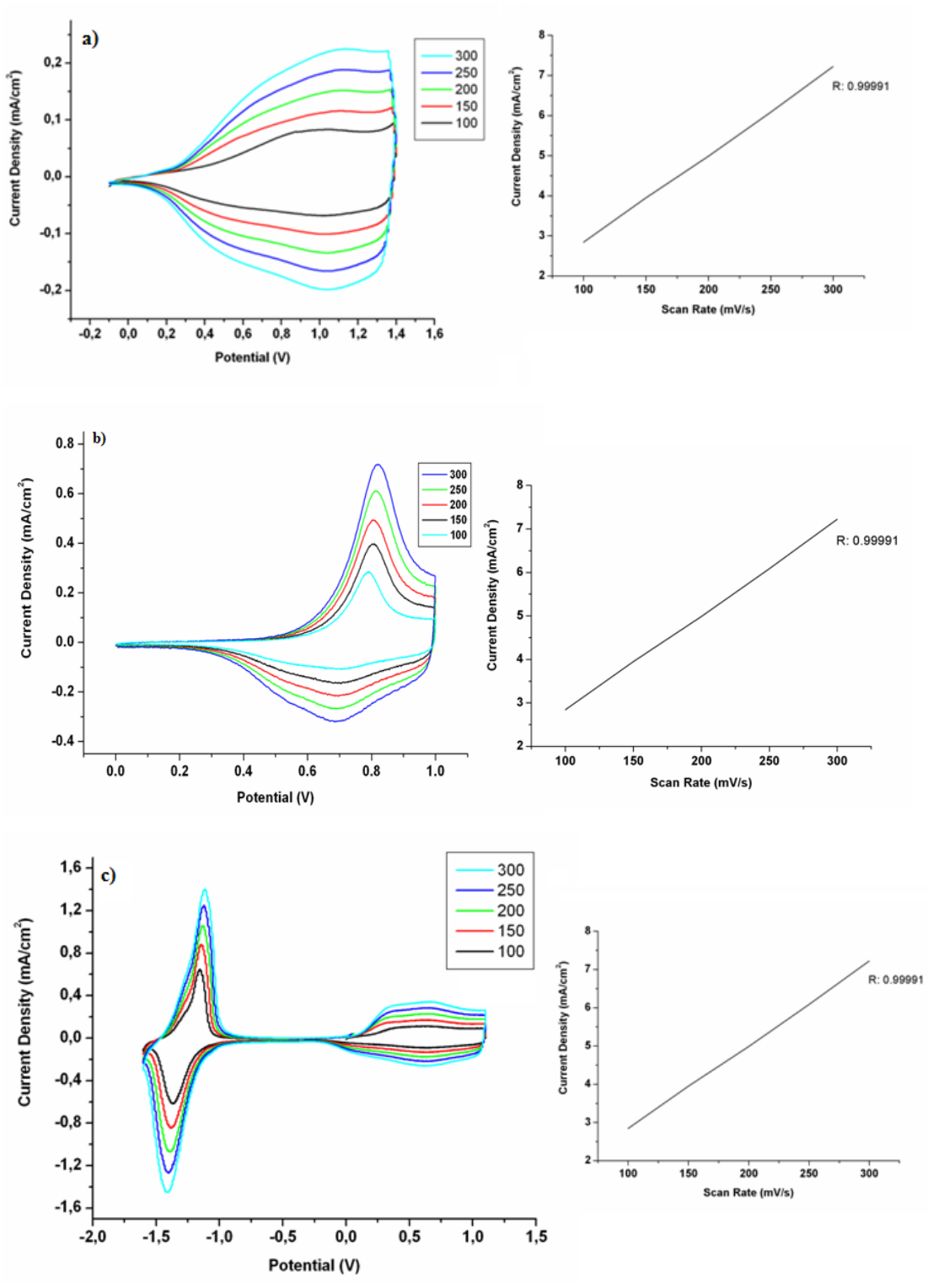

Figure 3.6 Cyclic voltammograms of a) P14 b) P15 c) P16 in 0.1 M $TBABF_4$/ACN/DCM at scan rates of 100, 150, 200, 250 and 300 mV/s.

3.5.1.2. Spectroelectrochemistry

Spectroelectrochemical measurements were performed in order to define the changes in optical properties that accompany the redox switching for **P14**, **P15** and **P16**. For these measurements, **P14** and **P16** films were electrochemically deposited on ITO-coated glass plates from $1x10^{-3}$ M monomer solutions in 0.1 M $TBABF_4$/ACN/DCM. **P15** film was electrochemically deposited on ITO-coated glass plates from $1x10^{-3}$ M monomer solutions in 0.1 M $NaClO_4$/ACN.

Changes in optical properties by increasing the applied potential were investigated using UV–Vis-NIR spectroscopy. The evolution of the electronic band structure during electrochemical p-doping of electrochromic polymers were recorded as a function of applied potential and shown in Figure 3.7. In the neutral state, **P14** absorbs across the entire visible region, exhibiting blue color with an optical band gap of 1.5 eV as calculated from the onset of the π-π* transition. Upon incremental stepping of the potential from -0.1V to +1.3 V, transition observed in the neutral polymer decrease in intensity. At intermediate potentials, a peak evolves at 896 nm attributable to the charge carriers that are formed, which is subsequently overwhelmed by the strong NIR absorption (1560 nm) upon further doping. The absorption is enhanced at lower energies [97].

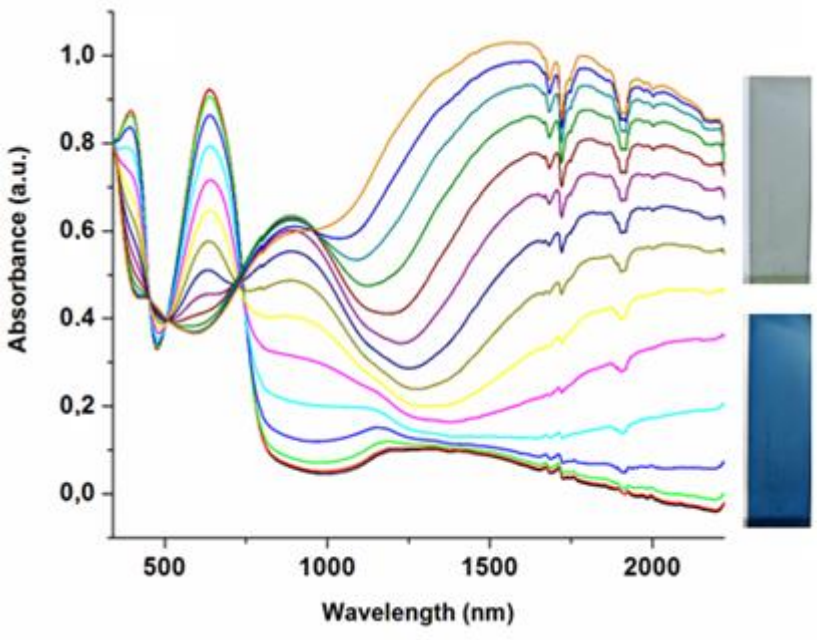

Figure 3.7. p-Doping spectroelectrochemistry of P14 film on an ITO coated glass slide in monomer free, 0.1 M $TBAPF_6$/DCM electrolyte-solvent couple at applied potentials.

Spectroelectrochemistry of **P15** shows a λ_{max} of 530 nm for the neutral polymer, which is red in color (Figure 3.8). Upon oxidation there is a decrease in the π-π* transition and the development of new transition bands at lower energy (at 856 and 1640 nm), corresponding to the polaronic and bipolaronic charge carriers. The electronic band gap of polymer, defined as the onset of the π-π* transitions, was determined as 1.82 eV. The different structures of the polymers due to the differences in donor moiety affect not only the monomer oxidation and the polymer redox couple potentials but also the maximum absorption wavelengths of the corresponding transition. The introduction of alkyl substituent on polymer causes steric hindrance, resulting in less order and less conjugation by the blue shift in absorption spectra and the increase in polymer's band gap.

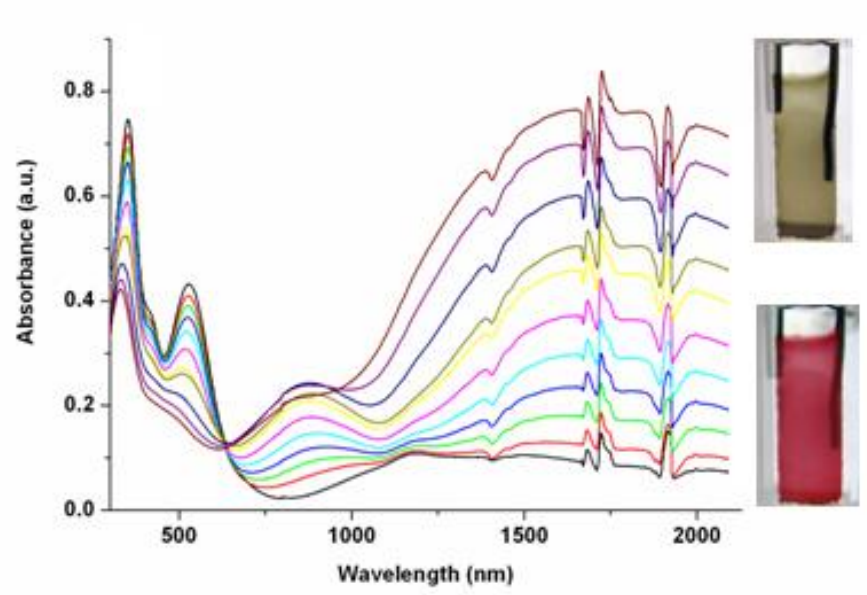

Figure 3.8. p-Doping spectroelectrochemistry of P15 film on an ITO coated glass slide in monomer free, 0.1 M $NaClO_4$/ACN electrolyte-solvent couple at applied potentials

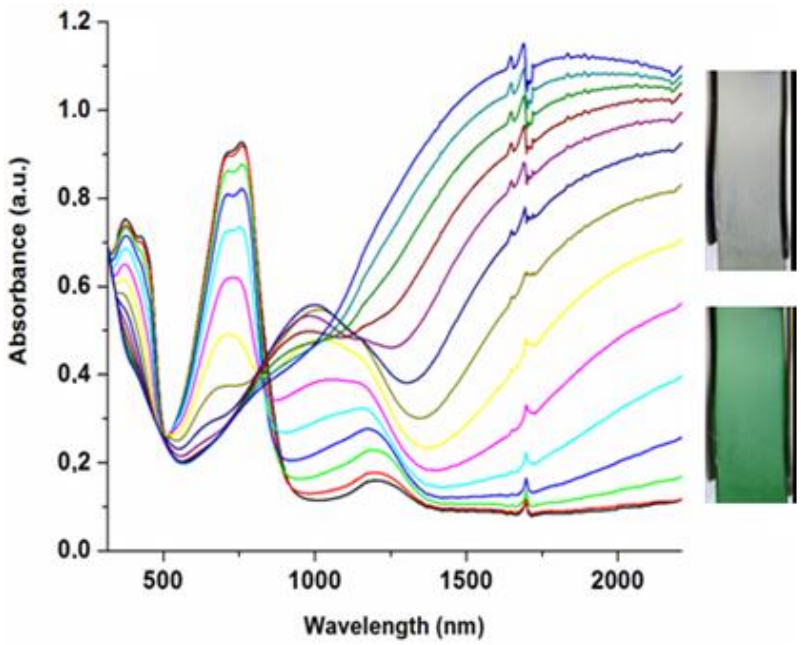

Figure 3.9. p-Doping spectroelectrochemistry of P16 film on an ITO coated glass slide in monomer free, 0.1 M $TBAPF_6$/DCM electrolyte-solvent couple at applied potentials.

Spectroelectrochemical studies of **P16** reveal two well-separated absorption maxima were centered at 423 and 738 nm which is a necessity to maintain a green reduced state (Figure 3.9). The intensity of both absorption bands decreases and a new absorption band in the NIR region arises due to the formation of charge carriers upon oxidation of **P16**. The band gap calculated from the onset π-π* transition is 1.3 eV. All the polymers show absorptions at around 1200 nm in their neutral state which may indicate that the films cannot be fully reduced. Incorporation of the EDOT unit in **P16**, causes a red shift in λ_{max} for that polymer to 720 nm. **P16** has the lowest band gap of all the polymers investigated of 1.3 eV due to the higher HOMO level of the EDOT unit compare to thiophene and 3-hexylthiophene. This can be rationalized by better intermolecular π-π* interaction with decreasing deviation from planarity. The fused thiophene ring helps stabilize the quinoidal form of **P14** as does the EDOT ring (**P16**), thereby leading to a polymer having a band gap lower than that PEDOT (Eg=1.6eV). The higher band gap of **P15** as compared to **P14** can be attributed to the difference in the stability of the quinoidal state by 3-hexylthiophene and thiophene ring, respectively. Meanwhile, the lowest-energy absorption band can be assigned to the intramolecular charge transfer between the donor and acceptor units. Compared with EDOT, thiophene and 3-hexylthiophene exhibit a rather large bathochromic shift (610 and 530 nm, respectively) of the absorption maximum.

The optical change that occurs during the n-doping of the polymer was examined to prove the introduction of charge carries to the conjugated system (Figure 3.10). The reductive absorption spectrum of **P16** was recorded at -1.7 V, which is the cathodic potential of the redox couple observed in the reduced state. **P16** film shows a green color at its neutral state and turned to red-purple at its n-doped state after reduction.

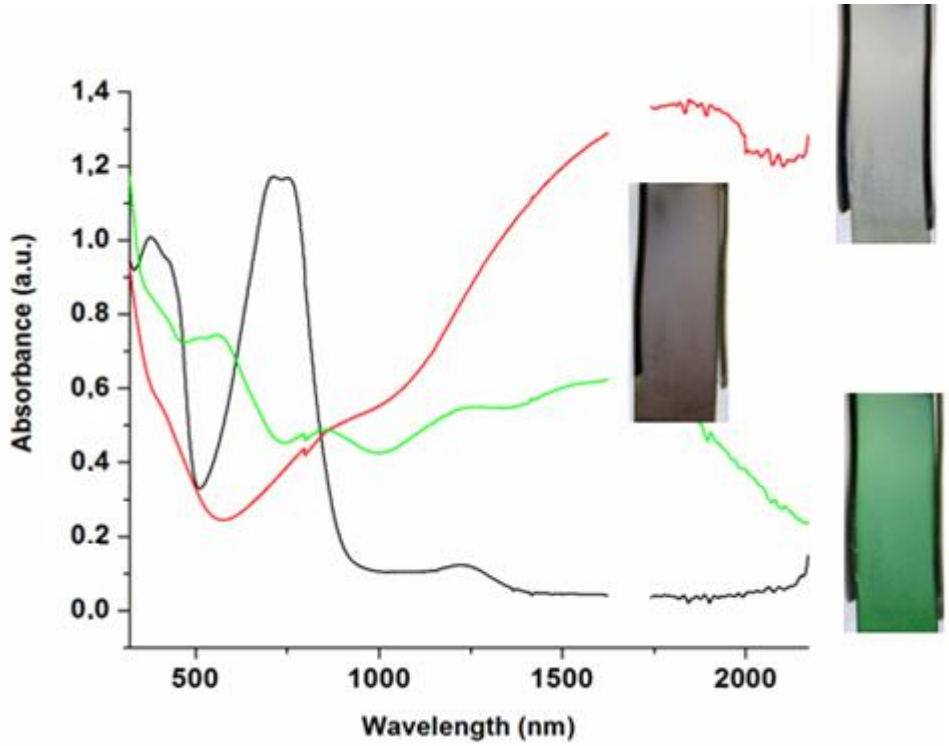

Figure 3.10. n-Doping spectroelectrochemistry of P16 at -0.2 V, -1.7 V and + 1.1. V

3.5.1.3. Electrochromic Switching Studies

Electrochromic switching studies were carried out to obtain an insight into changes in the optical contrast with time during repeated potential stepping between reduced and oxidized states. In these studies, the transmittance (%T) of the polymer films was recorded as a function of time at given wavelengths. Figure 3.11 shows the switching of **P14** between -0.1 V and + 1.3 V with a switching interval of 5 s in 0.1 M $TBABF_4$/ACN at three different wavelengths. In this instance, both the fully oxidized and fully reduced states were reached as evidenced by the leveling off of the optical response. At 395 nm, the optical contrast for **P14** was calculated as 20% and the switching time was 1.2 s. The polymer switches rapidly and achieves 35% and 77% of its total optical change in 0.6 s at 630 and 1560 nm, respectively.

The optical contrast for **P15** was 28% at 530 nm and 80 % at 1640 nm. The polymer revealed a switching time of 1.2 s at 530 nm and 1.5 s at 1640 nm while switched between -0.4 V and + 0.9 V.

P16 was switched from -0.2 V to +1.1 V at 5 s step intervals in 0.1 M $TBABF_4$/ACN while the change in transmittance was monitored. The optical contrasts for **P16** were calculated as 16% at 423 nm, 38% at 738 nm, and 71% at 1780 nm. **P16** revealed switching times of 0.6 s at 423 nm and 738 nm, 1.2 s at 1780 nm (Figure 3.11).

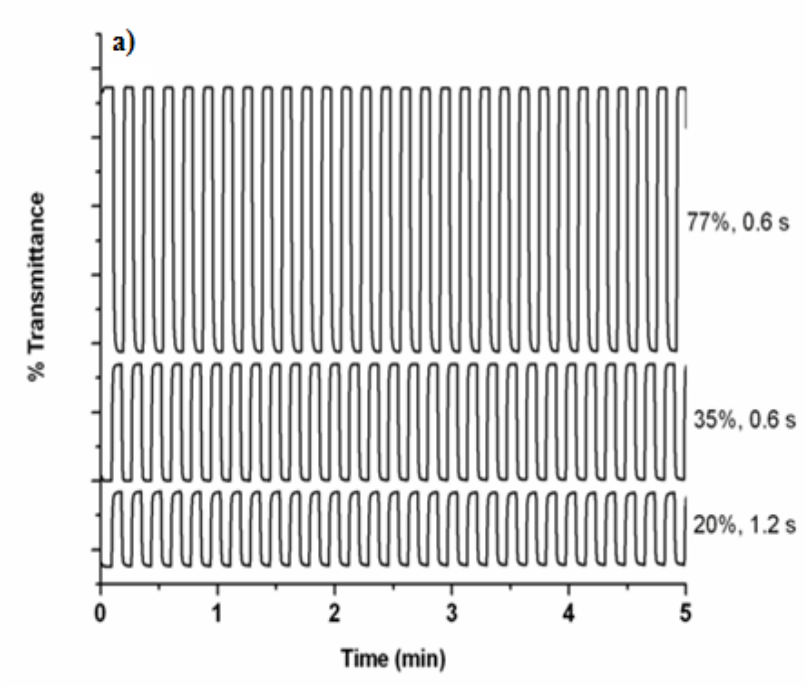

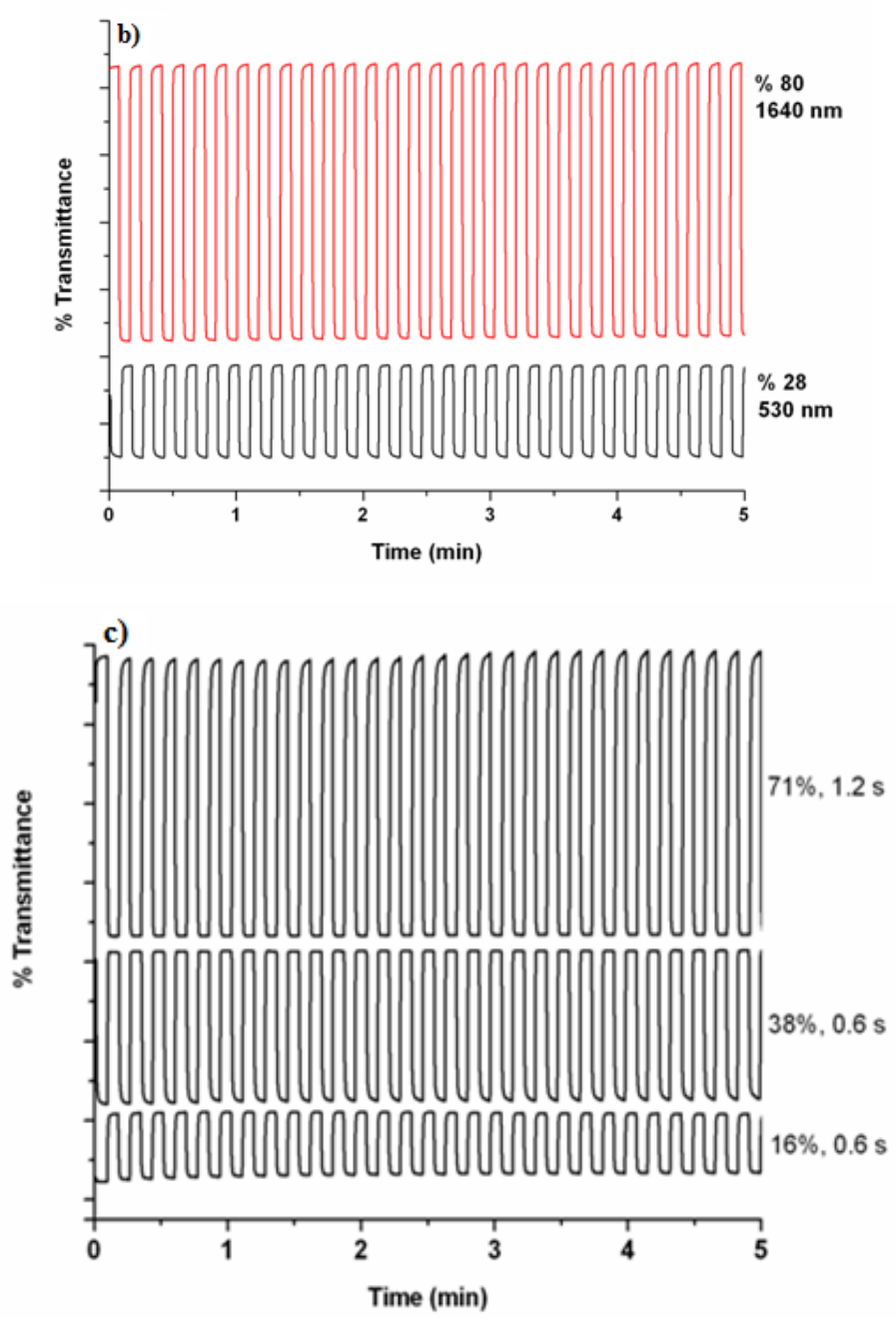

Figure 3.11. Electrochromic switching and optical absorbance change monitored at a) 395, 630 and 1560 nm for P14 in 0.1 M $TBABF_4$/ACN, b) 530 and 1640 nm for P15 in 0.1 M $NaClO_4$/ACN, c) 423, 738 and 1780 nm for P16 in 0.1 M $TBABF_4$/ACN.

3.5.1.4. Colorimetry Studies

The color changes were further investigated by colorimetry using the CIE 1931 Yxy color space to define color precisely. The color coordinates, Y, x, y values, were summarized in Table 3.2. **P14** becomes blue (Y, 470; x, 0.253; y, 0.296) in the neutral state as shown by its dominant wavelength of 610 nm. Upon incremental doping by application of oxidative potentials, **P14** changes to a transmissive gray color (Y, 915; x, 0.302; y, 0.331).

The neutral form of **P15** is red (Y, 20.3; x, 0.468; y, 0.318) in color, having an absorbance peak centered at 530 nm. Stepwise oxidation of the polymer shows that the color changes from red to green (Y, 41.0; x, 0.381; y, 0.419), while purple (Y, 13.8; x, 0.341; y, 0.298) and brown (Y, 22.4; x, 0.387; y, 0.357) color existed at intermediate potentials.

Increase of donor strength by the addition of EDOT group to form **P16** leads to a neutral green color (Y, 486; x, 0.293; y, 0.406) with two well-separated absorption maxima were centered at 423 and 738 nm. Upon oxidation the color changes to transmissive gray oxidized state (Y, 293; x, 0.314; y, 0.339). **P16** film shows a green color at its neutral state and turned to red-purple (Y, 299; x, 0.33; y, 0.34) at its n-doped state after reduction.

Table 3.2. Electrochromic properties of a) P14, b) P15,c) P16

a) Blue (-0.1 V)	Transmissive (+1.3V)
Y: 470 x:0.253 y:0.296	Y:915 x:0.302 y:0.331

b) Red (0.1 V)	Purple (0.5 V)	Brown (0.8 V)	Green(1.0 V)
Y: 20.3 x:0.468 y:0.318	Y: 13.8 x:0.341 y:0.298	Y: 22.4 x:0.387 y:0.357	Y: 41.0 x:0.381 y:0.419

c) Red-Purple (-1.7 V)	Green (-0.2 V)	Transmissive (+1.1 V)
Y: 299 x:0.330 y:0.340	Y:486 x:0.293 y:0.406	Y:293 x:0.314 y:0.339

3.5.2. Dibenzo[*a,c*]phenazine Inserted Quinoxaline Derivatives

3.5.2.1. Electrochemistry

Cyclic voltammetry was used to investigate electroactivity of **17, 18** and electrochemical redox behavior of the resulting polymers, **P17** and **P18**. The electrochemical oxidation of **P17** was carried out in a solution of $1x10^{-2}$ M monomer and 0.1 M $TBAPF_6$ in DCM at a scan rate of 100 mV/s. Electrochemical synthesis of **P18** was carried out in 0.1 M $TBAPF_6$/DCM supporting electrolyte-solvent couple potential scanning between -0.3 V and 1.0 V at a scan rate of 100 mV/s.

Oxidative electropolymerization of **17** was performed in 0.1 M $TBAPF_6$/DCM supporting electrolyte/solvent system at a scan rate of 100 mV/s. An irreversible oxidation wave appeared at 1.1 V vs Ag wire corresponding to the oxidation of monomer, **17** (Figure 3.12). An electroactive polymer film quickly grows on the indium tin oxide (ITO)-coated glass slide which was accompanied with an increase in the current intensity. Redox process of **P17** revealed a new reversible redox couple. Oxidation and reduction peaks centered at +0.87 and +0.80 V for the redox processes for **P17** (Scheme 3.11).

An irreversible anodic wave at 0.86 V vs Ag wire stands for the onset for monomer oxidation, **18** (Figure 3.12). Oxidation of monomer was followed by chemical coupling which leads to the formation of the dimers and the oligomers. These oligomers became insoluble and precipitated onto the electrode surface when the chain length of the oligomers increased. The reduction of the resulting polymer appeared at +0.38 V. Increase in the intensity of current response during subsequent scans indicates the increase in the polymer thickness and the amount of the electroactive material. A new oxidation peak appeared at +0.52 V due to the oxidation of the polymer upon consecutive cycle formation [98].

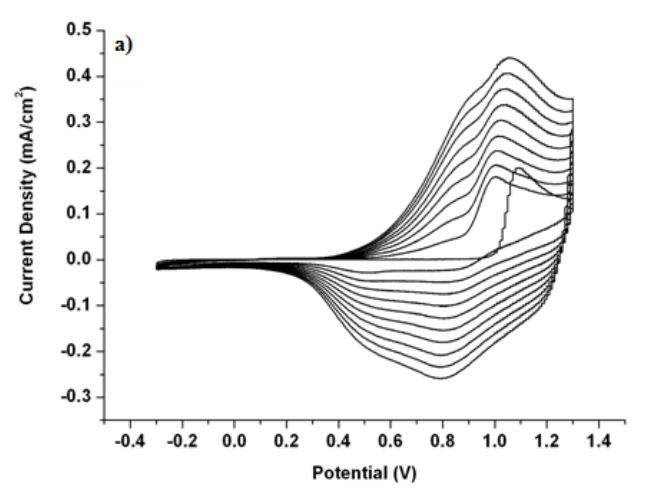

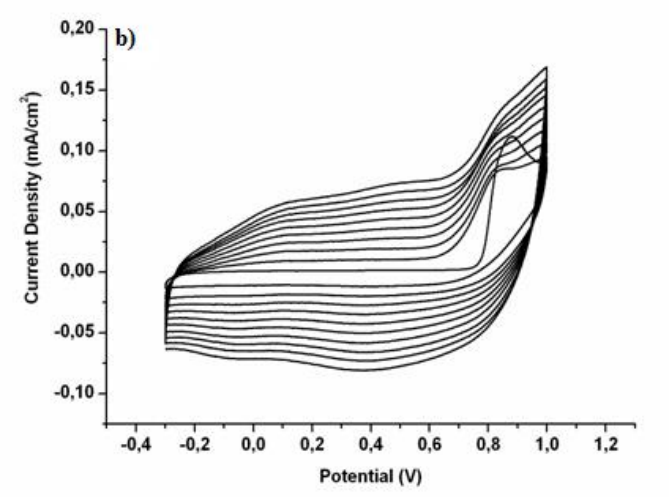

Figure 3.12. Repeated potential scan electropolymerization of a) **17** b) **18** at 100 mV/s in 0.1 M $TBAPF_6$/DCM on the ITO electrode.

Examination of elecetrochemical properties of two quinoxaline based monomers showed that oxidation potential of 3-hexylthiophene based monomer is more positive than that of EDOT derivative. This higher oxidation potential is expected since the terminal 3-hexylthiophene units are not electron-rich as EDOT. Reduction potential of **P18** which was lower than that of **P17** indicated the incorporation of electron-rich EDOT donor into the structure lead to more stabilized reduced state in the resulting polymer.

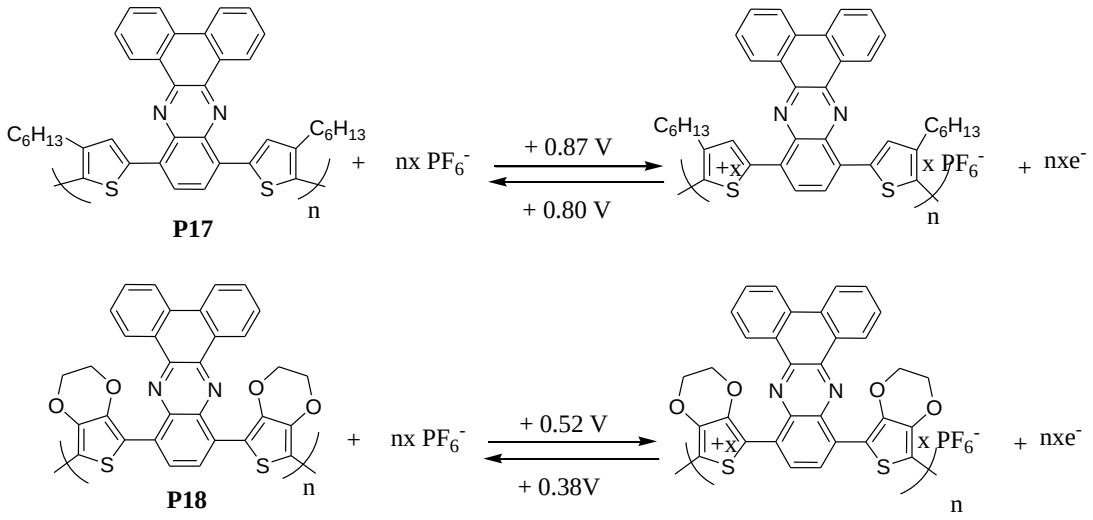

Scheme 3.11. p-Doping of **P17** and **P18**

A linear relationship was found between the peak current and the scan rate. This relationship indicates that the electroactive polymer films were well adhered and the redox processes were non-diffusion limited (Figure 3.13).

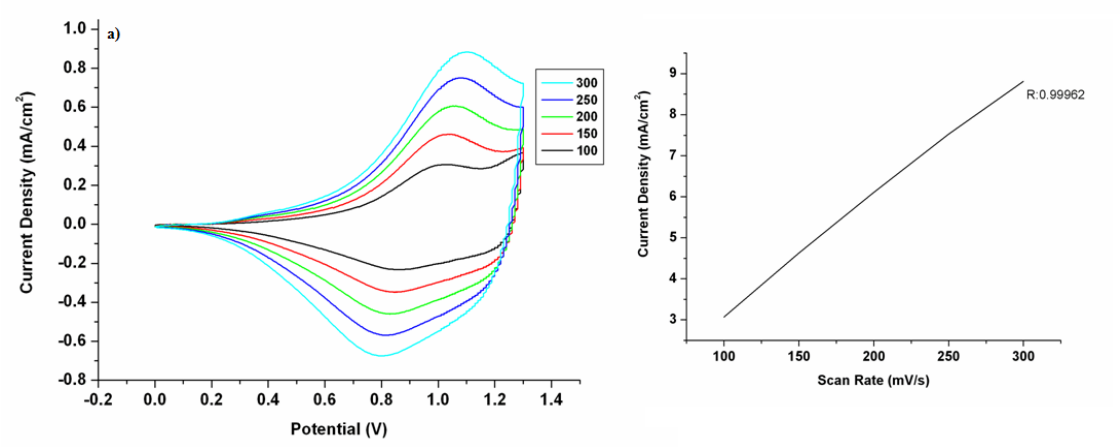

Figure 3.13. Cyclic voltammograms of P17 in 0.1 M $TBAPF_6$/DCM at scan rates of 100, 150, 200, 250 and 300 mV/s.

3.5.2.2. Spectroelectrochemistry

Spectroelectrochemical analysis was performed to examine the electronic structure of **P17** and **P18** using changes in electronic spectra under a voltage pulse. **P17** was electrodeposited onto ITO-coated glass slides potentiodynamically. A series of spectra were collected at various potentials ranging from +0.2 V to + 1.3 V as shown in Figure 3.14.

Polymer film switches between a blue neutral state, a gray intermediate state, and a green oxidized state. Neutral form of **P17** gives rise to π-π* absorption band centered at 570 nm. Band gap for the polymer was determined through the onset of π-π* absorption for the neutral polymer and found to be 1.65 eV. As polymer film was oxidized, the π-π* transition of absorption band was depleted at the expense of strong absorption bands in the NIR which correspond to the two low-energy charge carriers; polaronic state at 950 and bipolaronic state at 1700 nm.

The spectroelectrochemistry of **P18** was depicted in Figure 3.14 as the potential was increased stepwise from -0.3 V to + 1.3 V. **P18** was green at the neutral state. The π-π* transitions of the neutral polymer were split into two main absorption bands at 470 and 790 nm in the visible region as expected from a neutral state green polymer.

Electrochemical oxidation of the polymer resulted in a decrease in the π-π* transitions and in an increase in the transitions at 950 and 1600 nm which were characteristic of low energy charge carriers polaron and bipolaron, respectively. Since the polymer has two absorption bands in its neutral state, the optical bandgap was determined from the onset of the lower energy π-π* transition in the spectrum as 1.10 eV and therefore, this polymer meets the defined criterion for being a low band gap polymer. The difference between the band gaps of **P18** and PEDOT (Eg=1.6 eV) was 0.5 eV. The introduction of electron-accepting group results in a shift of the absorption onset towards longer wavelength compared to PEDOT underlines the effect of the acceptor moiety on the HOMO-LUMO gap of the molecule.

Although the backbone structure is the same, the optical properties of **P17** and **P18** are different with the variation of substitution. Π-Π* transition and low-energy absorption bands (polaronic and bipolaronic states) of **P17** show a blue shift compared to those of **P18**, indicating the presence of alkyl side chains on thiophene units lower the coplanarity between the benzene and thiophene rings. Thus the effective conjugation in the polymer decrease and maximum absorption band is blue shifted by 100 nm. Band gap of the hexyl-substituted polymer estimated from absorption onset wavelengths were 0.55 eV higher than that of the corresponding ethylenedioxy-substituted polymers. Replacement of ethylenedioxy unit on the thiophene ring with hexyl group may lead to decrease in the effective conjugated length in polymers by increasing the torsional angles between thiophene rings and benzene. Thus spectral results were blue shifted in the resulting polymers.

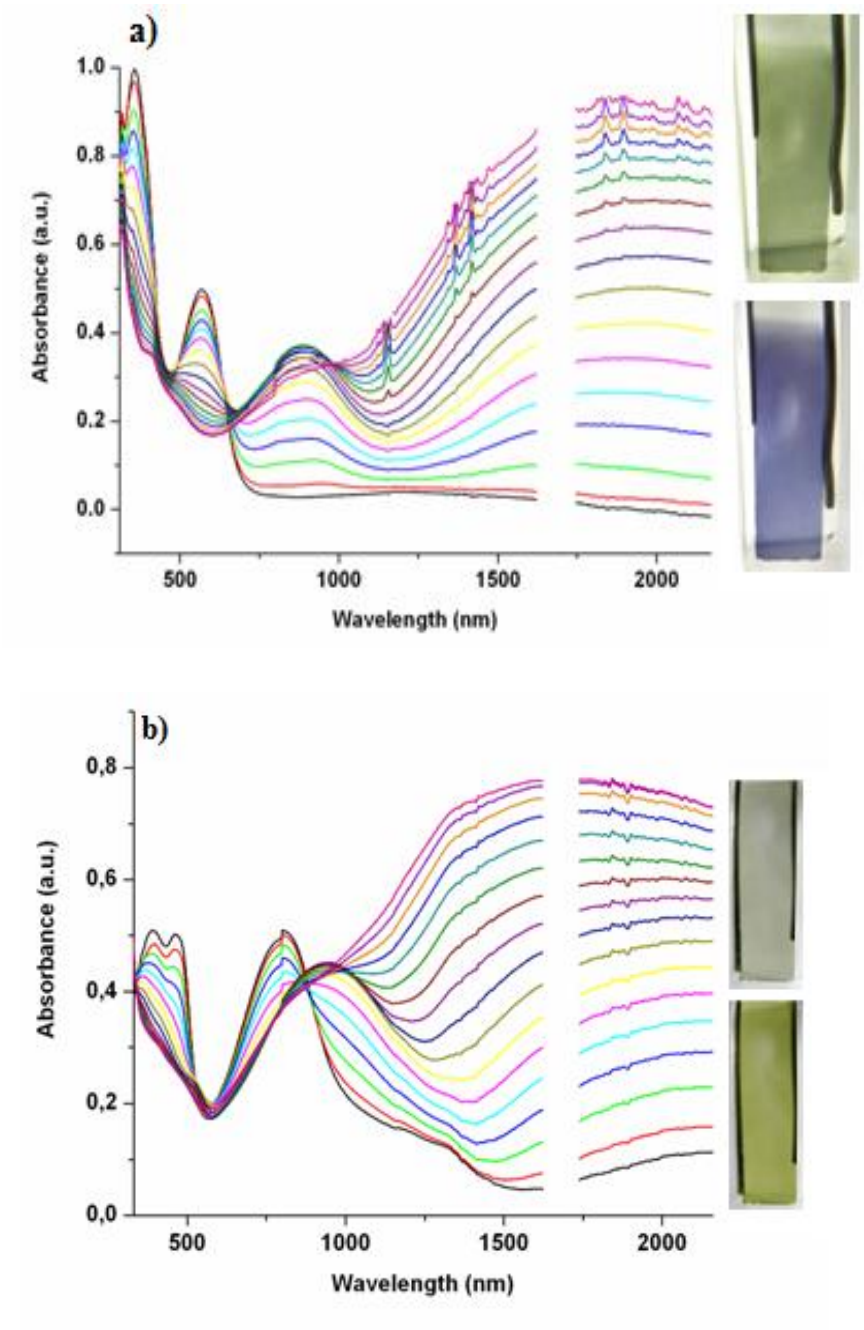

Figure 3.14. a) p-doping spectroelectrochemistry of P17 film on an ITO coated glass slide in monomer free, in 0.1 M $NaClO_4$/ACN electrolyte-solvent couple at applied potentials, b) p-doping Spectroelectrochemistry of P18 film on an ITO coated glass slide in monomer free, 0.1 M $TBAPF_6$/DCM electrolyte-solvent couple at applied potentials.

Table 3.3. Effects of changes in π-system of the central aromatic group on the absorption onset and electronic band gap of the resulting polymers

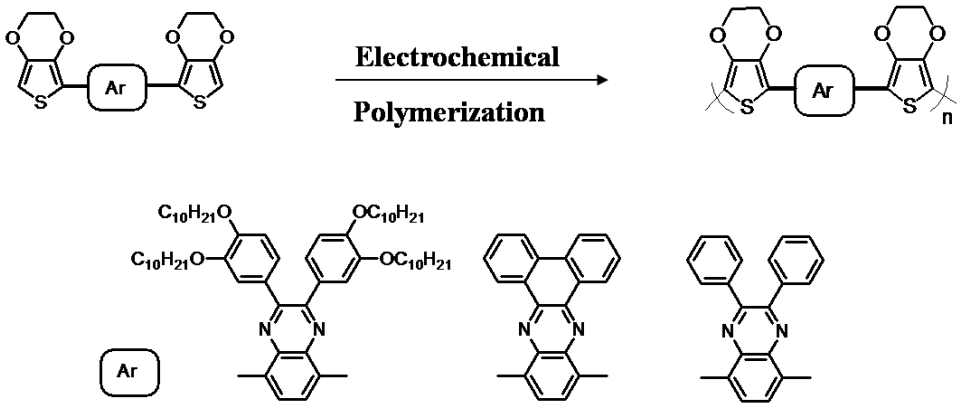

	I	II	III
λ_{max}(nm)	415 690	470 790	448 732
Eg(eV)	1.45	1.1	1.01

Electron-accepting property of the π-conjugated system of the central aromatic group **II** was compared with **I** [99] , and **III** [100] (Table 3.3). Differences in the intermolecular interaction between π-electrons led to shift of the absorption bands. Absorption bands of the alkoxy substituted analogous shifted to the blue since the coplanarization of the π-conjugated system decreased with the substitution of long alkyl chain on the acceptor unit. Insertion of dibenzo[a,c]phenazine acceptor unit in π-conjugated system increased rigidity thus better intermolecular interaction led to obtain lower band gap than that of the alkoxy substituted analogous. All these D-A-D type π-conjugated polymers are neutral state green polymer with two absorption bands around 400 and 700 nm as expected.

3.5.2.3. Electrochromic Switching

For electrochromic materials it is very important to switch rapidly between redox states and exhibit remarkable color change. The switching time of the polymer film is defined as the time needed to switch between the two extreme redox states of the polymer. In order to analyze the switching characteristics of the polymer film, the variation in percent transmittance at the wavelength of maximum contrast was monitored during repeated redox stepping experiments. In this experiment, the potential was set at an initial potential for a given period of time, and was stepped to a second potential for the same period of time before being switched back to the initial potential. Figure 3.15 shows the switching study of **P17** film when the potential is stepped between + 0.2 V and +1.3 V at 5 s step intervals in 0.1 M $TBAPF_6$/DCM at 570 nm and 1850 nm. **P18** film was switched by stepping the potential between –0.3 V and + 1.3 V with a switching interval of 5 s in 0.1 M $TBAPF_6$/DCM electrolyte-solvent system while the transmittance was measured at 470 nm, 790 nm and 1600 nm.

The percent transmittance (T %) at different wavelengths together with the λ_{max} of **P18** were measured. The optical contrast was found to be 27 % at 470 nm in 0.9 s. A transmittance value of 16 % was calculated with respect to the minimum absorption point on the absorption spectra of the polymer at 790 nm in 1.2 s. **P18** film showed 80% optical contrast and switched in 1.4 s at 1600 nm. The switching time was calculated at 95% of the full switch as is the common trend in literature.

P17 film showed 93% transmittance at the oxidized state and a 3% transmittance at the neutral state with an outstanding optical contrast of 90% in the NIR region which is 10% higher than **P18**. The high optical contrast (90%) at 1850 nm in less than 1 s makes this material a good candidate for NIR device applications. It reveals nearly 31% optical contrast with a switching time of 1.5 s.

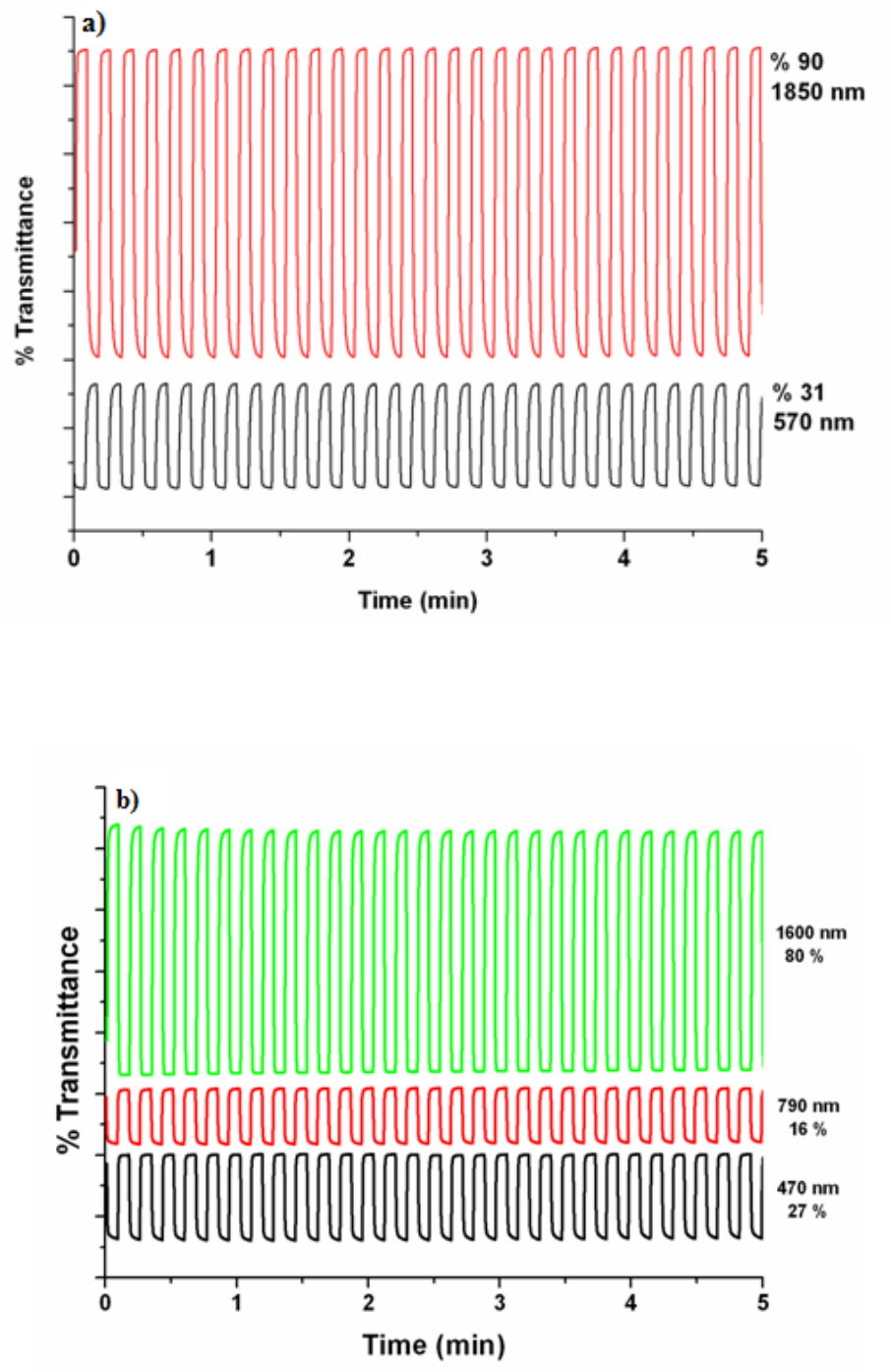

Figure 3.15. Electrochromic switching, optical absorbance change monitored at a) 570 and 1850 nm for P17 b) 470, 790 and 1600 nm for P18 in 0.1 M $TBAPF_6$/DCM.

3.5.2.4. Colorimetry

The range of color attainable from each polymer has been quantified by colorimetry using the CIE 1931 Yxy color space. The specific color states for the neutral and oxidized forms of each polymer are listed in the form of Yxy coordinates. **P17** shows multicolored electrochromic behavior with three distinct colors: blue (Y: 29.6, x:0.269, y:0.281) at -0.3V, gray (Y:41.2, x:0.351,y:0.372) at + 0.9 V, green (Y:36.2, x:0.345 y:0.409) at 1.3 V. **P18** reflects green light (Y: 71.398, x: 0.3500, y: 0.468) in the neutral state and is neutral blue-gray (Y: 86.099, x: 0.332, y: 0.379) in the oxidized state.

Table 3.4. Electrochromic properties of a) P17, b) P18.

a) Blue (-0.3 V)	Gray (+ 0.9 V)	Green (+ 1.3 V)
Y: 29.6 x:0.269 y:0.281	Y:41.2 x:0.351 y:0.372	Y:36.2 x:0.345 y:0.409

b) Green (-0.3 V)	Blue-Gray (+1.3V)
Y: 71.398 x:0.3500 y:0.4680	Y:86.099 x:0.332 y:0.379

3.6. Dipyrido[3,2-*a*:2,3-*c*]phenazine Inserted Quinoxaline Derivative

3.6.1. Electrochemistry

The new quinoxaline analogue, **21** exhibits redox behavior typical of the previous quinoxaline derivatives. The redox behavior of the monomer was examined using cyclic voltammetry. The electrochemical oxidation of the monomer was carried out in a solution of $1x10^{-2}$ M monomer and 0.1 M $TBAPF_6$ in DCM at a scan rate of 100 mV/s. **P21** was synthesized on indium tin oxide (ITO) coated glass slides by oxidative electropolymerization.

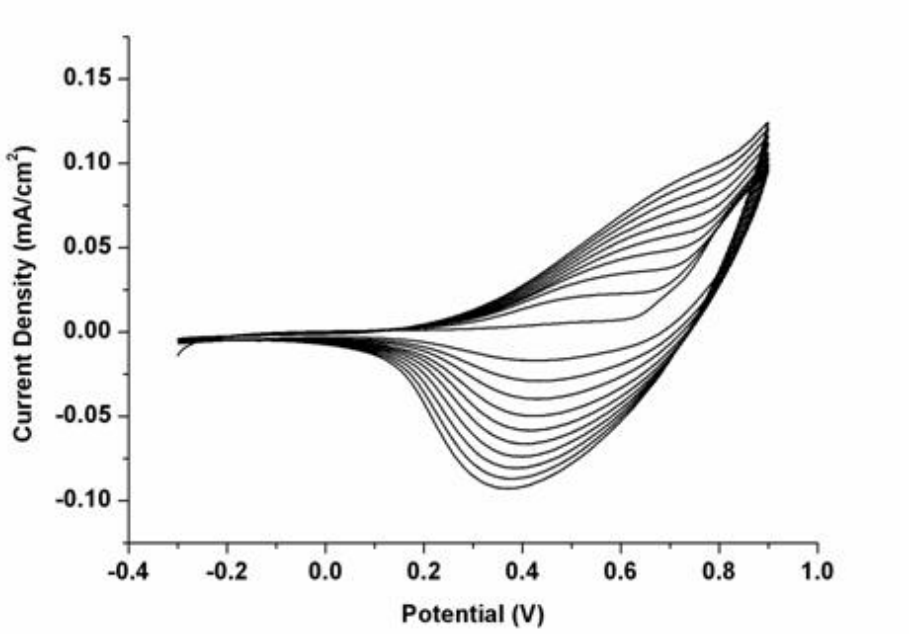

Figure 3.16. Repeated potential scan electropolymerization of 21 at 100 mVs^{-1} in 0.1 M $TBAPF_6/CH_2Cl_2$ on an ITO electrode

The cyclic voltammogram of **21** exhibits an irreversible oxidation wave at 0.85 V vs Ag wire (Figure 3.16). Following the monomer oxidation, an electroactive polymer film quickly grows on the indium tin oxide (ITO)-coated glass slide revealing new

reversible redox couple and accompanying increase in the current intensity.The redox processes for **P21** include oxidation and reduction peaks centered at +0.75 and +0.37 V (Scheme 3.12).

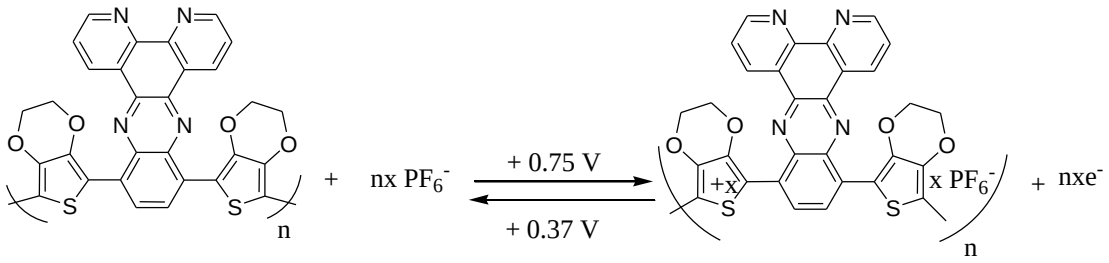

Scheme 3.12. p-Doping of **P21**

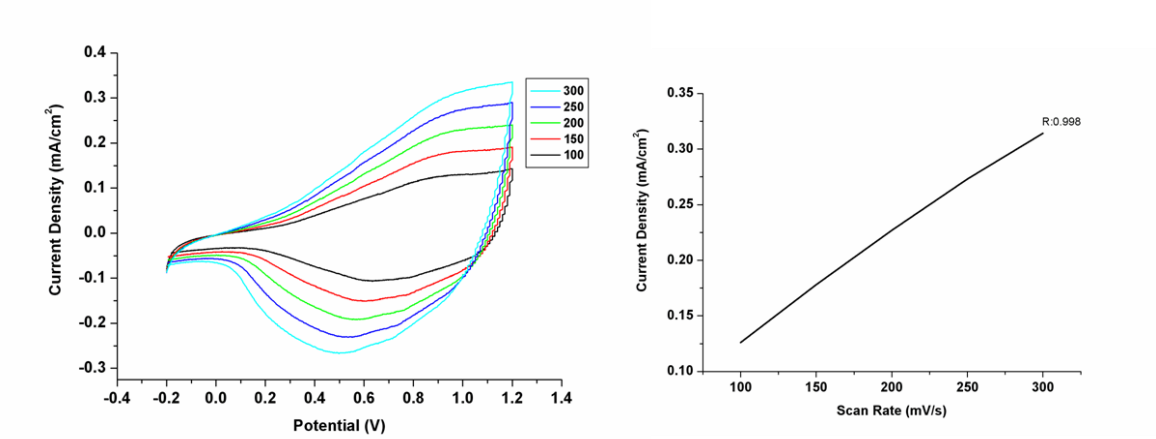

Figure 3.17. Cyclic voltammograms of P21 in 0.1 M $TBAPF_6$/DCM at scan rates of 100, 150, 200, 250 and 300 mV/s.

The scan rate dependence of the anodic and cathodic peak currents was studied in a monomer-free electrolyte solution (Figure 3.17). A linear relationship between the peak current and scan rate demonstrates that the films were well adhered and the electrochemical processes are reversible and non-diffusion-controlled.

3.6.2. Spectroelectrochemistry

Spectroelectrochemical analysis was performed to evaluate the optical properties of the electrochromic polymer, **P21**. Figure 3.18 shows the spectroelectrochemical series for p-doping between -0.3V and + 1.2 V. The neutral form of the polymer is brick red in color, having an absorbance peak centered at 820 nm. Stepwise oxidation of the polymer shows that the intensity of π-π* transition decreased as the color changes from brick red to gray, while passing through three intermediate states; orange, brown, green. Upon oxidation, new absorption bands which correspond to polaron and bipolaron species are built at 1250 and 1600 nm, respectively. The band gap (Eg), defined as the onset of the π-π* transition of the neutral **P21** film, was calculated to be 1.0 eV.

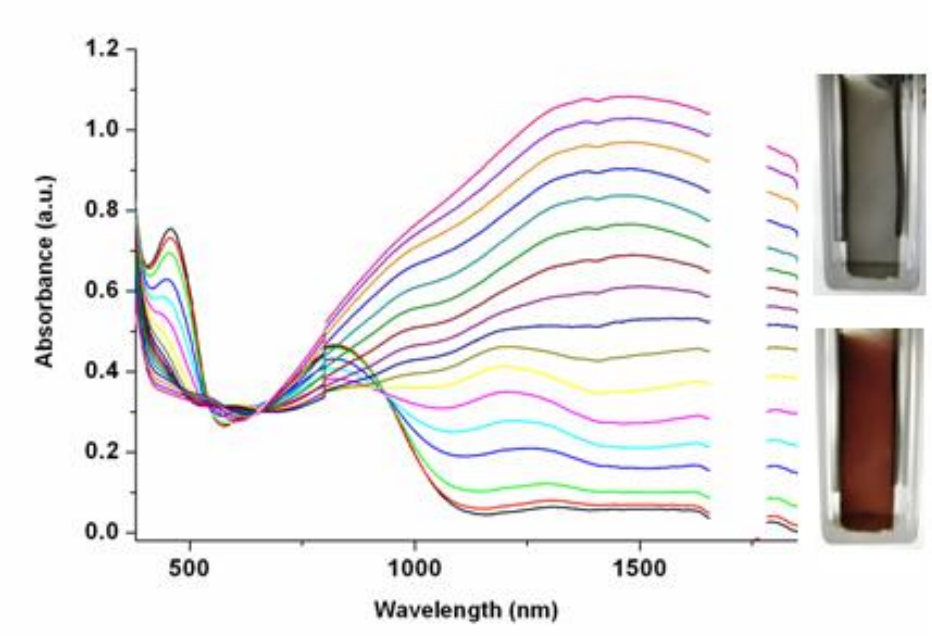

Figure 3.18. p-Doping spectroelectrochemistry of P21 film on an ITO-coated glass slide in monomer-free, 0.1 M $TBAPF_6$/DCM electrolyte–solvent couple at applied potentials.

In the neutral state the polymer film showed an absorption maxima at 820 nm which is red shifted by about 90 nm compared to the analogous polymer, PDPEQ **(II)** (λ_{max}=732 nm) [99]. This suggests that optical properties of **P21** are controlled by inductive effects rather than by delocalization along the polymer backbone. A considerable longer wavelength reflects a higher order of contribution of the charge-transferred structure in the electronic state of **16** due to its strong electron-accepting property. Electron-accepting property of the π-system of the central aromatic group **IV** was compared with **I** [101], **II** [100] and **III** [102] with respect to the number of electron-withdrawing imine(C=N) groups (Table 3.5). It can be concluded that the increase in the number of imine groups leads to a bathochromic shift.

Table 3.5. Effects of changes in π-system of the central aromatic group on the absorption onset and electronic band gap of the resulting polymers

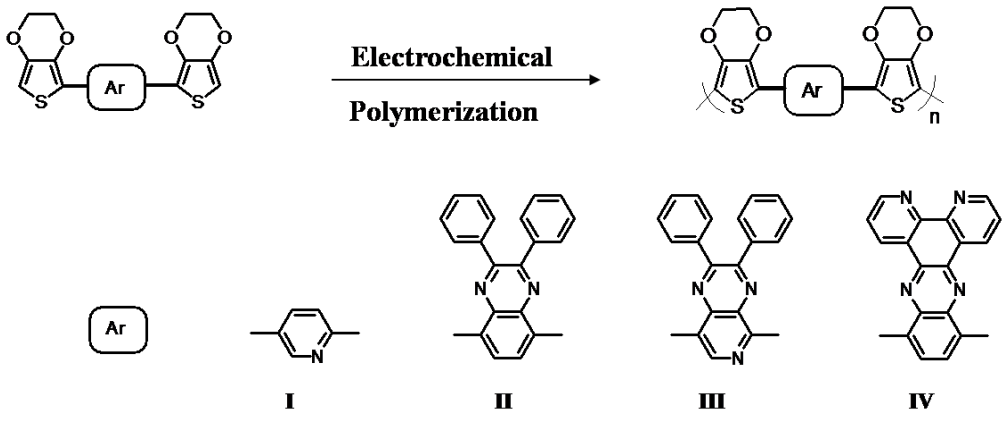

	I	II	III	IV
λ_{max}(nm)	478	732	750	820
Eg (eV)	1.9	1.01	1.2	1.0

3.6.3. Electrochromic Switching Studies

Electrochromic switching studies were performed to monitor the switching ability of the polymer. A square wave potential step method coupled with optical spectroscopy was used to probe switching times and contrast in the polymer. In this double potential step experiment, the potential was set at an initial potential (-0.3 V) for 5 s, and was switched to a second potential (+1.2 V) for 5 s before being switched back to the initial potential (-0.3V) again. The % transmittance was then monitored while the polymer was switched between -0.3 V and + 1.2 V with a switching interval of 5s in 0.1 M $TBAPF_6$/DCM at two different wavelengths (Figure 3.19). The optical contrast, measured as the difference in %T between the reduced and oxidized forms was determined as 34% at 460 nm.

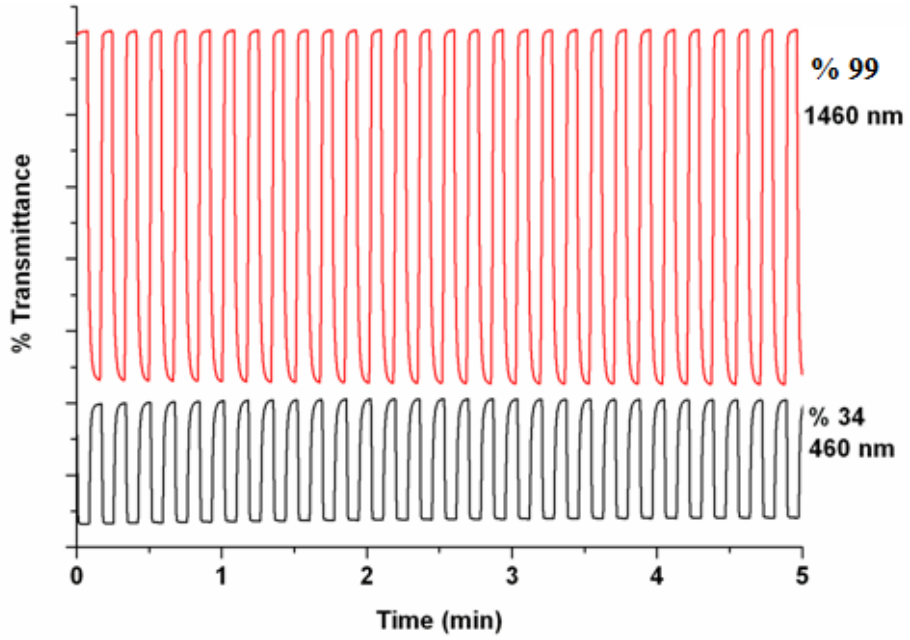

Figure 3.19. Electrochromic switching and optical absorbance change monitored at 460 nm and 1460 nm for P21 in 0.1 M $TBAPF_6$/DCM

An excellent optical contrast of 99 % in the NIR region (1460 nm) is a very significant property to be considered as an active electrochromic material for NIR applications. Response time on electrochromic switching of the polymer film between its neutral and oxidized states was also monitored. **P21** has a switching time of 1.8 s at 460nm. The polymer achieves an outstanding optical contrast of 99 % in the NIR region in only 1 s.

3.6.4. Colorimetry

Significant changes in absorption characteristics upon p-doping demonstrate the electrochromic properties of **P21**. Colorimetry analysis identify the color changes observed upon oxidation; the polymer is brick red at the reduced state (-0.3 V), gray at the oxidized state (+1.2 V) with three intermediate states; orange (+0.4 V), brown (+0.70 V), green (+0.85 V). The Commission Internationale de l'Eclairage (CIE) system was used as the quantitative scale to define and compare colors. The color coordinates, Y, x, y values, were measured and summarized in Table 3.6.

Table 3.6. Electrochromic properties of P21

Brick Red (-0.3 V)	**Orange (+0.4 V)**	**Brown (+0.7 V)**	**Green (+0.85 V)**	**Gray (+1.2 V)**
Y: 22.3 x:0.421 y:0.352	**Y: 32.2 x:0.464 y:0.424**	**Y: 32.6 x:0.438 y:0.432**	**Y: 32.6 x:0.365 y:0.423**	**Y: 31.5 x:0.312 y:0.335**

3.7. Thienopyrazine Derivative

3.7.1. Cyclic Voltammetry

The reversibility and relative potentials of the redox processes in this π-conjugated terthienyl system were examined in 0.1 M $TBAPF_6$/DCM solvent-electrolyte couple. Electrochemical polymerization of **26** was achieved using cyclic voltammetry by sweeping the potential between -0.2 V to +0.8 V at 100 mV/s. The voltammogram of **26** exhibits an irreversible oxidation wave at 0.56 V vs Ag wire (Figure 3.20).

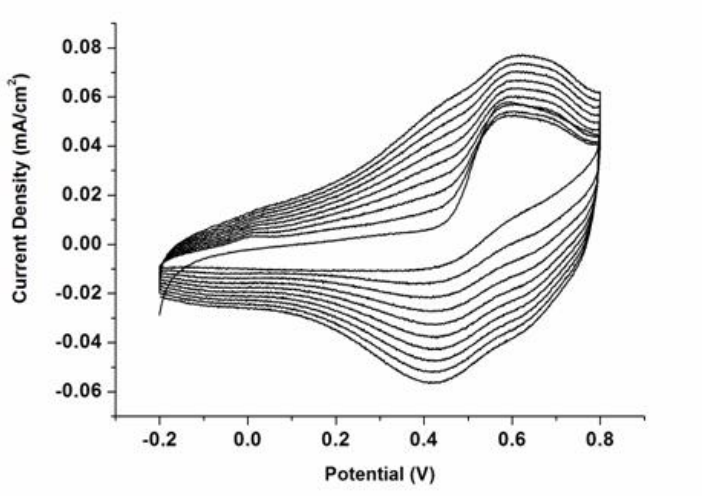

Figure 3.20. Repeated potential scan electropolymerization of P26 at 100 mV/s in 0.1 M $TBAPF_6$/DCM on ITO electrode.

Following the monomer oxidation, an electroactive polymer film quickly grows on the indium tin oxide (ITO)-coated glass slide revealing new reversible redox waves including oxidation and reduction peaks centered at +0.42 and +0.41 V, respectively (Scheme 3.13).

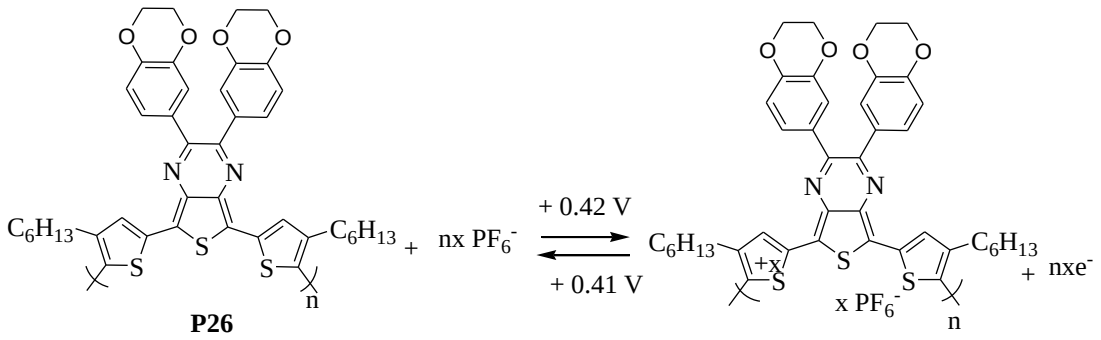

P26

Scheme 3.13. p-Doping of **P26**

3.7.2. Spectroelectrochemistry

Spectroelectrochemistry experiments were performed to investigate the optical changes of each of the π-conjugated terthienyl systems due to the formation of positively charged carriers upon electrochemical oxidation (p-type doping). Spectroelectrochemical studies of **P26** was performed in 0.1 M $TBAPF_6$/DCM electrolyte-solvent couple at applied potentials between -0.2 V and +0.8 V. The evolution of the electronic band structure during electrochemical p-doping of the polymers were recorded as a function of applied potential and shown in Figure 3.21. The ethylenedioxy pendant groups on phenyl rings affect not only the monomer oxidation and the polymer redox couple potentials but also the maximum absorption wavelengths of the corresponding transitions. For the neutral **P26**, two main absorptions were observed in the visible region at 410 nm and 751 nm. These absorption bands decrease as the doping proceeds and therefore this polymer meets the defined criteria for being a green polymer. The onset of the absorption edge gives the band gap for the π-conjugated terthienyl system, 1.0 eV. As the applied potential increased, new absorption bands which correspond to the formation of radical cations (polarons) and further dications (bipolarons) were observed at longer wavelength than the ones associated with the π-π* transitions.

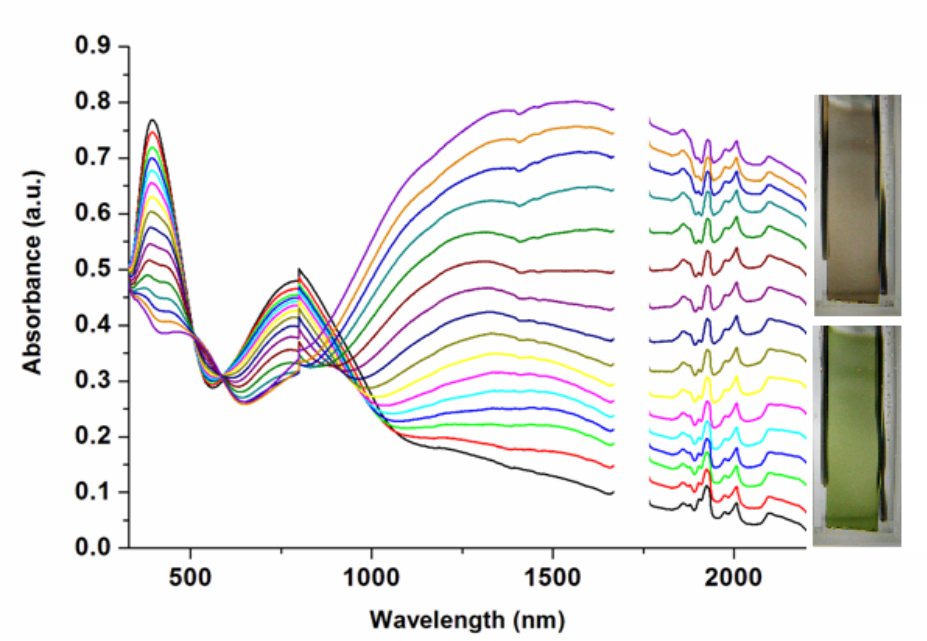

Figure 3.21. p-Doping spectroelectrochemistry of P26 film on an ITO coated glass slide in monomer free, 0.1M $TBAPF_6$/DCM electrolyte-solvent couple at applied potentials.

3.7.3. Electrochromic Switching Studies

Electrochromic switching studies were carried out to monitor the switching ability and changes in the optical contrast of the polymer with time during repeated potential stepping between neutral and oxidized states. In these studies, the transmittance (%T) of the polymer films was recorded as a function of time at given wavelengths (Figure 3.22). The contrast is given as the difference between T % in the neutral and oxidized states and reported as ΔT%. **P26** was switched from -0.2 V to + 0.8 V at 5 s step intervals in 0.1M $TBAPF_6$/DCM while the change in transmittance was monitored. The optical contrasts for the polymer were calculated as 22% at 410 nm, 22% at 751 nm, and 70% at 1550 nm. The polymer revealed switching times of 0.6 s at 410 nm and 751 nm, 1.2 s at 1550 nm.

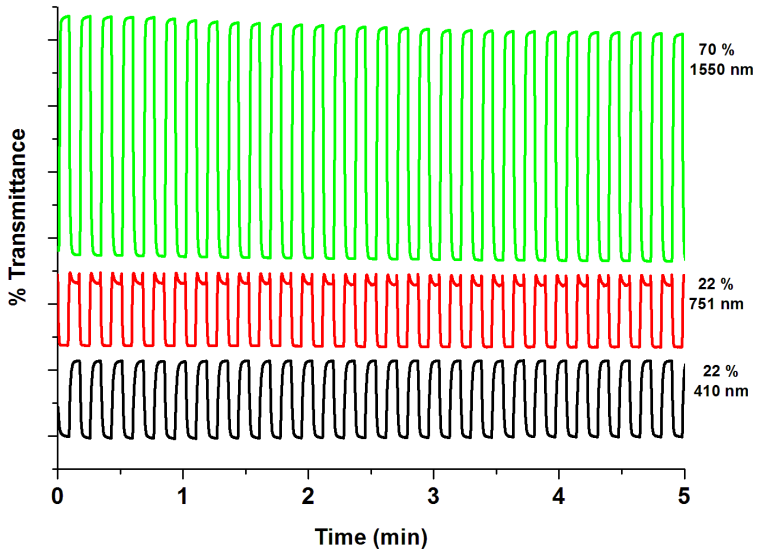

Figure 3.22. Electrochromic switching and optical absorbance change monitored at 410 nm, 751 nm and 1550 nm for P26 in 0.1M $TBAPF_6$/DCM.

3.7.4. Colorimetry

The change in optical properties that results from the redox switching of conjugated polymers was further examined through colorimetry using the Commission Internationale de l'Eclairage (CIE) 1931 Yxy color space. Colorimetry studies are performed to define the color of the polymer film in an objective and quantitative practice based on the CIE system. The color coordinates, Y, x, y values, were measured and summarized in Table 3.7.

Colorimetry analysis identifies the changes in the multi-colored **P26** observed upon oxidation; the polymer is dark green at the neutral state (-0.1 V), a brown intermediate state (+0.5V), and a violet-brown oxidized state (+0.9V).

Table 3.7. Electrochromic properties of P26

-0.1 V	0.5 V	1.3 V
Y:51.4 x:0.322 y:0.429	Y:41.4 x:0.342 y:0.360	Y:51.9 x:0.328 y:0.339

3.8. Electrochromic Device

3.8.1. Spectroelectrochemistry of ECD

A dual polymer ECD was constructed using **P18** as the anodically coloring polymer, and PEDOT as the cathodically coloring polymer [98]. ECD construction was carried out with on **P18** oxidatively doped while PEDOT was neutral. Application of voltage neutralizes the doped **P18** with concurrent oxidation of complementary polymer PEDOT. Spectroelectrochemical studies were performed to examine the optical properties of the ECD's that occur upon doping or dedoping process (Figure 3.23).

The alternation of the color from green to blue was observed upon stepwise increase of the potential from -1.8 V to 1.8 V. When a negative voltage (- 1.8 V) was applied to **P18** layer, the polymer film had a green color at 460 nm. At this point, cathodically coloring material, PEDOT, was in its oxidized state, revealing a transparent sky blue color.

When the voltage was stepwise increased to +1.8 V, **P18** layer started to get oxidized and intensity of peak at 610 nm increased. At this voltage, the PEDOT layer was reduced revealing a blue color.

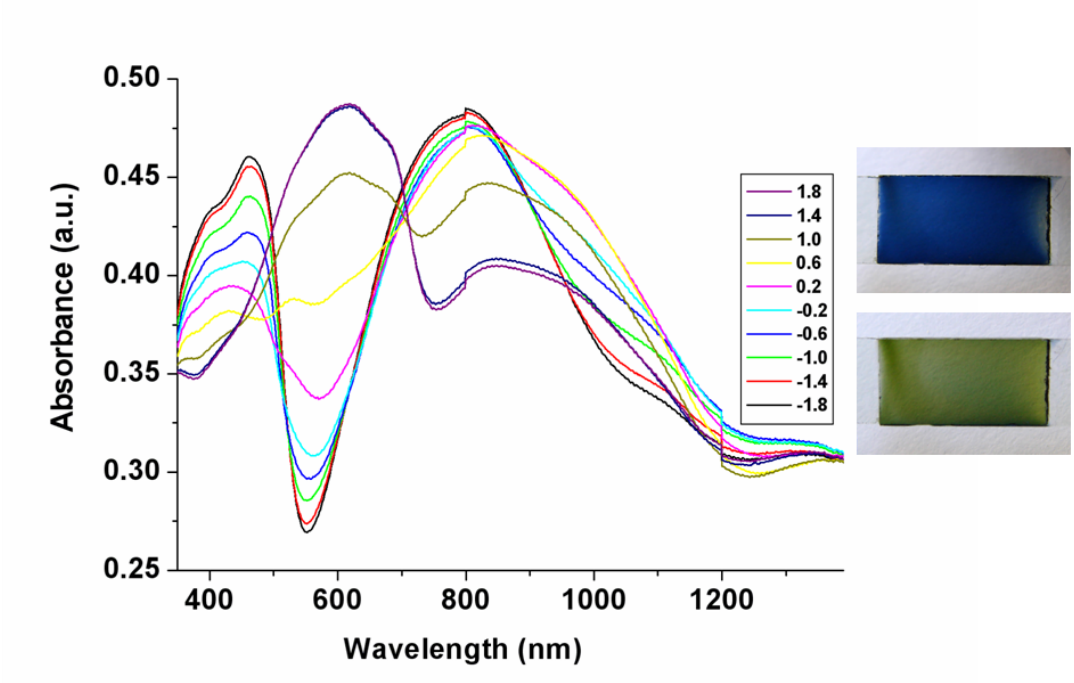

Figure 3.23. Optoelectrochemical spectrum of P18/PEDOT device

3.8.2. Electrochromic switching studies of ECDs

The switching characteristics of ECD were analyzed by monitoring the change in the transmittance during repeated redox switching experiments (Figure 3.24). Switching between square wave potentials of -1.8 V and 1.8 V with a residence time of 5 s, the optical contrast (T %) at 610 nm was found 18 % with less than 0.3 s switching time. The percentage transmittance was found to be 10 % for 460 nm with a fast switching time of approximately 0.6 s. These switching times are much better than the performances of similar devices.

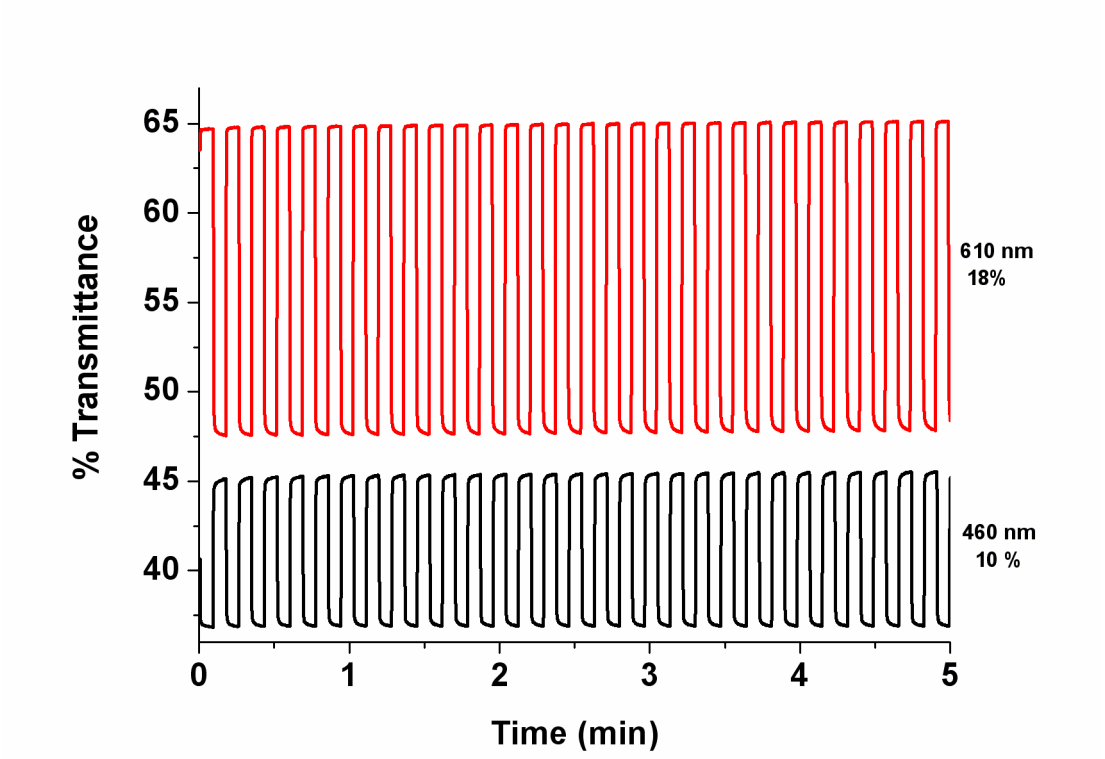

Figure 3.24. Electrochromic switching, optical absorbance monitored for P18/PEDOT device.

3.8.3. Open circuit memory

Open circuit memory is defined as the ability of an ECD to maintain its color whiles the current is off. The color persistence in the ECDs is a significant character since it is directly related to aspects involved in its utilization and energy consumption during application. In order to examine open circuit memory of the device, experiments were carried out by polarizing the device in the green/blue states by an applied pulse for 1 s and then holding at open circuit conditions for 200 s. Simultaneously the optical spectrum as a function of time was recorded (Figure 3.25).

When polarized in the green colored state (-1.8 V), the optical contrast of the device (63 %) decreases to 57 %. after 200 s. There is about 6% loss in optical contrast under open circuit conditions. Moreover, the device was more stable in blue colored state (+1.8V) as given by 3% decrease in the optical contrast. A reasonable optical memory in blue colored state was observed under open circuit conditions.

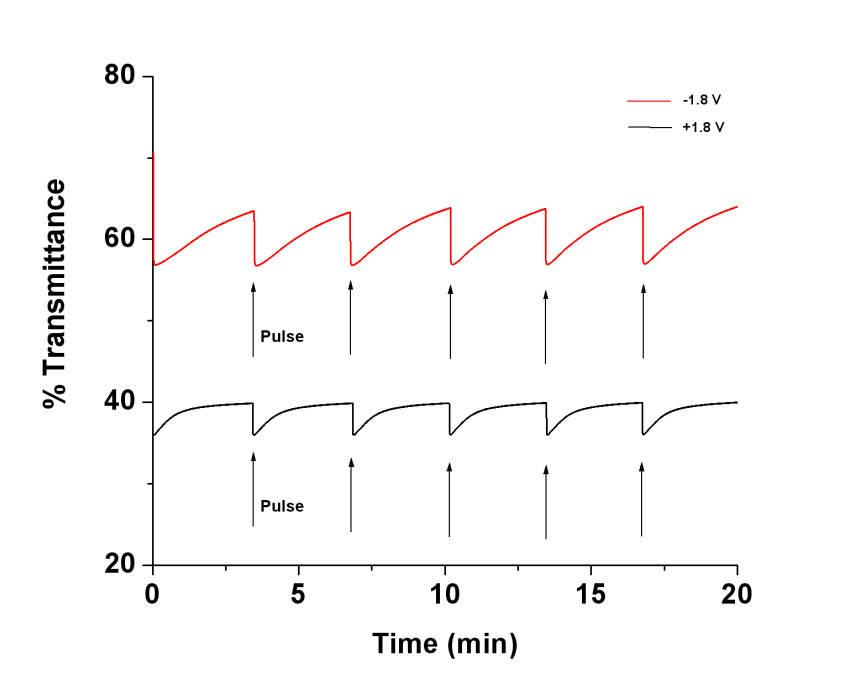

Figure 3.25. Open circuit memory of P18/PEDOT device monitored at −1.8 V and +1.8 V potentials were applied for one second for each 200 s time interval.

CHAPTER 4

CONCLUSION

Π-Conjugated monomers composed of aromatic donor and o-quinoid acceptor units were prepared via Stille coupling method. The polymers of the corresponding D-A-D type monomers were synthesized by electrochemical methods. Cyclic voltammetry experiments, spectroelectrochemistry and kinetic studies for all the polymers were performed in order to investigate the electrochemical and electrochromic properties. The different structures of the polymers due to the differences in donor/acceptor moiety affect not only the monomer oxidation and the polymer redox couple potential but also the maximum absorption wavelengths of the corresponding transition.

Target monomers based on 2-(2,3-dihydrobenzo[b][1,4]dioxin-5-yl)-3-(2,3-dihydrobenzo[b][1,4]dioxin-8-yl)quinoxaline as the common acceptor unit were synthesized to understand the effects of donor strength on the optoelectronic and redox properties of the resulting electropolymerized materials. The electrochemical cyclic voltammograms of the polymers showed a distinct reversible redox peaks. A stronger donor EDOT unit with the quinoxaline derivative as an acceptor unit had lower band gap relative to the thienyl derivative. The introduction of alkyl substituent on polymer causes steric hindrance, resulting in less order and less conjugation by the blue shift in absorption spectra and the increase in polymer's band gap.

The spectroelectrochemical analysis showed that the use of fused aromatics as an acceptor unit resulted in a shift in the onset of the π-π* transition towards longer wavelengths. These results confirmed that the rigidification of the π-conjugated system constitutes an efficient strategy for band gap reduction.

Ethylenedioxybenzene functionalized thieno[3,4-b]pyrazine was synthesized as precursors to investigate the effect of changes in π-conjugated terthienyl system on the electronic and optoelectronic properties of the resulting polymers. The terthienyl system lowered the band gap value from 1.8 eV to 1.0 eV. Thieno[3,4-b]pyrazine unit provides a more planar backbone between repeating units due to less steric hindrance of the thiophene compared to the benzene ring in quinoxaline derivative. In addition, the fused-ring thienopyrazine unit allowed fine-tuning of the polymer band gap due to the enhanced π-π stacking between the polymeric chains.

In conclusion, all these results showed that electrochemical and optoelectrochemical properties of the π-conjugated polymer can be fine-tuned by changing the nature of acceptor and donor moieties.

REFERENCES

[1] H. Letheby, J. Chem. Soc. 15 (1862) 161.

[2] P. M. Shumbula, MS Thesis, University of the Western Cape, 2005.

[3] W. H. Jr. Watson, W. C. Jr. McMordie, L. G. Lands, J. Polym. Sci. 55 (1961) 137.

[4] M. Hatano, S. Kambara, S. Okamoto, J. Polym. Sci. 51(1961) S26.

[5] F. D.Kleist, N. R. Byrd, J. Polym. Sci., Polym. Chem. Ed. 7 (1969) 3419.

[6] H. Shirakawa, T Ito, S. Ikeda, Makromol. Chem. 179 (1978) 1565.

[7] H. Shirakawa, E. J. Louis, A. G. MacDiarmid, C. K. Chiang, A. J. Heeger, J. Chem. Soc., Chem. Commun. (1977) 578.

[8] A. F. Diaz, K. K. Kanazawa, G. P. Gardini, J. Chem. Soc., Chem. Commun. (1979) 635.

[9] A. G. MacDiarmid, Angew. Chem. Int. Ed. 40 (2001) 2581.

[10] K. K. Kanazawa, A. F. Diaz, R. H. Geiss, W. D. Gill, J. F. Kwak, J. A. Logan, J. F. Rabolt, G. B. Street, J. Chem. Soc., Chem. Commun. (1979) 854.

[11] C. L. Gaupp, J. R. Reynolds, Macromolecules 36 (2003) 6305.

[12] P. M. Beaujuge, W. Pisula, H. N. Tsao, S. Ellinger, K. Müllen, J. R. Reynolds, J. Am. Chem. Soc. 131 (2009) 7514.

[13] C. C. Chueh, M. H. Lai, J. H. Tsai, C. F. Wang, W. C. Chen, J. Polym. Sci. Part A: Polym. Chem. 48 (2010) 74.

[14] L.S. Hwang, J.M. Ko, H.W. Rhee, C.Y. Kim, Synth. Met. 55 (1993) 3671.

[15] J. Bobacka, Anal. Chem. 71 (1999) 4932.

[16] C. J. Tonzola, M. M. Alam, B. A. Bean, S. A. Jenekhe, Macromolecules 37 (2004) 3554.

[17] B. Winkler, F. Meghdadi, S. Tasch, R. Mtillner, R. Resel, R. Saf, G. Leising, F. Stelzer, Optical Materials 9 (1998) 159.

[18] A. P. Zoombelt, M. Fonrodona, M. G. R. Turbiez, M. M. Wienkab, R. A. J. Janssen, J. Mater. Chem. 19 (2009) 5336.

[19] Q. Zhang, A. Cirpan, T. P. Russell, T. Emrick, Macromolecules 42 (2009) 1079.

[20] L. J. Maa, Y. X. Li, X. F. Yu, Q. B. Yang, C. H. Noh, Sol. Energy Mater. Sol. Cells 93 (2009) 564.

[21] I. Schwendeman, R. Hickman, G. Sonmez, P. Schottland, K. Zong, D. M. Welsh, J. R. Reynolds, Chem. Mater. 14 (2002) 3118.

[22] W. Y. Lee, K. F. Cheng, T. F. Wang, C. C. Chueh, W.C. Chen, C. S. Tuan, J. L. Lin, Macromol. Chem. Phys. 208 (2007) 1919.

[23] T. T. Steckler, K. A. Abboud, M. Craps, A. G. Rinzler, J. R. Reynolds, Chem. Commun. (2007) 4904.

[24] I. Schwendeman, PhD Thesis, University of Florida, 2002.

[25] J. A. A. Irvin PhD Thesis, University of Florida, 1998.

[26] W. P. Su, J. R. Schrieffer, A. J. Heeger, J. Phys. Rev. B 28 (1980) 2099.

[27] A. J. Heeger, Rev. Mod. Phys. 73 (2001) 681.

[28] C.K. Chiang, C.R. Fischer, Y.W. Park, A.J. Heeger, H. Shirakawa, E.J. Louis, S.C. Gau, A.G. MacDiarmid, Phys. Rev. Lett. 39 (1977) 1098.

[29] C. K. Chiang, M. A. Druy, S. C. Gau, A. J. Heeger, E. J. Louis, A. G. MacDiarmid, J. Am. Chem. Soc. 100 (1978) 1013.

[30] K. E. Ziemelis, A. T. Hussain, D. D. C. Bradley, R. H. Friend, J. Rilhe, G. Wegner, Phys. Rev. Lett. 66 (1991) 2231.

[31] P. J. Nigrey, A. G. MacDiarmid, A. J. Heeger, J. Chem. Soc. Chem. Commun. (1979) 594.

[32] I. F. Perepichka, D. F. Perepichka, H. Meng, F. Wudl, Adv. Mater 17 (2005) 2281.

[33] J.Lin, L. P. Dudek, J. Polym. Sci.: Polym. Chem. Ed. 18 (1980) 2869.

[34] R.D. McCullough, R.D. Lowe, M. Jayaraman, D.l. Anderson, J. Org. Chem. 58(1993) 904.

[35] J. Roncali, J. Mater. Chem. 9 (1999) 1875.

[36] J.Roncali, Chem. Rev. 97 (1997) 173.

[37] C. A. Thomas, PhD Thesis, University of Florida, 2002.

[38] J. P. Lowe, S. A. Kafafi, J. Am. Chem. Soc. 106 (1984) 5837.

[39] J. L.Bredas, J. Chem Phys. 82(1985) 3808.

[40] B. Liu, W. L. Yu, Y. H. Lai, W. Huang, Chem. Mater. 13(2001) 1984.

[41] F. Wudl, M. Kobayashi, A. J. Heeger, J. Org. Chem. 49 (1984) 3382.

[42] J. Roncali, J. Mater. Chem. 9 (1999) 1875.

[43] R. H. L. Kiebooms, H. Goto, K. Akagi, Macromolecules 34 (2001) 7989.

[44] R. Kiebooms, I. Hoogmartens, D. Vanderzande, P. Adriaensens, D. Vanderzande, J. Gelan, 28 (1995) 4961.

[45] Y. S. Lee, M. Kertesz, J. Chem. Phys. 88(1988) 2609.

[47] A. 0. Patil, A. J. Heeger, F. Wudl, Chem. Rev 88 (1988) 183.

[48] D. M. Welsh, PhD Thesis, University of Florida, 2002.

[49] P. Blanchard, H. Brisset, B. Illien, A. Riou, J. Roncali, J. Org. Chem. 62 (1997) 2401.

[50] P. R. Somani, S. Radhakrishnan, Mater. Chem. and Phys. 77 (2002) 117.

[52] T. Kaniowski, W. Luzny, S. Niziol, J. Sanetra, M. Trznadel, Synth Met. 92 (1998) 7.

[55] R. J. Mortimer, Electrochimica Acta 44 (1999) 2971.

[56] T. L.Rose, S. D'Antonio,M. H. Jillson, A. B. Kon, R. Suresh, F. Wang, Synth. Met. 85 (1997) 1439.

[57] E. B. Franke, C. L. Trimble, J. S. Hale, M. Schubert, J. A. Woollam, J. Appl. Phys. 88 (2000) 5777.

[58] P. Topart, P. Hourquebie, Thin Solid Films 352 (1999) 243.

[59] C. L. Gaupp, J. R. Reynolds, Macromolecules 36 (2003) 6305.

[60] V. Seshadri, J. Padilla, H. Bircan, B. Radmard, R. Draper, M. Wood, T. F. Otero, G. A. Sotzing, Org. Electron. 8 (2007) 367.

[61] N. M. Rowley, R. J. Mortimer, Science Progress 85 (2002) 243.

[62] R. J. Mortimer, A. L. Dyer, J. R. Reynolds, Displays 27 (2006) 2.

[63] M. De Paoli, W. A. Gazotti, J. Braz., Chem. Soc. 13(2002) 410.

[64] G. Sonmez, I. Schwendeman, P. Schottland, K. Zong, J. R. Reynolds, Macromolecules 36 (2003) 639.

[65] G. A. Sotzing, J. L. Reddinger, A. R. Katritzky, J. Soloducho, R. Musgrave, J. R. Reynolds, Chem. Mater. 9 (1997) 1578.

[66] C. L. Gaupp, D. M. Welsh, J. R. Reynolds, Macromol. Rapid. Commun. 23 (2002) 885.

[67] J. Subbiah, P. M. Beaujuge, K. R. Choudhury, S. Ellinger, J. R. Reynolds, F. So, Applied Materials and Interfaces 1(2009) 1154.

[68] S. Gunes, H. Neugebauer, N. S. Sariciftci, Chem. Rev. 107 (2007) 1324.

[69] R. S. Ashraf, M. Shahid, E. Klemm, M. A. Ibrahim, S. Sensfuss, Macromol. Rapid Commun. 27 (2006) 1454.

[70] I. Schwendeman, R. Hickman, G. Sonmez, P. Schottland, K. Zong, D. M. Welsh, J. R. Reynolds, Chem. Mater. 14 (2002) 3118.

[71] G. Sonmez, H. B. Sonmez, C. K. F. Shen, F. Wudl, Adv. Mater. 16 (2004) 1905.

[72] G. Sonmez, F. Wudl, J. Mater. Chem. 15(2005) 20.

[73] D. Mecerreyes, R. Marcilla, E. Ochoteco, H. Grande, J. A. Pomposo, R. Vergaz, J. M. S. Pena, Electrochim. Acta 49 (2004) 3555.

[74] D. Rosseinsky, R. J. Mortimer, Adv. Mater. 13 (2001) 783.

[75] J.H. Burroughes, D.D.C. Bradley, A.R Brown, R.N Marks, K. Mackay, R.H Friend, P.L Burn, A.B Holmes, Nature 347(1990) 539.

[76] A. Moliton, C. R. Hiorns, Polym. Int. 53 (2004) 1397.

[77] M. A. Green, Physica E 14 (2002) 11.

[78] D. Mühlbacher, M. Scharber, M. Morano, Z. Zhu, D. Waller, R. Gaudiana, C. Brabec, Org. Lett. 11 (2009) 903.

[79] J. Wang, Analytical Electrochemistry, Wiley, NY, 2001.

[80] P.M.S. Monk, R. J. Mortimer, D. R. Rosseinsky, Electrochromism: Fundamentals and Applications, VCH, Weinheim, 1995.

[81] E. Lavion, J. Electroanal Chem. 39 (1972) 1.

[82] G. Sonmez, C. K. F. Shen, Y. Rubin, F. Wudl, Angew. Chem. Int. Ed. 43 (2004) 1498.

[83] L. B. Groenendaal, G. Zotti,P. H. Aubert, S. M. Waybright, J. R. Reynolds, Adv. Mater. 15 (2003) 855.

[84] Q. Hou, Q. Zhou, Y. Zhang, W. Yang, R.Yang, Y. Cao, Macromolecules 37 (2004) 6299.

[85] S. S. Zhu, T. M. Swager, J Am Chem Soc 119 (1997) 12568.

[86] B. A. D. Neto, A. S. Lopes, G. Ebeling, R. S. Goncalves, V. E. U. Costa, F. H. Quina FH, Tetrahedron 61 (2005) 10975.

[87] Y. Tsubata, T. Suzuki, T. Miyashi, Y. Yamashita, J. Org. Chem. 57 (1992) 6749.

[88] B. Mohr, V. Enkelmann, G. Wegner, J. Org. Chem. 59 (1994) 635.

[89] H. Becker, K. Treacher, H. Spreitzer, A. Falcou, P. Stoessel, A. Buesing, A. Parham PCT International Patent WO 2003020790; 2003.

[90] G. Che, W. Li, Z. Kong, Z. Su, B. Chu, B. Li, Z. Zhang, Z. Hu, H. Chi, Synth. Commun. 36 (2006) 2519.

[91] A. Agrawal, P. G. Tratnyek, Environ. Sci. Technol. 39 (1996) 153.

[92] A. Durmus, G. Gunbas, L. Toppare Chem. Mater. 25 (2007) 6247.

[93] J. K. Stille, Angew. Chem. Int. Ed. Engl. 25 (1986) 508.

[94] D. Aldakov, M. A. Palacios, P. Anzenbacher, Jr. Chem. Mater. 17 (2005) 5238.

[95] B. P. Karsten, R. A. J. Janssen, Org. Lett. 16 (2008) 3513.

[96] L. Wen, S.C. Rasmussen, Journal of Chemical Crystallography 37 (2007) 6.

[97] S. Tarkuc, Y. A. Udum, L. Toppare, Polymer 50 (2009) 3458.

[98] S. Tarkuc, Y. A. Udum, L. Toppare, J. Electroanal. Chem. 64 (2010) 89.

[99] G. Gunbas, A. Durmus, L. Toppare, Adv. Funct. Mater. 18 (2008) 2026.

[100] G. Gunbas, A. Durmus, L. Toppare, Adv. Mater. 20 (2008) 691.

[101] D. J. Irvin, Jr. C. J. DuBois, J. R. Reynolds, Chem. Commun. (1999) 2121.

[102] Jr. C. J. DuBois, F. Larmat, D. J. Irvin, J. R. Reynolds, Synth. Met. 119 (2001) 321

APPENDIX A: SELECTED NMR DATA

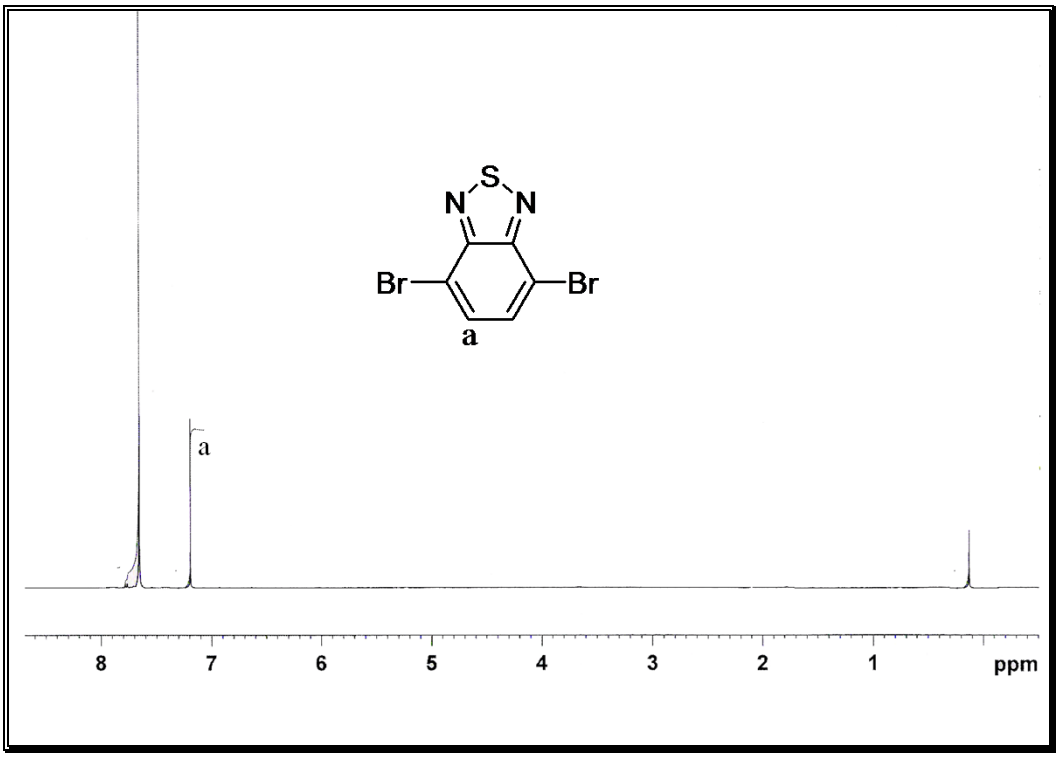

Figure A.1. ^{1}H-NMR spectrum of 4,7-dibromobenzo[c][1,2,5]thiadiazole (5)

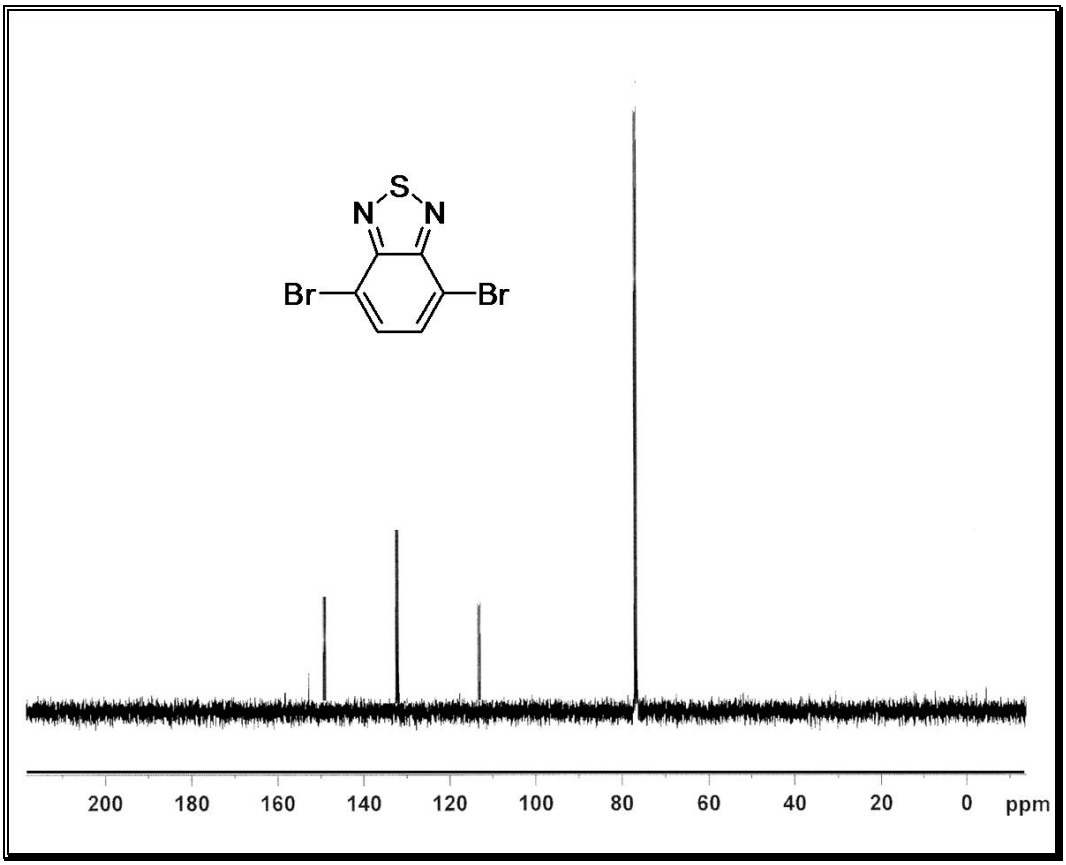

Figure A.2. ^{13}C-NMR spectrum of 4,7-dibromobenzo[c][1,2,5]thiadiazole (5)

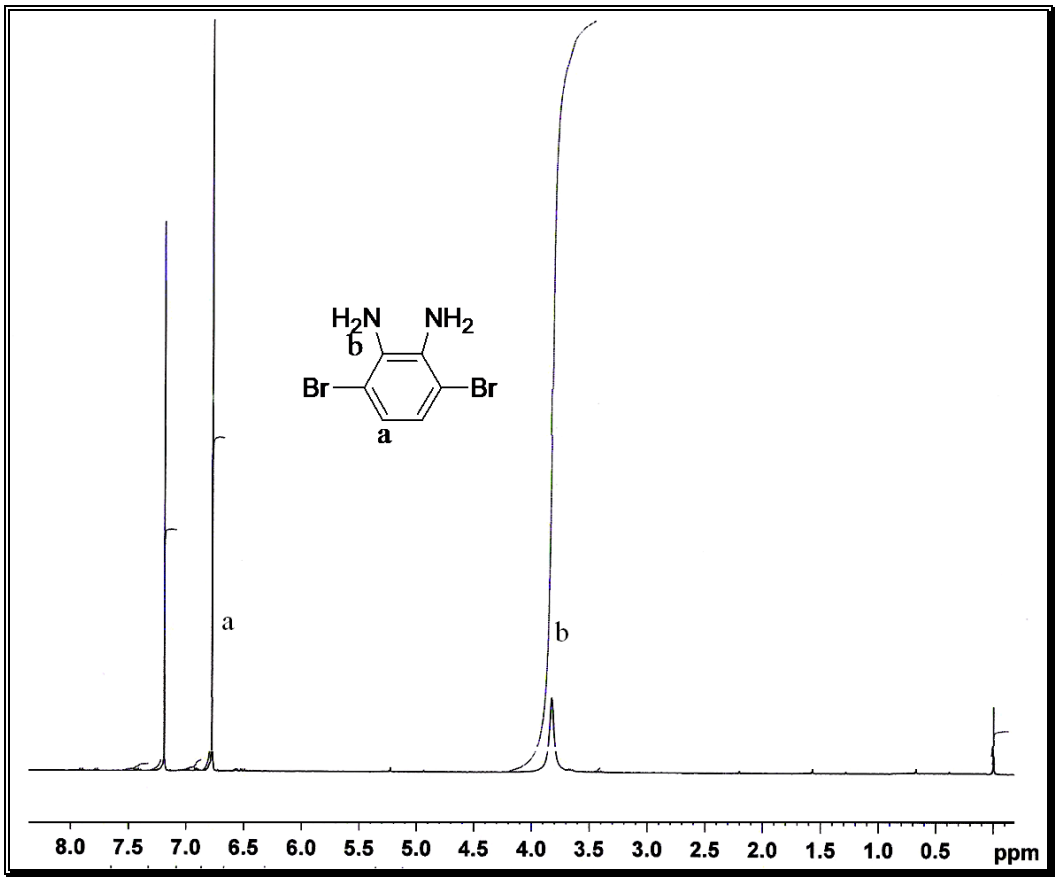

Figure A. 3. ^{1}H-NMR spectrum of 3,6-dibromobenzene-1,2-diamine (6)

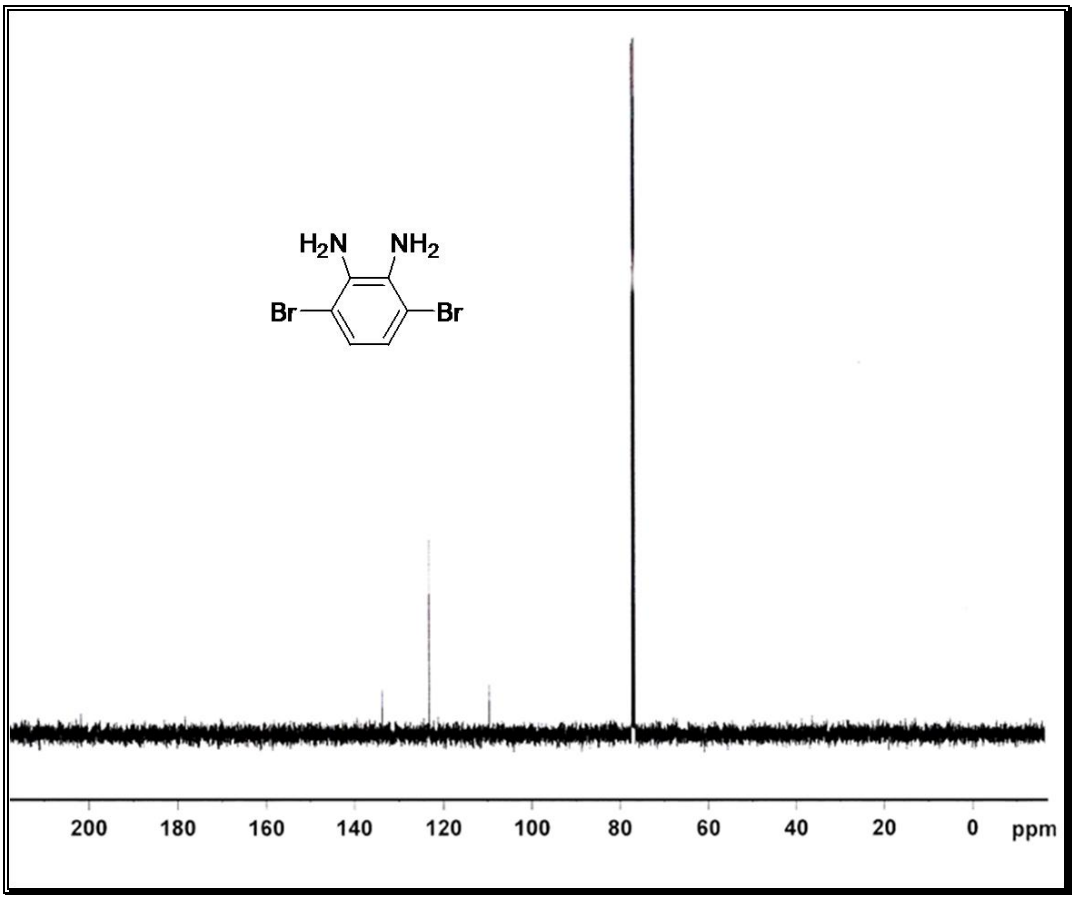

Figure A.4. ^{13}C-NMR spectrum of 3,6-dibromobenzene-1,2-diamine (6)

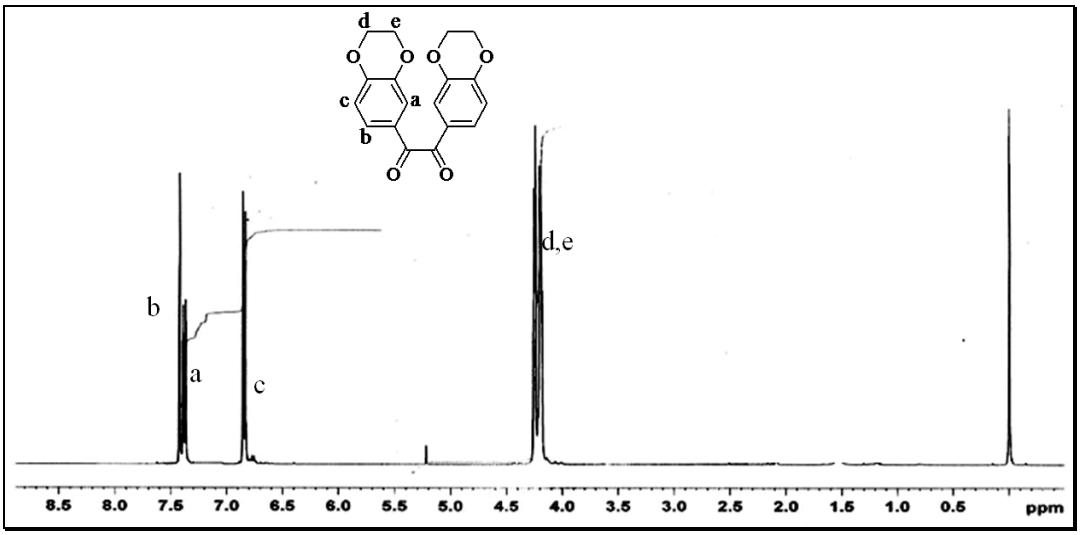

Figure A.5. 1-(2,3-dihydrobenzo[b][1,4]dioxin-6-yl)-2-(2,3-dihydrobenzo [b][1,4] dioxin-7-yl)ethane-1,2-dione (8)

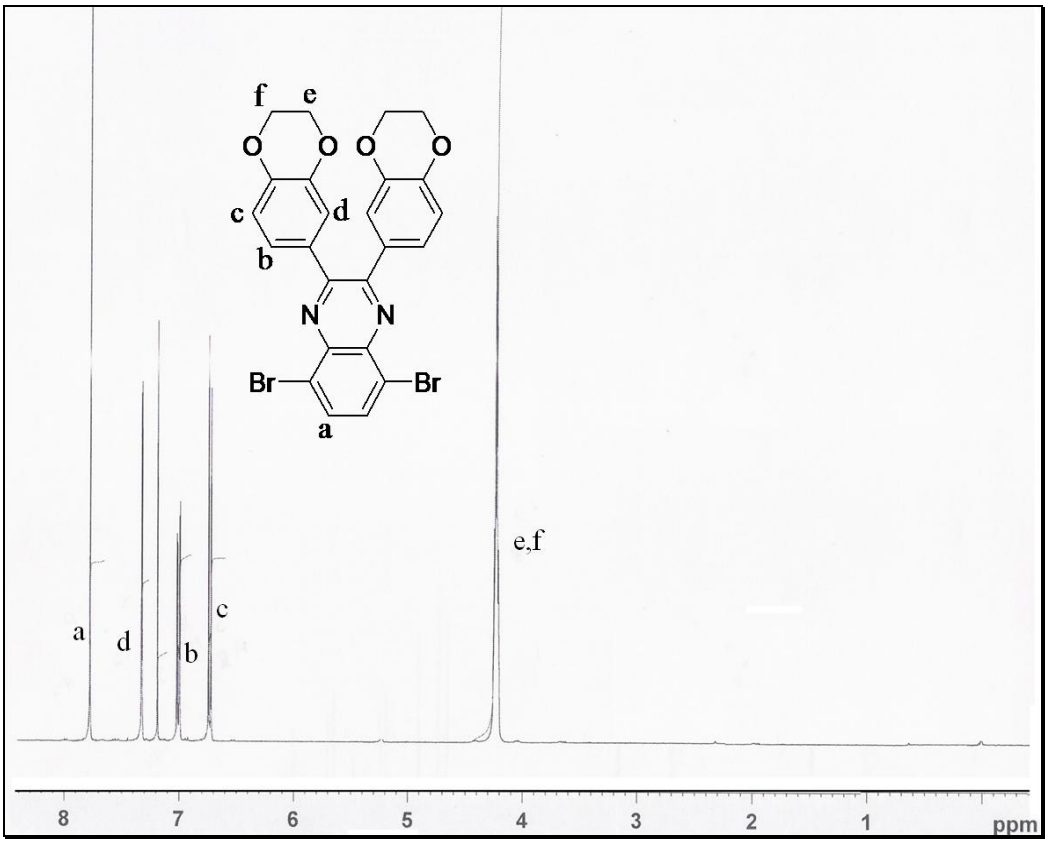

Figure A.6. ^{1}H-NMR spectrum of 5,8-dibromo-2-(2,3-dihydrobenzo[b][1,4]dioxin-6-yl)-3-(2,3-dihydrobenzo[b][1,4]dioxin-7-yl)quinoxaline (9)

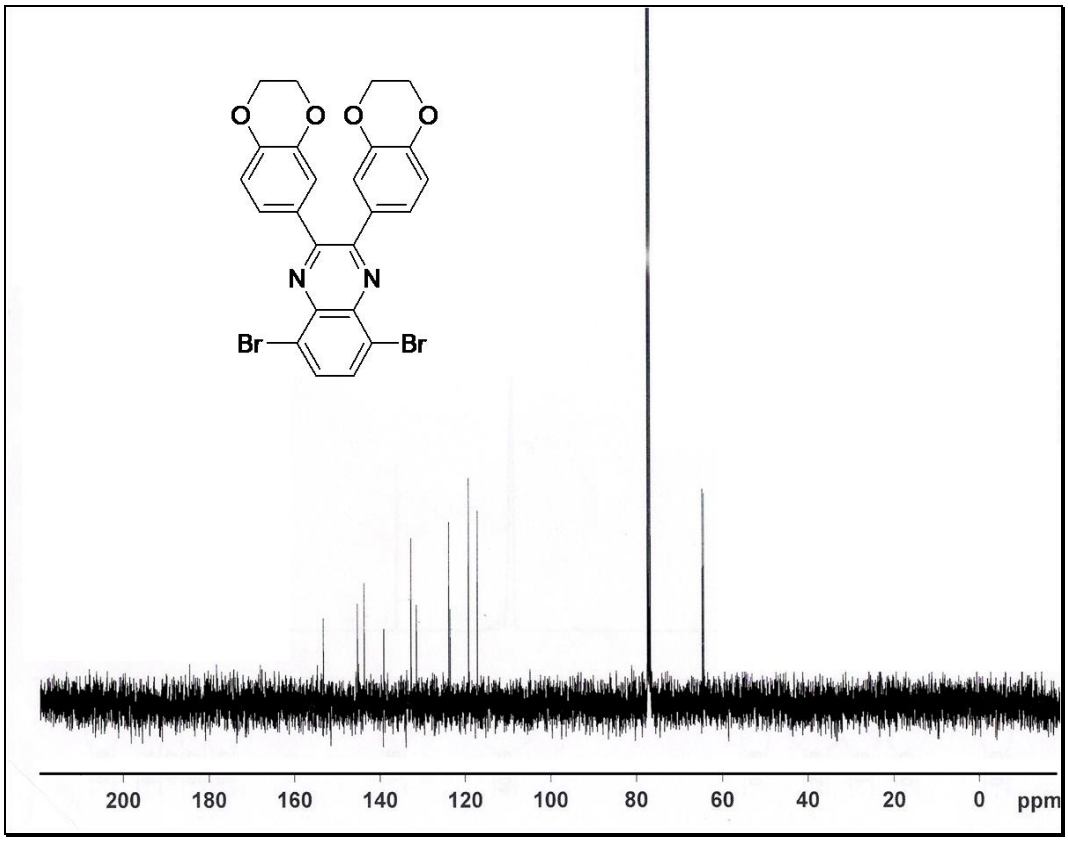

Figure A.7. ^{13}C-NMR spectrum of 5,8-dibromo-2-(2,3-dihydrobenzo[b][1,4]dioxin-6-yl)-3-(2,3-dihydrobenzo[b][1,4]dioxin-7-yl)quinoxaline (9)

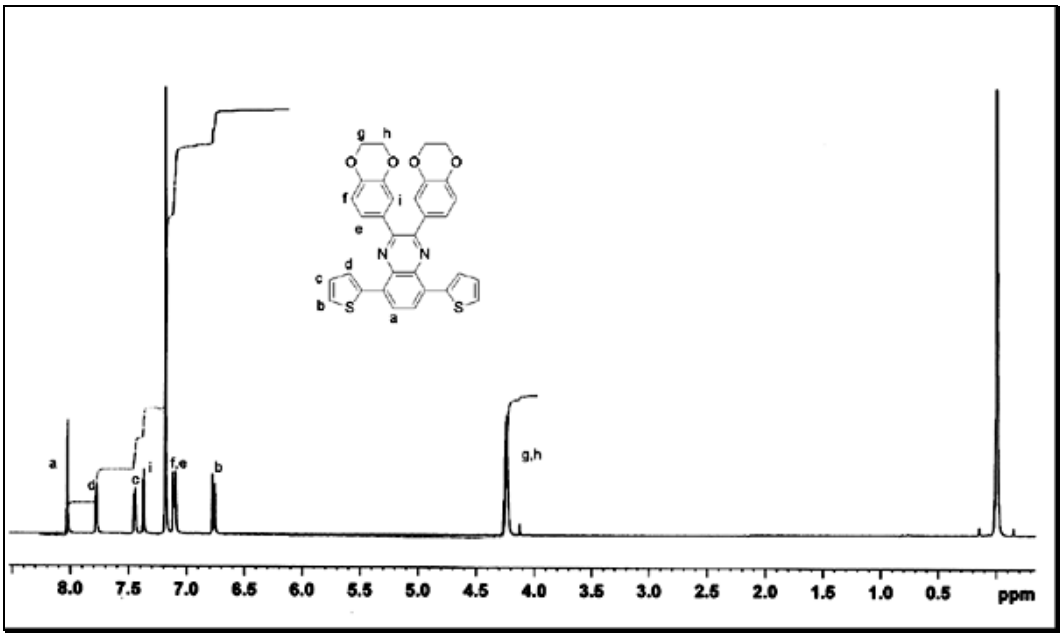

Figure A.8. ^{1}H-NMR spectrum of 2-(2,3-dihydrobenzo[b][1,4]dioxin-6-yl)-3-(2,3-dihydrobenzo [b][1,4]dioxin-7-yl)-5,8-di(thiophen-2-yl)quinoxaline (14)

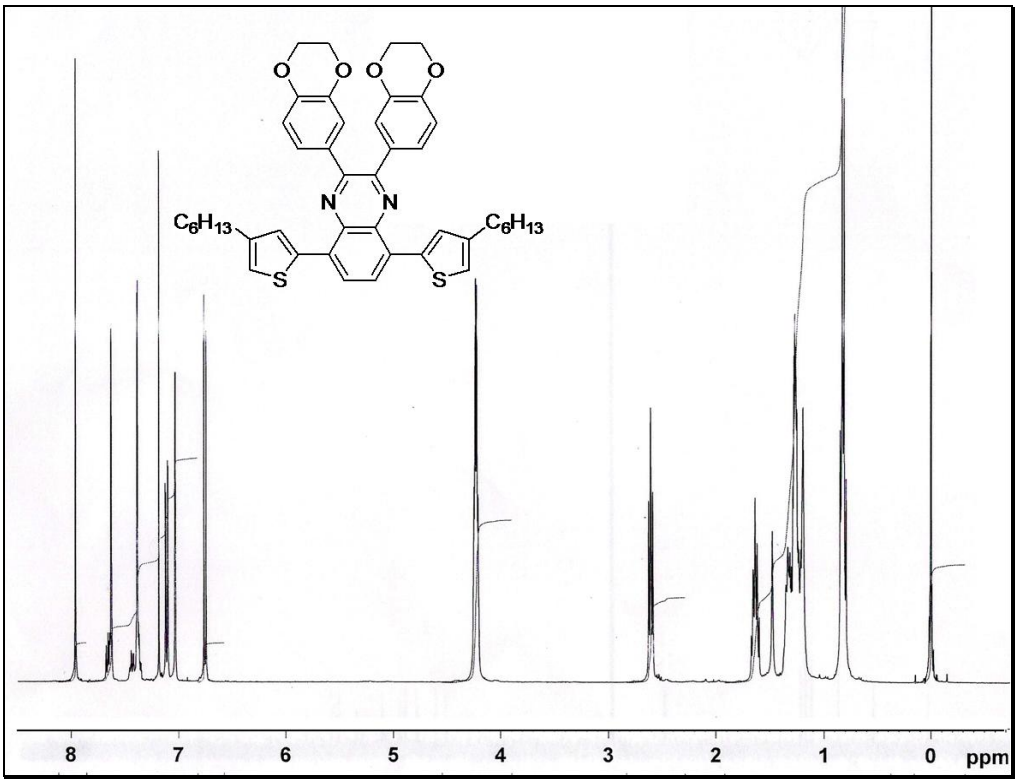

Figure A. 9. ^{1}H-NMR spectrum of 5,8-bis(4-hexylthiophen-2-yl)-2-(2,3-dihydro benzo[b] [1,4] dioxin-6-yl)-3-(2,3-dihydrobenzo[b][1,4]dioxin-7-yl)quinoxaline(15)

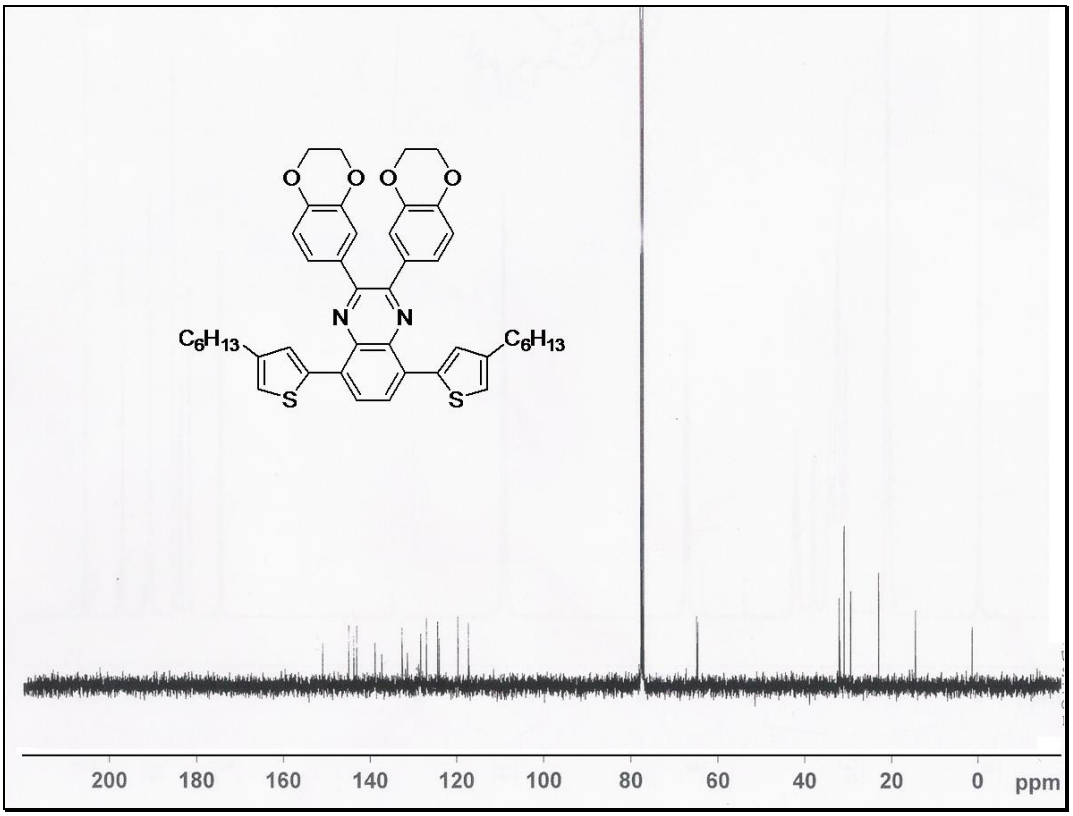

Figure A. 10. ^{13}C-NMR spectrum of 5,8-bis(4-hexylthiophen-2-yl)-2-(2,3-dihydro benzo[b] [1,4] dioxin-6-yl)-3-(2,3-dihydrobenzo[b][1,4]dioxin-7-yl)quinoxaline (15)

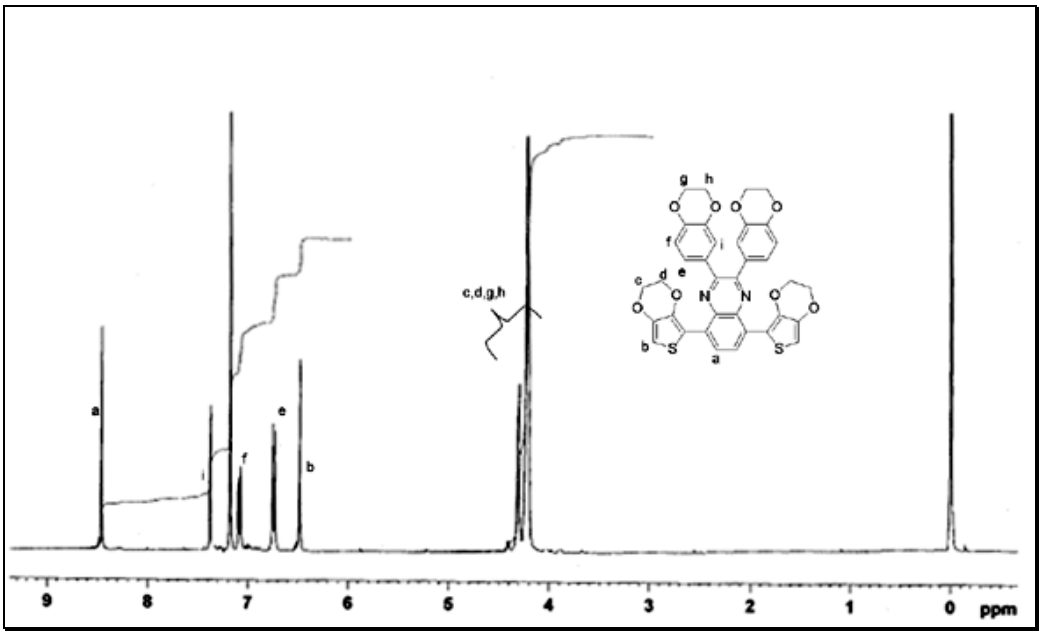

Figure A. 11. ^{1}H-NMR spectrum of 2-(2,3-dihydrobenzo[b][1,4]dioxin-6-yl)-3-(2,3-dihydrobenzo [b][1,4]dioxin-7-yl)-8-(2,3-dihydrothieno[3,4-b][1,4]dioxin-5-yl)-5-(2,3-dihydrothieno[3,4-b] [1,4]dioxin-7-yl)quinoxaline (16)

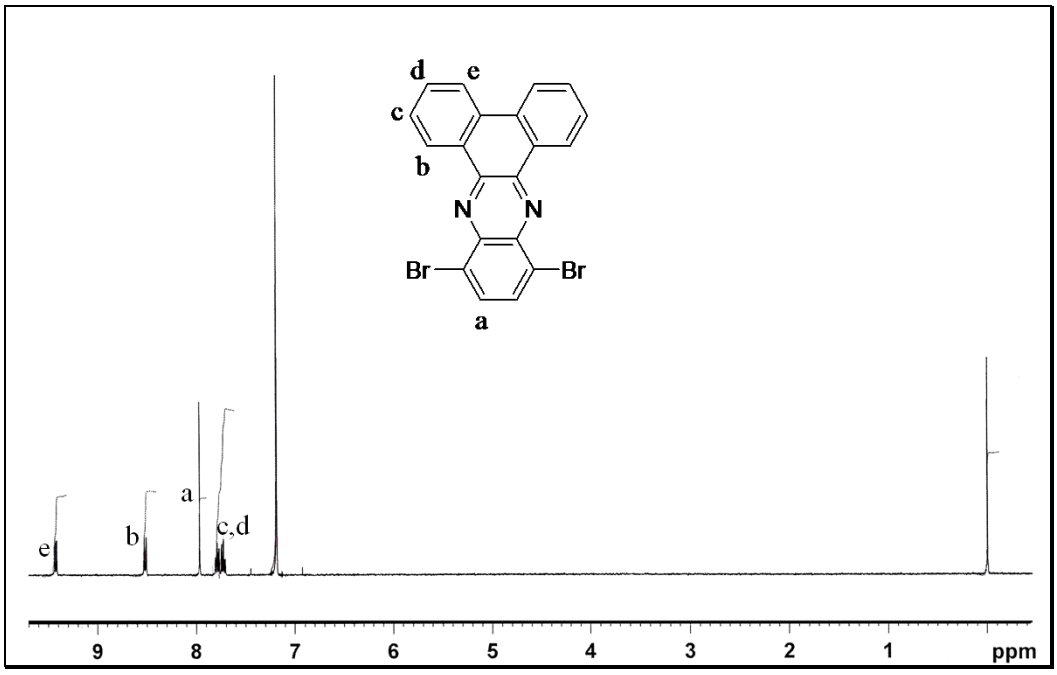

Figure A. 12. ^{1}H-NMR spectrum of 10,13-dibromobenzo[*a*,*c*]phenazine (10)

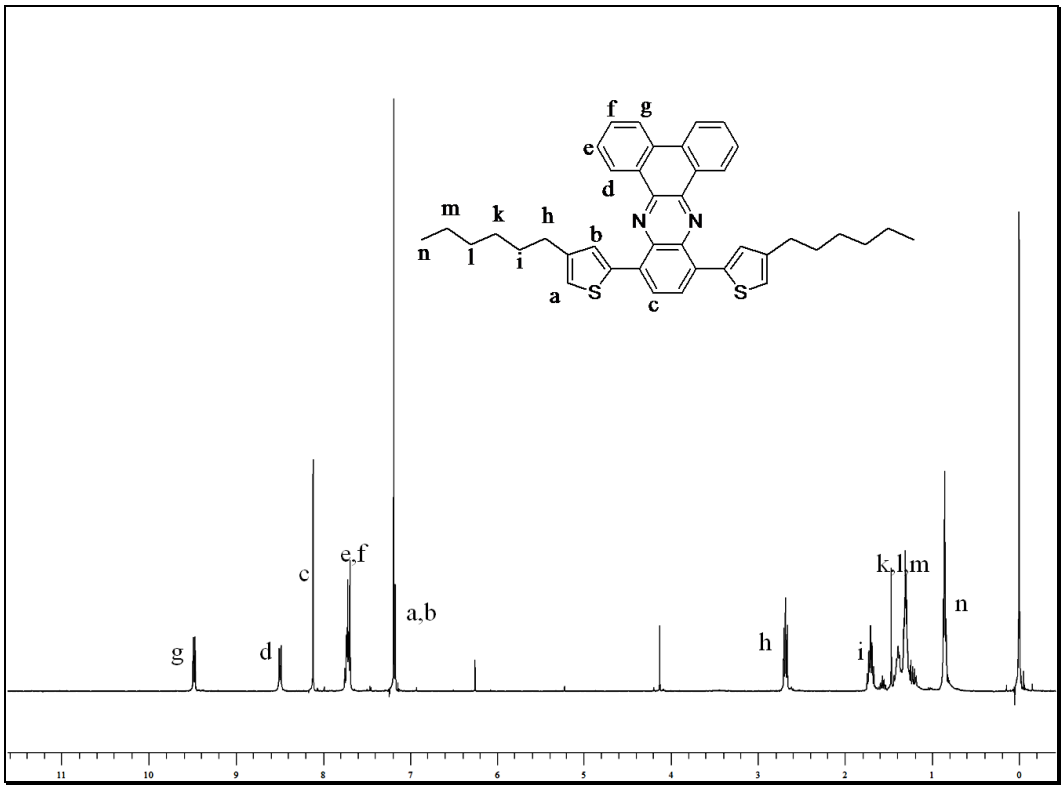

Figure A. 13. ^{1}H-NMR spectrum of 17

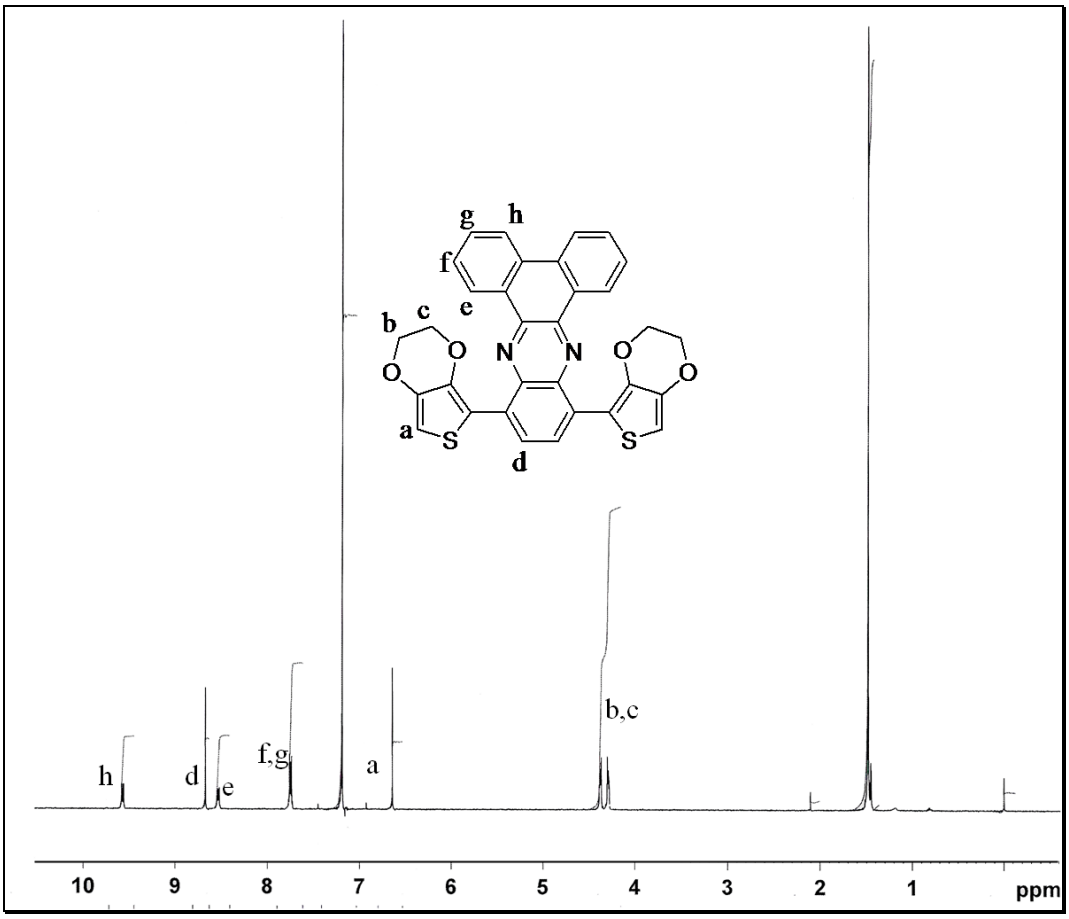

Figure A. 14. ^{1}H-NMR spectrum of 18

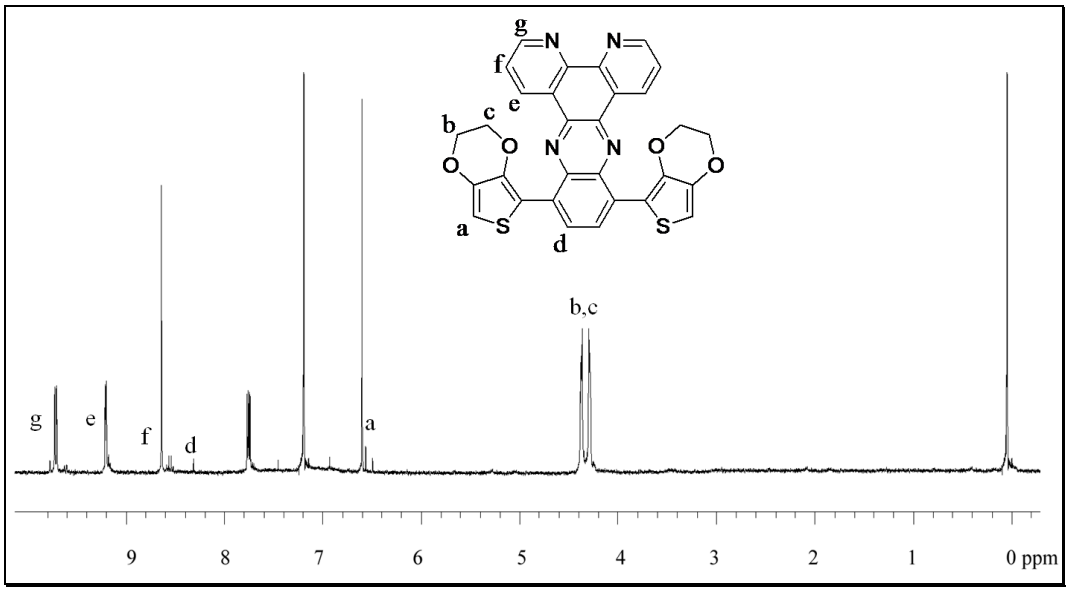

Figure A. 15. ^{1}H-NMR spectrum of 21

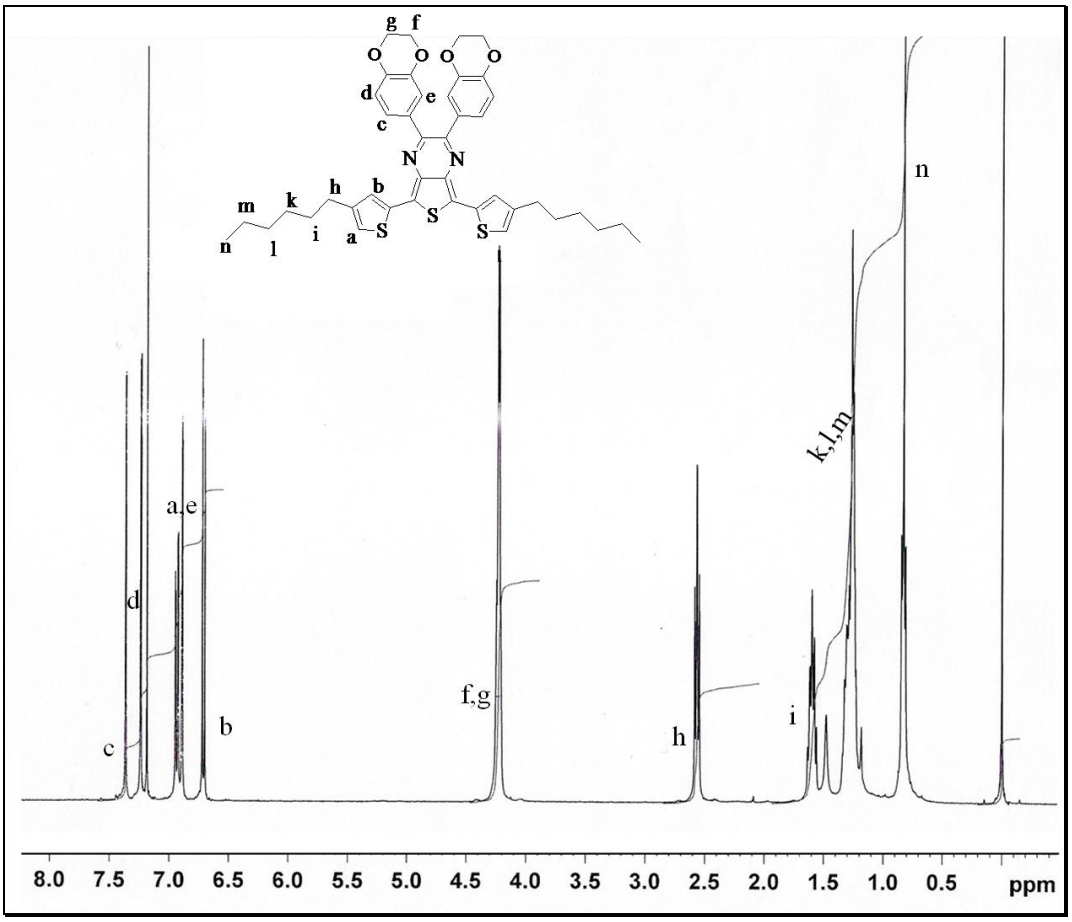

Figure A. 16. [1]H-NMR spectrum of 5,7-bis(4-hexylthiophen-2-yl)-2-(2,3-dihydro-benzo[b][1,4] dioxin-6-yl)-3-(2,3-dihydrobenzo[b][1,4]dioxin-7-yl)thieno[3,4-b] pyrazine (26)

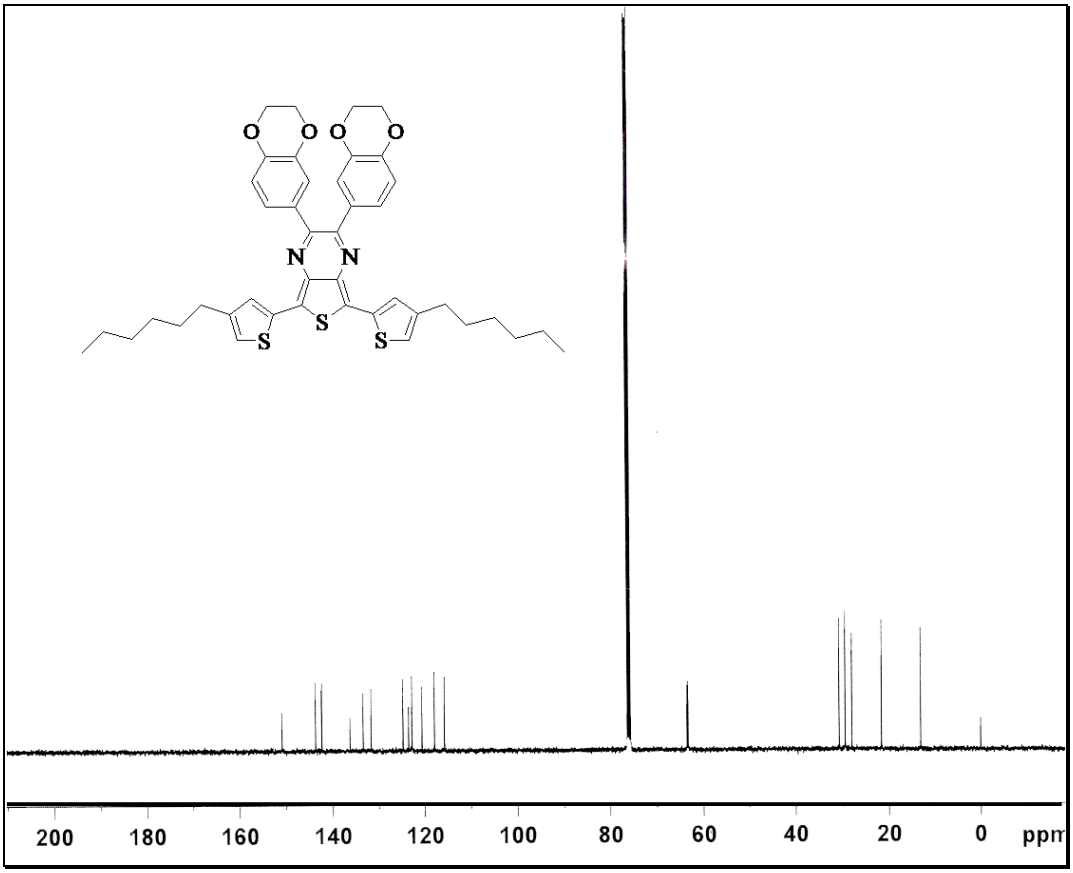

Figure A. 17. ^{13}C-NMR spectrum of 5,7-bis(4-hexylthiophen-2-yl)-2-(2,3-dihydro-benzo[b][1,4] dioxin-6-yl)-3-(2,3-dihydrobenzo[b][1,4]dioxin-7-yl)thieno[3,4-b] pyrazine (26)

CURRICULUM VITAE

PERSONAL INFORMATION

Surname, Name: Tarkuç, Simge

Nationality: Turkish Cypriot (KKTC)

Date and Place of Birth: 30 August 1982 , Gazi Magosa

Phone: +90 392 366 43 82

email: starkuc@yahoo.com

EDUCATION

Degree	Institution	Year of Graduation
MS	METU Chemistry Department	2006
BS	METU Chemistry Education	2005
High School	20 July Science High School, Cyprus	1999

FOREIGN LANGUAGES

Advanced English.

PUBLICATIONS

1. S. Tarkuc, E. Sahin, L. Toppare, D. Colak, I. Cianga, Y. Yagci "Synthesis, characterization and electrochromic properties of a conducting copolymer of pyrrole functionalized polystyrene with pyrrole", Polymer, 47(6),2001-2009 (2006)

2. S. Tarkuc, E. Sahmetlioglu, C. Tanyeli, I.M. Akhmedov, L. Toppare "A soluble conducting polymer: 1-Phenyl-2,5-di(2-thienyl)-1H-pyrrole and its electrochromic application", Electrochimica Acta,51 (25), 5412-5419 (2006)

3. S. Tarkuc, E. Sahmetlioglu, C. Tanyeli, I.M. Akhmedov, L. Toppare, "Electrochromic properties of a soluble conducting polymer of 1-benzyl-2,5-di(thiophene-2-yl)-1H-pyrrole", Sensors and Actuators B: Chemical, 121(2), 622-628 (2007).

4. P. Camurlu, S. Tarkuc, E. Sahmetlioglu, C. Tanyeli, I.M. Akhmedov, L. Toppare, "Multichromic conducting copolymer of 1-benzyl-2,5-di(thiophen-2-yl)-1H-pyrrole with EDOT", Solar Energy Materials and Solar Cells, 92 (2),154-159 (2008).

5. A. Yildirim, S. Tarkuc, M. Ak, L. Toppare, "Syntheses of electroactive layers based on functionalized anthracene for electrochromic applications", Electrochimica Acta, 53(14), 4875-4882 (2008).

6. S. Tarkuc, E. Sahmetlioglu, C. Tanyeli, I.M. Akhmedov, L. Toppare , "Electrochromic properties of poly (1-(phenyl)-2,5-di(2-thienyl)-1H-pyrrole-co-3,4-ethylenedioxy thiophene) and its application in electrochromic devices", Optical Materials, 30 (10), 1489-1494, 2008.

7. K. Aydemir, S. Tarkuc, A. Durmus, G. E. Gunbas, L.Toppare, "Synthesis, characterization and electrochromic properties of a near infrared active conducting polymer of 1,4-di(selenophen-2-yl)-benzene", Polymer, 4(8), 2029-2032 (2008).

8. Y. Arslan Udum, S. Tarkuc, L. Toppare, “A bis-selenophene substituted alkoxy benzene derivative as a highly stable novel electrochromic polymer”, Synthetic Metals, 156 (5-6), 361-365 (2009).

9. S. Tarkuc, Y. Arslan Udum, L. Toppare, “Tuning of the neutral state color of the π-conjugated donor–acceptor–donor type polymer from blue to green via changing the donor strength on the polymer”, Polymer, 50(15), 3458-3464 (2009).

10. E. K. Unver, S. Tarkuc, Y. Arslan Udum, C. Tanyeli, L. Toppare , “Effect of Conjugated-Core Building Block Dibenzo[a,c]phenazine Unit on π-Conjugated Electrochromic Polymers: Red-Shifted Absorption”, Journal of Polymer Science Part A: Polymer Chemistry, 48 (8) , 1714-1720 (2010).

11. S.Tarkuc, Y. Arslan Udum, L. Toppare, “Molecular Architecture: Another Plausible Pathway Toward Low Band Gap Polymer”, Journal of Electroanalytical Chemistry, 643, 89-93 (2010).

12. S. Tarkuc, E. K. Unver, Y. Arslan Udum, C. Tanyeli, L. Toppare, “Multi-Colored Electrochromic Polymer with Enhanced Optical Contrast”, submitted to Optical Materials (2010).

13. S. Tarkuc, E. K. Unver, Y. Arslan Udum, C. Tanyeli, L. Toppare, “The Effect of Changes In Π-Conjugated Terthienyl Systems Using Thienyl and Ethylenedioxybenzene Functionalized Thieno[3,4-b]pyrazine Precursors: Multicolored Low Band Gap Polymers”, submitted to Electrochimica Acta (2010).